ISSN 1732-9353 (suspended)
eISSN 2543-7496

Scientific Review

Engineering and Environmental Sciences

Przegląd Naukowy
Inżynieria i Kształtowanie Środowiska

Vol. 33 (4) 2024 Issue 106
Quarterly

SCIENTIFIC REVIEW
ENGINEERING AND ENVIRONMENTAL SCIENCES
Quarterly

EDITORIAL OFFICE ADDRESS
Wydział Budownictwa i Inżynierii Środowiska SGGW, ul. Nowoursynowska 159, 02-776 Warsaw, Poland
tel. (+48 22) 59 35 363, 59 35 210, 59 35 302
e-mail: srees@sggw.edu.pl
https://srees.sggw.edu.pl

Electronic version of the Scientific Review Engineering and Environmental Sciences is primary version

All papers are indexed in the data bases as follows: AGRO(Poznań), BazTech, Biblioteka Nauki, **CrossRef**, **DOAJ**, **Google Scholar**, **Index Copernicus**, INFONA, POL-Index, **SCOPUS**, SIGŻ(CBR)

Scientific Review

Engineering and Environmental Sciences

Przegląd Naukowy

Inżynieria i Kształtowanie Środowiska

Vol. 33 (4) 2024 Issue 106

Contents

Wydawnictwo SGGW, Warsaw 2024

Wydawnictwo SGGW wydawnictwosggw

Editorial work – Anna Dołomisiewicz, Tomasz Ruchniewicz

ISSN 1732-9353 (suspended) eISSN 2543-7496

Scientific Review Engineering and Environmental Sciences (2024), 33 (4), 329–351

Sci. Rev. Eng. Env. Sci. (2024), 33 (4) https://srees.sggw.edu.pl

ISSN 1732-9353 (suspended) eISSN 2543-7496 DOI 10.22630/srees.9939

Received: 11.09.2024
Accepted: 01.10.2024

Marta STACHOWICZ[1]✉
Piotr BANASZUK[2]
Pouya GHEZELAYAGH[1]
Andrzej KAMOCKI[2]
Dorota MIROSŁAW-ŚWIĄTEK[1]
Mateusz GRYGORUK[1]

[1] Institute of Environmental Engineering, Warsaw University of Life Sciences – SGGW, Poland
[2] Faculty of Civil Engineering and Environmental Sciences, Bialystok University of Technology, Poland

Estimating mean groundwater levels in peatlands using a Bayesian belief network approach with remote sensing data

Keywords: groundwater table, Sentinel-1, SAR, wetlands, subsidence

Introduction

Contemporary management of peatlands requires documentation of their current state to serve as a baseline for future evaluations within an adaptive management approach (United Nations Environment Programme [UNEP], 2022). One critical aspect of this documentation is assessing greenhouse gas (GHG) fluxes. There is a pressing global demand for accurate estimates of GHG emissions from peatlands to inform management strategies and enhance decision-making processes. This need

✉marta_stachowicz@sggw.edu.pl

is underscored by the challenges associated with implementing policies such as the recently enacted EU Nature Restoration Law (European Commission [EC], 2022), which calls for measures that incentivize farmers to mitigate GHG emissions from drained peatlands by raising groundwater levels (GWL) on their lands (Liu et al., 2023). Rewetting is usually the first step in the restoration process of peatlands (Grand-Clement et al., 2015), as all the other elements and functions are dependent on the presence of water (Jones et al., 2018). Accurate GHG emission data is crucial for providing indicators of the effectiveness of rewetting activities (Nielsen et al., 2023). This is especially important for determining appropriate subsidies based on the activities undertaken by farmers. However, direct measurement of GHG fluxes is often unfeasible due to the high costs, time, and specialized personnel required (Cieśliński, 2024). As a result, there is a growing demand for alternative, simplified methods of estimating GHG emissions from drained peatlands.

Peatlands' GWL is recognized as the most informative proxy for GHG emissions (Tanneberger et al., 2024). It was found to be the most sensitive and influential factor affecting gas fluxes, with even minor changes in GWL (on the order of centimeters) capable of causing significant variations in carbon dioxide emissions (Tiemeyer et al., 2020; Evans et al., 2021; Koch et al., 2023). Yet, measuring the GWL also requires field inspections, and obtaining multi-year average GWL data to assess the status or pre- and post-rewetting differences is equally costly, time-consuming (Ghazaryan et al., 2024) and requires meticulous planning of the location of monitoring wells. Therefore, developing a method for predicting the GWL in peatlands using readily available, long-term datasets, such as those derived from remote sensing, is essential.

Various remote sensing data types and sources are widely used in peatland monitoring (Harris & Bryant, 2009; Lees et al., 2018; Millard et al., 2018; Food and Agriculture Organization of the United Nations [FAO], 2021; Habib & Connolly, 2023; Ghezelayagh et al., 2024). However, no universally applicable and accurate tool or methodology has been implemented to assess GWL in peatlands globally. The choice of remote sensing datasets depends on the specific parameters that need to be monitored, as some can also be used for vegetation or soil moisture monitoring. Several options are available for soil moisture, which is strongly connected to GWL (Irfan et al., 2020). It is important to note that regional-scale peatland monitoring requires data with high spatial resolution. Therefore, datasets such as NASA's soil moisture active passive (SMAP) instrument, with a spatial resolution of 36 km, are unsuitable. Synthetic aperture radar (SAR) has proven to be a valuable tool in land monitoring, particularly in forestry and agriculture. Dual-polarized radar backscatter, which is sensitive to soil moisture content,

can thus help predict the GWL in peatlands (Kim et al., 2017; Lees et al., 2021). Consequently, this data can be effectively integrated as input into predictive models, such as Bayesian belief networks.

The Bayesian belief network (BBN) is a probabilistic model in the form of a directed acyclic graph (DAG) that defines conditional dependencies between variables using Bayes' theorem (Neapolitan, 2007; Liu et al., 2016). The network consists of nodes representing model variables and arcs, which determine the nodes' influence on each other (Henriksen et al., 2007; Rao & Rao, 2014). It provides a range of possible outcomes with a certain level of uncertainty in the form of conditional probabilities (Rohmer, 2020). These results can also be presented as conditional probability tables. Bayesian networks are used in many fields, including environmental studies, and they are helpful in decision-making in environmental management (Marcot & Penman, 2019).

In this paper, we apply the BBN approach to estimate the GWL in peatlands using remote sensing. The study is based on data from the Biebrza National Park area (BbPN; NE Poland), which has a long history of GWL monitoring in natural and drained peatlands (Kardel et al., 2009). This allows the use of multi-year mean GWLs as input to the model together with multi-year remote sensing imagery, including data derived from SAR (backscatter coefficient) and InSAR (vertical peat displacement), to build a BBN capable of predicting the occurrence of specific GWLs in peatlands. The main goal of developing the model is to create cost-effective monitoring options in peatlands that currently lack monitoring infrastructure and long-term data. Our hypothesis is that the approach involving the use of BBN alongside remote sensing can serve this purpose.

Material and methods

Study area

Biebrza National Park (BbPN) is located in north-eastern Poland, in the Biebrza river valley (Fig. 1). The entire BbPN area (59,233 ha) was nominated as a Ramsar site in 1995, recognizing its significance as one of the most extensive floodplain and peatland complexes in Central Europe. Despite the relatively well-preserved state of the Biebrza marshes, which support a high diversity of flora and fauna, the area has experienced considerable anthropogenic pressure, particularly from agricultural activities (Okruszko & Byczkowski, 1996). Extensive drainage projects

Stachowicz, M., Banaszuk, P., Ghezelayagh, P., Kamocki, A., Mirosław-Świątek, D., Grygoruk, M. (2024). Estimating mean groundwater levels in peatlands using a Bayesian belief network approach with remote sensing data. *Sci. Rev. Eng. Env. Sci.*, *33* (4), 329–351. DOI 10.22630/srees.9939

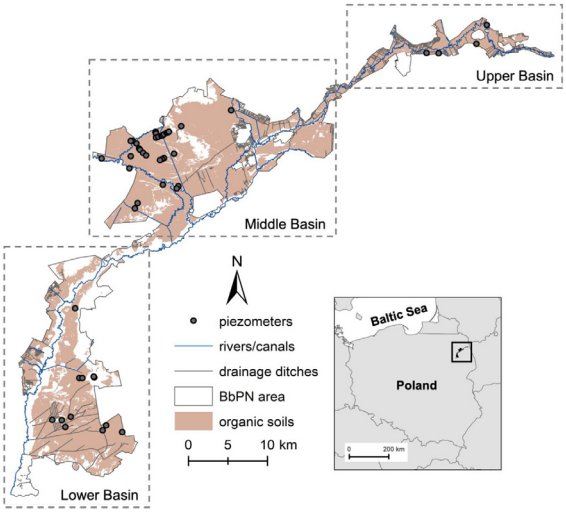

FIGURE 1. Map of the Biebrza National Park with hydrological network and locations of the piezometers
Source: own work.

in the 19th and 20th centuries, comprising the construction of major canals such as the Woźnawiejski Canal and Rudzki Canal and drainage ditches (with a total length of approx. 540 km), have led to the significant lowering of groundwater levels in surrounding peatlands, contributing to their degradation (Stachowicz et al., 2023). Restoration efforts began in the second half of the 20th century.

The study area within BbPN offered a representative sample of various mire and peatland types, including bogs, fluviogenous and topogenous mires, and drained and restored peatlands. For the terminology of mires and peatlands, please refer to e.g. Joosten and Clarke (2002). The Biebrza valley is in a temperate continental climate zone, with mean annual air temperatures varying between 6.6°C and 9.0°C, an average annual sum of precipitation of 561 mm in the period 1951–2021, and – interestingly – a predominantly negative multi-year water balance (Venegas-Cordero et al., 2024).

Input data

Groundwater levels

Groundwater data were obtained from a network of piezometers installed at various locations across BbPN, either alone or arranged in transects. Each piezometer was equipped with an automatic water level logger. Data collection

began in 1994 in some places, while others had shorter recording periods (with the shortest being 4 years and an average of 18 years). Detailed information about the piezometers can be found in Supplementary Material A. This study analyzed data from 32 piezometers in the middle Biebrza basin, 4 in the upper Biebrza basin, and 10 in the lower Biebrza basin. The data from all 45 selected piezometers were used for model training. The GWL values used in the study were multi-year averages from each piezometer. The locations of the piezometers are shown in Figure 1. Each piezometer used for model training was assigned to a specific GWL class to construct the Bayesian network. The classes were developed based on studies by Tiemeyer et al. (2020) and Koch et al. (2023), which revealed a relationship between GHG emissions and peatland GWLs. It was found that the reduction of GHG emissions is expected to occur for groundwater at a depth of 0.40 m. Emissions are stable below this depth (for deeper GWLs), but changes are dynamic above it until the GWL reaches the surface. Based on this, the GWL was divided into six classes: below −0.4 m, four intervals of 0.1 m between −0.4 m and 0.0 m (surface level) and above surface level (Table 1).

TABLE 1. Classification of parameters used in the Bayesian network model[a]

Parameter	Class	Value
Groundwater level [m]	C1	< −0.4
	C2	−0.4 to −0.3
	C3	−0.3 to −0.2
	C4	−0.2 to −0.1
	C5	−0.1 to 0.0
	C6	> 0.0
SAR backscatter coefficient (σ°) [dB]	SAR1	< −18
	SAR2	−18 to −16
	SAR3	> −16
Peat subsidence rate [m·year^{-1}]	Subs1	−0.05 to −0.02
	Subs2	−0.02 to −0.01
	Subs3	−0.01 to 0.05
Distance to the watercourse [m]	D1	0 to 25
	D2	25 to 100
	D3	100 to 440
	D4	> 440

[a]The rationale behind the class intervals of remote sensing parameters is explained in subsequent subsections.

Source: own work.

Stachowicz, M., Banaszuk, P., Ghezelayagh, P., Kamocki, A., Mirosław-Świątek, D., Grygoruk, M. (2024). Estimating mean groundwater levels in peatlands using a Bayesian belief network approach with remote sensing data. *Sci. Rev. Eng. Env. Sci.*, *33* (4), 329–351. DOI 10.22630/srees.9939

Synthetic aperture radar backscatter coefficient

The Copernicus Sentinel-1's C-band SAR imagery data, expressed in decibels (dB) as the backscatter coefficient (σ°), was among the remote sensing parameters utilized for the model's training. This data was chosen because it is sensitive to soil moisture content, making it relevant for estimating groundwater levels (Asmuß et al., 2018; Bechtold et al., 2018; Räsänen et al., 2022). The SAR imagery used in the model was a multi-year average derived from images captured between 1 January 2015 and 8 July 2024, processed in Google Earth Engine. A total of 3,281 images were utilized to create the mean raster of the SAR backscatter coefficient. All images were pre-processed using the Sentinel-1 Toolbox – S1TBX (Veci et al., 2012), which included thermal noise removal, radiometric calibration, and terrain correction. The image collection used in the study was captured in interferometric wide (IW) swath mode, providing a high resolution of 10 m and a swath width of 250 km.

VH polarization was selected for the study, as the relationship between σ° and in-situ measured GWL was tested with both VH and VV polarizations, and Spearman's rank correlation coefficient (ρ) indicated a better correlation with VH (−0.818 vs. −0.762). The Spearman's rank correlation test was selected due to the GWL data's deviation from a normal distribution. The analysis revealed that a lower backscatter coefficient corresponds to a shallower GWL (Fig. 2). The values of the backscatter coefficient were categorized into three classes, as shown in Table 1. This classification was based on the data distribution in the peatlands, where the backscatter coefficient ranged from −21 dB to −14 dB.

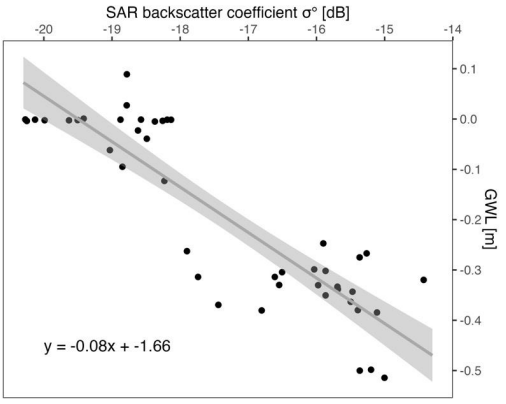

FIGURE 2. Correlation between synthetic aperture radar backscatter coefficient and groundwater level (gray line represents the regression line; gray area represents the confidence interval of 95%; linear model equation: $y = -0.08x + -1.66$)

Source: own work.

Peat subsidence rate

The peat subsidence (vertical displacement) rate, a remote sensing-derived parameter correlated with GWL, was also utilized in the model. The decline in GWL, leading to increased soil respiration, has been identified as a primary factor contributing to the acceleration of subsidence rates (Ma et al., 2022). The subsidence data were obtained from the study by Ghezelayagh et al. (2024), which employed the InSAR technique to measure the vertical displacement of the peat surface within the BbPN area. Changes in peat surface elevation using InSAR are estimated based on InSAR coherence, which is the correlation between two subsequent SAR images (Abdel-Hamid et al., 2021; Hrysiewicz et al., 2024) and can provide centimeter to millimeter precision (Hoyt et al., 2020). This parameter was categorized into three intervals: −0.05 to −0.02 m·year^{-1}, −0.02 to −0.01 m·year^{-1} and −0.01 to 0.05 m·year^{-1} (Table 1).

Distance to watercourses (ditches, canals, rivers)

The third parameter used to build the BBN was the distance to ditches, canals, or rivers. These data were compiled from digitized vector layers of watercourses within the BbPN and created through orthophoto mapping and field verification. The classification of this parameter was based on the meta-analysis by Bring et al. (2022), who identified specific thresholds for the impact of drainage on a peatland's GWL. The study indicated that the effect of ditching on the GWL diminishes by 50% at a distance of 21 m and by 75% at 97 m relative to the immediate vicinity of the ditch. Moreover, the drainage effect is negligible beyond approximately 440 m. For the model, four distance classes were established based on the findings of this study, as outlined in Table 1.

Data processing, building Bayesian network and statistical analyses

All data were pre-processed in the ArcGIS 10.7.1 software. The remote sensing data, provided as raster layers, were spatially extracted to each point feature corresponding to the piezometer locations and their associated multi-year GWL records. The extracted values were subsequently classified according to the categories outlined in Table 1. This classification was a critical step, as BBNs utilize conditional probability tables, which are more effectively managed with discrete variables (Cobb et al., 2007). The BBN was built in GeNIe Academic Version 4.1 (BayesFusion, LLC) by learning the parameters. The network graphs presenting example results were exported from Netica 7.01 (Norsys

Stachowicz, M., Banaszuk, P., Ghezelayagh, P., Kamocki, A., Mirosław-Świątek, D., Grygoruk, M. (2024). Estimating mean groundwater levels in peatlands using a Bayesian belief network approach with remote sensing data. *Sci. Rev. Eng. Env. Sci.*, *33* (4), 329–351. DOI 10.22630/srees.9939

Software Corp). The network structure was designed as depicted in Figure 3, where the remote sensing data serve as parent nodes, and the GWL acts as the child node. This configuration allows the model to estimate the probability of a specific GWL class occurring based on the provided remote sensing parameters. The model was trained using data from the whole Biebrza basin area.

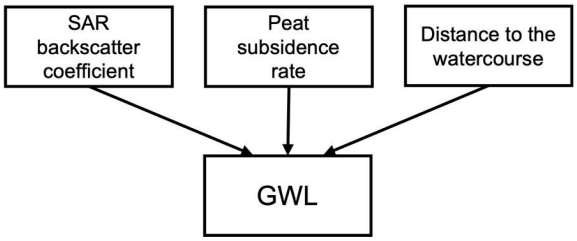

FIGURE 3. Conceptual model of the Bayesian belief network
Source: own work.

The Bayesian belief network's probability results were analyzed using Microsoft Excel and RStudio Version 2023.12.0+369 (R Core Team, 2023). The packages used included 'caret' (Kuhn, 2008), 'ggplot2' (Wickham, 2016) and 'Metrics' (Hamner & Frasco, 2018). Unlike deterministic models, a BBN estimates the probability distribution of potential outcomes rather than predicting exact values. Due to limited data availability, two approaches for network validation were applied. The first approach involved creating 12 random polygons of 100 ha (Fig. 4A), each covering at least two piezometers, to calculate the mean GWL within each extent. The area percentage contribution of each model parameter class was then determined within each polygon. The second validation approach used 26 BbPN plots (cadaster-based, real parcels) with areas ranging from 0.9 ha to 450 ha, with an average of 42 ha (Fig. 4B). In the case of the BbPN plots, the GWL value for each plot was derived from either one piezometer or an average of several piezometers located within the polygon, depending on the number of piezometers intersecting the plot. Then, the percentage contribution of each model variable class (SAR backscatter coefficient, peat subsidence rate, and distance to watercourses) was used as an input in the Bayesian belief network to generate conditional probabilities of different classes of GWL. The class with the highest probability (referred to as a prediction or predicted class later in this study) was then compared with the class of the mean observed GWL at each polygon/plot. However, it should be stressed that the prediction from the model is not a deterministic value and is only one from the possible set of outcomes.

The model's performance was assessed using a confusion matrix and predictive accuracy. The confusion matrix summarizes the model performance by comparing the predicted and actual classes and is a valuable tool for validating probabilistic models in classification tasks (Chen & Pollino, 2012; Marcot, 2012). The predictive accuracy was calculated as the ratio of correct predictions to the total number of predictions. Additionally, a sensitivity analysis, as sensitivity to findings specific to Bayesian networks (Rositano et al., 2017), was performed to determine which model variables had the most significant influence on the GWL prediction. The indicator used for the sensitivity analysis was entropy reduction, with entropy being a measure of uncertainty of variables (Villaverde et al., 2014).

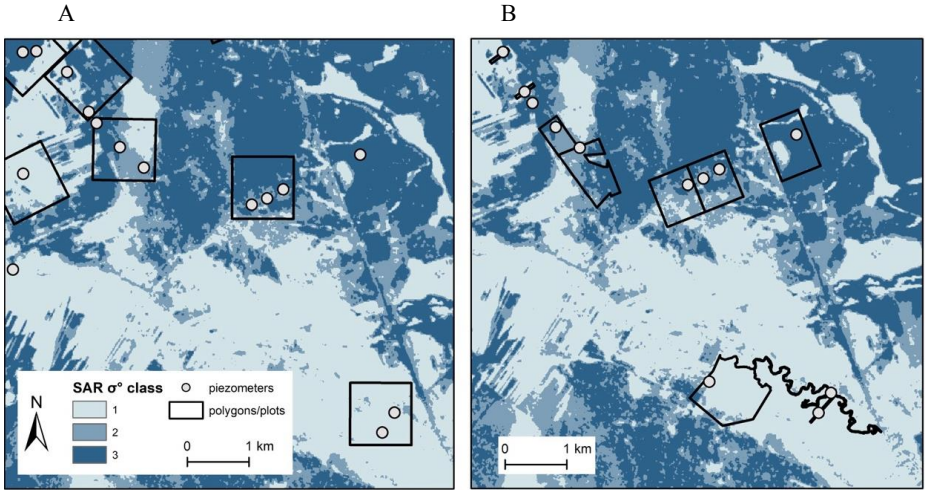

FIGURE 4. Maps showing 100-hectare polygons (A) and the Biebrza National Park plots (B) with a synthetic aperture radar backscatter coefficient raster layer as a background

Source: own work.

Statistical independence of model variables

The statistical independence of the model variables was evaluated. The Shapiro–Wilk test assessed whether the datasets conformed to the normal distribution assumption. The findings indicated that the SAR backscatter coefficient and distance to the watercourse data deviated from a normal distribution (p-value < 0.05), necessitating the application of the Spearman's rank correlation coefficient to investigate the independence of the variables. The Spearman's rank correlation coefficient (ρ) was −0.11 between SAR backscatter and subsidence, with a p-value of 0.47, indicating that there is no significant association between

the variables in the dataset. Similarly, the test showed no correlation between SAR backscatter and distance to the watercourses (ρ = 0.11; p-value = 0.45) and between subsidence and distance (ρ = −0.03; p-value = 0.82), thus making these variables suitable to be used in the BBN approach (Table 2).

TABLE 2. Spearman's rank correlation results between model variables

Pair of compared model variables	Spearman's rank correlation parameters	
	ρ	p-value
Synthetic aperture radar backscatter coefficient–subsidence	−0.11	0.47
Synthetic aperture radar backscatter coefficient–distance to the watercourses	0.11	0.45
Subsidence–distance to the watercourses	−0.03	0.82

Source: own work.

Results

The model's conditional probability table (CPT) generated 36 possible combinations of remote sensing classes. However, due to limited data, some combinations are not present in the model. Therefore, the model was tested using two approaches, as described in the "Data processing, building Bayesian network and statistical analyses" subsection. The percentage contributions of the model variables' classes were calculated for each polygon and BbPN plot used for validation (Table 3). Based on these contributions, the distribution of probabilities of the occurrence of GWL classes was generated (Table 4). The BBNs for one 100-hectare polygon (Polygon 9) and one BbBN plot (Plot 26) selected randomly are shown in Figure 5 to present how the results are generated. Belief bars visually represent conditional probabilities on the BBN, which reflect the likelihood of different outcomes for the child node based on the contributions of the model parameters. In Polygon 9, the presented percentage contribution of the model parameters' classes indicates that the GWL in class C5 (with a 58.2% probability) is most likely to occur within its boundaries. The probabilities of the GWL falling into classes C1, C2, C3, C4 and C6 are 6%, 10.3%, 5.5%, 15% and 5%, respectively. In Plot 26, the GWL in class C2 is most likely to occur (with a 50.3% probability). The probabilities for the GWL being in classes C1 and C3 are 23.9% and 11.7%, respectively. Additionally, the probability of the GWL being in classes C4, C5, and C6 is 4.7% for each.

TABLE 3. Area percentage contributions of each model variables class in polygons and plots used for validation

V.m.	No	Area [ha]	Avg. obs. GWL [m]	SAR backscatter coefficient class distribution [%]			Subsidence class distribution [%]			Distance to the watercourse class distribution [%]			
				1	2	3	1	2	3	1	2	3	4
Polygon	1	100	−0.364	48.3	21.9	29.8	21.7	60	18.3	0	4	53.4	42.6
	2	100	−0.293	3.5	26.7	69.8	0.6	31.4	68	0	0	0	100
	3	100	−0.391	6.6	11.9	81.5	64.3	34.6	1.1	3.6	10.4	71.6	14.4
	4	100	−0.314	30.1	41.0	28.9	17.1	76	6.9	0	0	0	100
	5	100	−0.309	23.2	22.8	54.0	11.1	57.2	31.7	0	0.7	35.3	64
	6	100	−0.332	29.6	4.4	66.0	52.9	44.8	2.3	5.8	13.5	40.4	40.3
	7	100	−0.001	96.0	4.0	0.0	24.3	65.6	10.1	10.6	23.4	66	0
	8	100	−0.006	79.9	10.3	9.8	11	55.9	33.1	15.5	41.2	43.3	0
	9	100	−0.004	81.5	13.6	4.9	63.3	35.6	1.1	0	0	3	97
	10	100	−0.002	48.6	46,0	5.4	22.6	60.5	16.9	0.3	1.7	25.9	72.1
	11	100	−0.109	79.8	6.6	13.6	22.6	65.2	12.2	0	0	14.1	85.9
	12	100	−0.012	96.7	3.3	0.0	34.6	61.5	3.9	4	10.8	42.4	42.8
BbPN plot	1	5.72	−0.002	64.6	27.4	8	30	60	10	0	0	18.5	81.5
	2	4.75	−0.338	20.3	65.8	13.9	10	80	10	0	1.3	53.9	44.8
	3	1.41	−0.5	10.7	44.3	45	33.3	66.7	0	13.6	45.5	40.9	0
	4	0.92	−0.338	1.1	78.4	20.5	0	100	0	0	0	0	100
	5	1.74	−0.351	6.9	24.7	68.4	33.3	66.7	0	0	0	100	0
	6	1.73	−0.267	14.4	29.3	56.3	0	100	0	0	0	0	100
	7	7.21	0.001	100	0	0	33.3	41.7	25	22.5	25	52.5	0
	8	1.3	−0.002	100	0	0	0	33.3	66.7	4.8	19	76.2	0
	9	53.24	−0.304	19.3	56.1	24.6	1.1	47.8	51.1	0	0	0	100
	10	38.63	−0.001	29.2	50.7	20.1	32.8	61.2	6	3.3	10.2	52.6	33.9
	11	18.46	−0.003	76.7	23.3	0	9.1	63.6	27.3	0	0	0	100
	12	53.57	−0.287	6.8	47.8	45.4	0	18.7	81.3	0	0	0	100
	13	50.47	−0.314	2.6	46.9	50.5	18.9	71.1	10	0	0	0	100
	14	65.53	−0.514	12.3	9.9	77.8	53.8	43.4	2.8	3.6	9.8	52.8	33.8
	15	19.53	−0.247	0.7	73.6	25.7	5.7	80	14.3	0	0	0	100
	16	50.94	−0.333	19.4	20.3	60.3	9	64	27	0	0	8.8	91.2
	17	39.29	−0.372	4.7	10	85.3	57.1	42.9	0	2.1	8.9	76.1	12.9
	18	61.39	−0.062	50.6	22.4	27	4.6	55	40.4	2.4	8.9	54.4	34.3
	19	87.01	−0.005	87	10.1	2.9	31	65.2	3.8	2.3	7.5	50	40.2
	20	2.01	−0.023	100	0	0	33.3	66.7	0	3.1	15.6	81.3	0
	21	450.55	−0.001	90.3	5.2	4.5	44.3	51.1	4.6	2	4.8	21.4	71.8
	22	3.86	−0.001	100	0	0	28.6	71.4	0	0	0	0	100
	23	41.17	−0.001	86.5	10.7	2.8	13.7	64.4	21.9	21.9	47.7	30.4	0
	24	2.19	−0.001	50.9	12.7	36.4	0	66.7	33.3	14.7	50	35.3	0
	25	1.78	−0.001	44.3	19.9	35.8	0	66.7	33.3	14.3	35.7	50	0
	26	24.2	−0.320	0	1.2	98.8	53.5	41.8	4.7	0	0	48.1	51.9

V.m. – validation method; Avg. obs. GWL – average observed groundwater level; SAR – synthetic aperture radar; BbPN – Biebrza National Park.

Source: own work.

Stachowicz, M., Banaszuk, P., Ghezelayagh, P., Kamocki, A., Mirosław-Świątek, D., Grygoruk, M. (2024). Estimating mean groundwater levels in peatlands using a Bayesian belief network approach with remote sensing data. *Sci. Rev. Eng. Env. Sci.*, *33* (4), 329–351. DOI 10.22630/srees.9939

TABLE 4. Conditional probabilities of groundwater level classes generated from the Bayesian belief network

V.m.	No	Avg. obs. GWL [m]	GWL class probability [%]						GWL class	
			C1	C2	C3	C4	C5	C6	Obs.	Pred.
Polygon	1	−0.364	10	28.5	10.6	6.95	37.8	6.05	C2	C5
	2	−0.293	5.96	22.5	52	5.83	7.85	5.82	C3	C3
	3	−0.391	20.8	50.8	7.07	5.87	9.66	5.79	C2	C2
	4	−0.314	7.38	39.1	14	6.76	27	5.73	C2	C2
	5	−0.309	10.6	34.4	20.8	6.52	21.4	6.19	C2	C2
	6	−0.332	16.9	35.4	9.91	7.63	23.4	6.77	C2	C2
	7	−0.001	6.94	8.55	7.25	6.94	59.7	10.6	C5	C5
	8	−0.006	8.67	12.6	9.17	7.98	48.8	12.8	C5	C5
	9	−0.004	6.02	10.3	5.52	15	58.2	4.99	C5	C5
	10	−0.002	7.03	29.1	10.5	8.04	38.8	6.51	C5	C5
	11	−0.109	6.17	13.5	8.09	7.99	59.4	4.89	C4	C5
	12	−0.012	5.74	7.16	5.88	8.61	65.6	6.98	C5	C5
BbPN plot	1	−0.002	6.68	21	8.24	8.87	49.5	5.71	C5	C5
	2	−0.338	7.9	50.4	9.52	6.23	19.9	6.05	C2	C2
	3	−0.500	14.2	34.2	16.6	9.9	14.7	10.4	C1	C2
	4	−0.338	5.26	67.8	10.4	5.26	6.08	5.26	C2	C2
	5	−0.351	20.6	56.2	4.64	4.64	9.24	4.64	C2	C2
	6	−0.267	4.57	52.3	18.6	4.57	15.4	4.57	C3	C2
	7	0.001	7.75	7.75	7.75	7.75	55.2	14.2	C6	C5
	8	−0.002	6.06	6.06	6.06	6.06	67.8	7.93	C5	C5
	9	−0.304	6.49	30.2	32.1	6.44	18.4	6.4	C2	C3
	10	−0.001	10.2	38.7	10.5	7.78	25.3	7.45	C5	C2
	11	−0.003	5.72	15.6	8.9	7.11	57	5.72	C5	C5
	12	−0.287	6.65	16.9	52.8	6.65	10.4	6.65	C3	C3
	13	−0.314	9.32	49.5	20.8	6.24	7.95	6.14	C2	C2
	14	−0.514	19.6	44.7	9.63	6.48	13.4	6.13	C1	C2
	15	−0.247	6.51	56	18.9	6.03	6.52	6.02	C3	C2
	16	−0.333	8.04	35.7	26.6	5.77	18.4	5.45	C2	C2
	17	−0.372	21.7	52.8	6.65	5.35	8.17	5.3	C2	C2
	18	−0.062	9.27	24.3	12.8	7.14	39	7.47	C5	C5
	19	−0.005	6.14	11.8	6.24	7.86	61.6	6.37	C5	C5
	20	−0.023	6.51	6.51	6.51	6.51	66.4	7.54	C5	C5
	21	−0.001	5.81	8.9	5.78	10.9	63	5.61	C5	C5
	22	−0.001	3.93	3.93	3.93	3.93	74.6	3.93	C5	C5
	23	−0.001	8.24	10.6	9.72	8.08	47.8	15.6	C5	C5
	24	−0.001	11.8	17.5	11.7	9.62	36.4	12.9	C5	C5
	25	−0.001	12.1	22	11.5	9.08	33.5	11.9	C5	C5
	26	−0.320	23.9	50.3	11.7	4.71	4.71	4.71	C2	C2

V.m. – validation method; Avg. obs. GWL – average observed groundwater level; Obs. – observed; Pred. – predicted; BbPN – Biebrza National Park.

Source: own work.

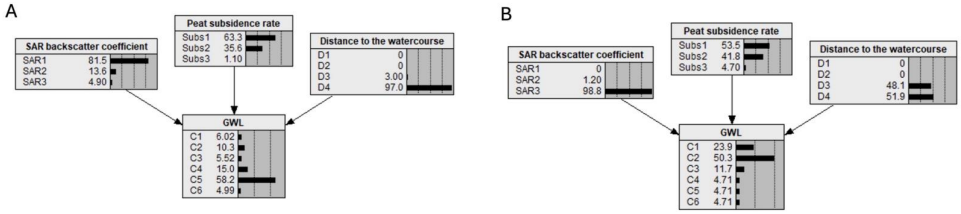

FIGURE 5. Example results from the Bayesian belief network: A – percentage contribution of model parameters in Polygon 9, B – percentage contribution of model parameters in Biebrza National Park Plot 26. Groundwater level node represents the results as a probability distribution of the occurrence of certain GWL classes

Source: own work.

The confusion matrices assessing the performance of the model for both sets of 100-hectare polygons and BbPN plots are shown in Figure 6. Diagonal elements on the matrix represent correctly predicted classes, while off-diagonal elements indicate misclassifications. Using 100-hectare polygons as a validation set, 10 out of 12 predictions were correct, resulting in a prediction accuracy of 83.3% (Fig. 6A). Validating the network with a set of BbPN plots resulted in an accuracy of 73.1%, where 19 out of 26 predictions were correct. Sensitivity analysis revealed that the entropy reduction was 0.315, 0.066, and 0.038 for SAR backscatter coefficient, distance to the watercourse, and peat subsidence rate, respectively. This means that the SAR backscatter coefficient is the parameter with the highest influence over the GWL result in the model.

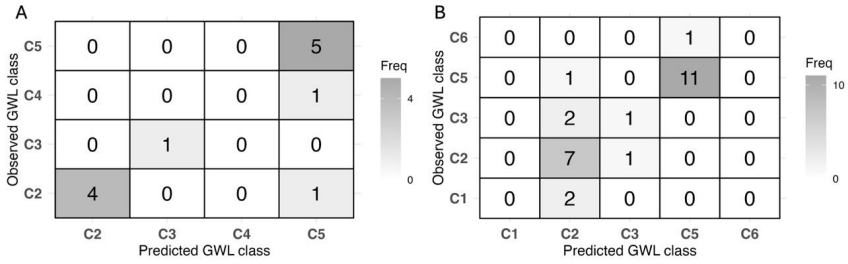

FIGURE 6. Confusion matrices displaying the number of matched and unmatched classes between predicted and actual groundwater level values for 100 ha polygons (A) and the Biebrza National Park plots (B) used as the validation set

Source: own work.

Discussion

The results of this study highlight the potential of using BBN in conjunction with remote sensing data to address the challenge of estimating GWLs in peatlands, particularly in the context of environmental management and GHG mitigation. The model achieved predictive accuracies of 73.1–83.3%, proving its effectiveness as a cost-efficient alternative to traditional GWL measurement methods, which are often hindered by logistical constraints and high costs. The results demonstrate that remote sensing can serve as a reliable proxy for groundwater dynamics, which are vital for understanding and managing peatland ecosystems. These findings are particularly important as they provide a means to evaluate the hydrological status of peatlands that lack extensive monitoring infrastructures, ultimately supporting restoration efforts aimed at enhancing carbon sequestration in peat soils. By linking GWL estimates to GHG emissions, this research can contribute to the broader goal of developing adaptive management strategies that can support policy decisions and promote sustainable land use practices.

Numerous approaches have been explored to estimate GWLs in peatlands without direct measurements, often by testing a range of remote sensing and non-remote sensing indicators to identify the most accurate and sensitive proxies for GWL prediction (Kameoka et al., 2021; Georgiou et al., 2023). Some of them reached higher (Hikouei et al., 2023) or lower (Bechtold et al., 2014) accuracy, although they had much more input data to teach the model. However, a significant challenge emerges from upscaling these indicators and models for application beyond the specific environments where they were initially built. For instance, Adinugroho et al. (2021) developed a model using Indonesian peatlands to estimate soil moisture using Sentinel imagery as a proxy for groundwater level. This model is available as an open-source SEPAL tool (FAO, 2021), but it did not perform well in the peatlands in BbPN. Ideally, an extensive monitoring network across diverse types and conditions of peatlands would be required to provide spatially comprehensive GWL data, facilitating robust model development and validation. Unfortunately, establishing and managing such a network is generally not feasible due to the significant financial, time, and logistical resources required and the different monitoring protocols in peatlands across countries (Gutierrez Pacheco et al., 2021). The Bayesian belief network employed in this study faces similar challenges. Several uncertainties emerged during data preparation, model construction, and validation. A primary concern lies in the inherent limitations of remote sensing data, such as the constraints imposed by spatial resolution and satellite

revisit intervals. Additionally, because synthetic aperture radar (SAR) cannot penetrate dense tree canopies, some datasets had to be excluded to prevent the introduction of inaccuracies. Further complications arise from temporal discrepancies between the multi-year GWL measurements and the remote sensing data, as these datasets were collected over differing timeframes. For instance, the SAR backscatter coefficient used in this study was averaged from all available Sentinel-1 imagery since its launch. In contrast, the multi-year GWL data from some piezometers represents a more extended period, potentially leading to inconsistencies. Other uncertainties arise from the limited size of the training dataset, which reduces the variety of variable class combinations within the model due to limitations in piezometer coverage, potentially leading to inaccurate predictions. The possibility of mismatching definitions of intervals or classes of variables aggravates this issue. The obtained accuracy in the built model may be somewhat misleading due to unbalanced proportions in the class distributions, as class C5 in the validation set was much more frequent than the others, and some classes were even missing (C1 and C3 in the 100-hectare polygon validation set). Moreover, it is crucial to address whether the level of accuracy in GWL prediction is sufficient for practical applications, such as estimating greenhouse gas emissions.

The most common way to teach Bayesian networks is using observational data and/or expert knowledge (Daly et al., 2011). However, the data is often insufficient to capture all model variables (Masegosa et al., 2016), which was the case in this study. One approach to addressing this issue would be to obtain missing data from other models. In terms of the future development of the BBN created in this study, there are plans to construct a multiple regression model. This model would facilitate the generation of new GWLs based on the known remote sensing parameters used in the study. The generated data could then be used to update the developed BBN. Additionally, the data from the BbPN area should be complemented and tested with data from other peatlands across all of Poland and outside of the country, especially since other studies found that results obtained at one peatland using SAR imagery cannot be compared with different sites (Lees et al., 2021). Incorporating data from various peatlands will improve the accuracy of future models and provide a more comprehensive understanding of the relationship between the GWL and parameters derived from remote sensing. Furthermore, the potential of other remote sensing data sources could also be investigated to improve the prediction accuracy.

Despite the indicated limitations, the presented assessment methodology may be one of the few that can be applied under operational conditions to determine

the multi-year average GWL in peatlands, where necessary (e.g., for the purpose of assessing the hydrological status of remote/unmonitored peatlands before undertaking restoration measures) and where hydrological monitoring has never been conducted and the use of more complex methods will be pointless due to the long analysis time, its complexity and data requirements. Indeed, under the assumptions of implementing programs that encourage carbon retention in rewetted peat soils, there will be a need for an ex-ante evaluation of the effectiveness and scale of success of these measures. Under such conditions, a rapid assessment of the average state of groundwater will prove necessary. So far, published experience of the uncertainty in the success of peatland rewetting and the resulting increase in GWL of a few centimeters (Karimi et al., 2024) indicates that even an uncertainty-laden assessment of water levels using the Bayesian belief network presented here can become a useful, and perhaps even the only, tool that provides a meaningful quantification of peatland GWL from a multi-year period. However, this will certainly require calibration and verification of the method on other, possibly numerous, peatlands with available data from long-term GWL monitoring.

Conclusions

This research demonstrates the application of a BBN model integrated with remote sensing data to estimate the mean groundwater levels in peatlands, with a specific focus on the Biebrza National Park in Poland. The developed Bayesian network can predict GWLs within the defined classes with an accuracy of 73.1–83.3%. Additionally, dual-polarized radar backscatter has been validated as a proxy for GWL, showing a high correlation with field-measured GWL data. Among the remote sensing variables considered, the SAR backscatter coefficient was the most sensitive in predicting the GWL in peatlands. The study emphasizes the potential of the Bayesian network model as a cost-effective and efficient alternative to traditional GWL measurement techniques. It also highlights the critical role of high-resolution remote sensing data in improving GWL estimates and the effectiveness of Bayesian networks in managing uncertainties and providing conditional probabilities for different outcomes. This underscores the importance of the continued development and refinement of predictive models for environmental management. Developing this modeling

approach to other peatland areas globally is recommended, particularly in regions where ground-based monitoring is logistically challenging or costly. Future research should also explore incorporating additional remote sensing parameters and the potential impact of climatic variables on the model's predictive accuracy. In conclusion, the study demonstrates the feasibility and effectiveness of using Bayesian networks and remote sensing data to estimate GWLs in peatlands. This approach remains a valuable next step in achieving efficient peatland monitoring and management, despite its uncertainties. However, further improvements in the prediction of GWL by utilizing available hydrological and remote sensing data are required, especially including testing alternative modeling approaches.

Acknowledgments

The research leading to these results has received funding from the Norwegian Financial Mechanism 2014–2021 (project no. 2019/34/H/ ST10/00711).

References

Abdel-Hamid, A., Dubovyk, O., & Greve, K. (2021). The potential of Sentinel-1 InSAR coherence for grasslands monitoring in Eastern Cape, South Africa. *International Journal of Applied Earth Observation and Geoinformation*, *98*, 102306. https://doi.org/10.1016/j.jag.2021.102306

Adinugroho, W. C., Imanuddin, R., Krisnawati, H., Syaugi, A., Santosa, P. B., Qirom, M. A., & Prasetyo, L. B. (2021). Exploring the potential of soil moisture maps using Sentinel Imagery as a Proxy for groundwater levels in peat. *IOP Conference Series: Earth and Environmental Science*, *874* (1), 012011. https://doi.org/10.1088/1755-1315/874/1/012011

Asmuß, T., Bechtold, M., & Tiemeyer, B. (2018). Towards Monitoring Groundwater Table Depth in Peatlands from Sentinel-1 Radar Data. *IGARSS 2018 - 2018 IEEE International Geoscience and Remote Sensing Symposium*, *2018*, 7793–7796. https://doi.org/10.1109/IGARSS.2018.8518838

Bechtold, M., Schlaffer, S., Tiemeyer, B., & De Lannoy, G. (2018). Inferring Water Table Depth Dynamics from ENVISAT-ASAR C-Band Backscatter over a Range of Peatlands from Deeply-Drained to Natural Conditions. *Remote Sensing*, *10* (4), 536. https://doi.org/10.3390/rs10040536

Bechtold, M., Tiemeyer, B., Laggner, A., Leppelt, T., Frahm, E., & Belting, S. (2014). Large-scale regionalization of water table depth in peatlands optimized for greenhouse gas emission upscaling. *Hydrology and Earth System Sciences*, *18* (9), 3319–3339. https://doi.org/10.5194/hess-18-3319-2014

Bring, A., Thorslund, J., Rosén, L., Tonderski, K., Åberg, C., Envall, I., & Laudon, H. (2022). Effects on groundwater storage of restoring, constructing or draining wetlands in temperate and boreal climates: a systematic review. *Environmental Evidence*, *11* (1), 38. https://doi.org/10.1186/s13750-022-00289-5

Chen, S. H., & Pollino, C. A. (2012). Good practice in Bayesian network modelling. *Environmental Modelling & Software*, *37*, 134–145. https://doi.org/10.1016/j.envsoft.2012.03.012

Cieśliński, R. (2024). The use of the GEST method to estimate greenhouse gases uptake or emissions in the absence of data for a raised bog. *Journal of Water and Land Development*, *60*, 59–64. https://doi.org/10.24425/jwld.2023.148460

Cobb, B. R., Rumí, R., & Salmerón, A. (2007). Bayesian network models with discrete and continuous variables. In P. Lucas, J. A. Gámez, A. Salmerón (Eds.), *Advances in probabilistic graphical models* (pp. 81–102). Springer. https://doi.org/10.1007/978-3-540-68996-6_4

Daly, R., Shen, Q., & Aitken, S. (2011). Learning Bayesian networks: approaches and issues. *The Knowledge Engineering Review*, *26*(2), 99–157. https://doi.org/10.1017/S0269888910000251

European Commission [EC]. (2022). *Nature restoration law: for people, climate, and planet.* Publications Office of the European Union. https://data.europa.eu/doi/10.2779/86148

Evans, C. D., Peacock, M., Baird, A. J., Artz, R. R. E., Burden, A., Callaghan, N., Chapman, P. J., Cooper, H. M., Coyle, M., Craig, E., Cumming, A., Dixon, S., Gauci, V., Grayson, R. P., Helfter, C., Heppell, C. M., Holden, J., Jones, D. L., Kaduk, J., Levy, P., Matthews, R., McNamara, N. P., Misselbrook, T., Oakley, S., Page, S. E., Rayment, M., Ridley, L. M., Stanley, K. M., Williamson, J. L., Worrall, F., & Morrison, R. (2021). Overriding water table control on managed peatland greenhouse gas emissions. *Nature*, *593* (7860), 548–552. https://doi.org/10.1038/s41586-021-03523-1

Food and Agriculture Organization of the United Nations [FAO]. (2021). *Practical guidance for peatland restoration monitoring in Indonesia – A remote sensing approach using FAO-SEPAL platform. Technical working paper.* Food and Agriculture Organization of the United Nations.

Georgiou, S., Mitchard, E. T. A., Crezee, B., Dargie, G. C., Young, D. M., Jovani-Sancho, A. J., Kitambo, B., Papa, F., Bocko, Y. E., Bola, P., Crabtree, D. E., Emba, O. B., Ewango, C. E. N., Girkin, N. T., Ifo, S. A., Kanyama, J. T., Mampouya, Y. E. W., Mbemba, M., Ndjango, J-B. N., Palmer, P. I., Sjögersten, S., & Lewis, S. L. (2023). Mapping water levels across a Region of the Cuvette Centrale Peatland Complex. *Remote Sensing*, *15* (12), 3099. https://doi.org/10.3390/rs15123099

Ghazaryan, G., Krupp, L., Seyfried, S., Landgraf, N., & Nendel, C. (2024). Enhancing peatland monitoring through multisource remote sensing: optical and radar data applications. *International Journal of Remote Sensing*, *45* (18), 6372–6394. https://doi.org/10.1080/01431161.2024.2387133

Ghezelayagh, P., Oleszczuk, R., Stachowicz, M., Eini, M. R., Kamocki, A., Banaszuk, P., & Grygoruk, M. (2024). Developing a remote-sensing-based indicator for peat soil vertical displacement. A case study in the Biebrza Valley, Poland. *Ecological Indicators*, *166*, 112305. https://doi.org/10.1016/j.ecolind.2024.112305

Grand-Clement, E., Anderson, K., Smith, D., Angus, M., Luscombe, D. J., Gatis, N., Bray, L. S., & Brazier, R. E. (2015). New approaches to the restoration of shallow marginal peatlands. *Journal of Environmental Management*, *161*, 417–430. https://doi.org/10.1016/j.jenvman.2015.06.023

Gutierrez Pacheco, S., Lagacé, R., Hugron, S., Godbout, S., & Rochefort, L. (2021). Estimation of Daily Water Table Level with Bimonthly Measurements in Restored Ombrotrophic Peatland. *Sustainability*, *13* (10), 5474. https://doi.org/10.3390/su13105474

Habib, W., & Connolly, J. (2023). A national-scale assessment of land use change in peatlands between 1989 and 2020 using Landsat data and Google Earth Engine – a case study of Ireland. *Regional Environmental Change*, *23* (4), 124. https://doi.org/10.1007/s10113-023-02116-0

Hamner, B., & Frasco, M. (2018). *Metrics: Evaluation metrics for machine learning. R package version 0.1.4.* Retrieved from: https://CRAN.R-project.org/package=Metrics

Harris, A., & Bryant, R. G. (2009). A multi-scale remote sensing approach for monitoring northern peatland hydrology: Present possibilities and future challenges. *Journal of Environmental Management*, *90* (7), 2178–2188. https://doi.org/10.1016/j.jenvman.2007.06.025

Henriksen, H. J., Rasmusssen, P., Brandt, G., Bulow, D. von, & Jensen, F. V. (2007). Bayesian networks as a participatory modelling tool for groundwater protection. In A. Castellati & R. Soncini-Sessa (Eds.), *Topics on System Analysis and Integrated Water Resources Management* (pp. 49–72). Elsevier. https://doi.org/10.1016/B978-008044967-8/50003-8

Hikouei, I. S., Eshleman, K. N., Saharjo, B. H., Graham, L. L. B., Applegate, G., & Cochrane, M. A. (2023). Using machine learning algorithms to predict groundwater levels in Indonesian tropical peatlands. *Science of The Total Environment*, *857* (part 3), 159701. https://doi.org/10.1016/j.scitotenv.2022.159701

Hoyt, A. M., Chaussard, E., Seppalainen, S. S., & Harvey, C. F. (2020). Widespread subsidence and carbon emissions across Southeast Asian peatlands. *Nature Geoscience*, *13* (6), 435–440. https://doi.org/10.1038/s41561-020-0575-4

Hrysiewicz, A., Williamson, J., Evans, C. D., Jovani-Sancho, A. J., Callaghan, N., Lyons, J., White, J., Kowalska, J., Menichino, N., & Holohan, E. P. (2024). Estimation and validation of InSAR-derived surface displacements at temperate raised peatlands. *Remote Sensing of Environment*, *311*, 114232. https://doi.org/10.1016/j.rse.2024.114232

Irfan, M., Kurniawati, N., Ariani, M., Sulaiman, A., & Iskandar, I. (2020). Study of groundwater level and its correlation to soil moisture on peatlands in South Sumatra. *Journal of Physics: Conference Series*, *1568* (1), 012028. https://doi.org/10.1088/1742-6596/1568/1/012028

Jones, C. N., Evenson, G. R., McLaughlin, D. L., Vanderhoof, M. K., Lang, M. W., McCarty, G. W., Golden, H. E., Lane, C. R., & Alexander, L. C. (2018). Estimating restorable wetland water storage at landscape scales. *Hydrological Processes*, *32* (2), 305–313. https://doi.org/10.1002/hyp.11405

Joosten, H., & Clarke, D. (2002). *Wise use of mires and peatlands - background and principles including a framework for decision-making.* International Mire Conservation Group and International Peat Society.

Kameoka, T., Kozan, O., Hadi, S., Asnawi, & Hasrullah. (2021). Monitoring the groundwater level in tropical peatland through UAV mapping of soil surface temperature: a pilot study in Tanjung Leban, Indonesia. *Remote Sensing Letters*, *12* (6), 542–552. https://doi.org/10.1080/2150704X.2021.1906974

Kardel, I., Chormański, J., Mirosław-Świątek, D., Okruszko, T., Grygoruk, M., & Wassen, M. J. (2009). Decision support system for Biebrza National Park. In Ch. Jao (Eds.), *Hydroinformatics in Hydrology, Hydrogeology and Water Resources* (pp. 441–458). IAHS Publications.

Karimi, S., Hasselquist, E. M., Salimi, S., Järveoja, J., & Laudon, H. (2024). Rewetting impact on the hydrological function of a drained peatland in the boreal landscape. *Journal of Hydrology*, *641*, 131729. https://doi.org/10.1016/j.jhydrol.2024.131729

Kim, J. W., Lu, Z., Gutenberg, L., & Zhu, Z. (2017). Characterizing hydrologic changes of the Great Dismal Swamp using SAR/InSAR. *Remote Sensing of Environment*, *198*, 187–202. https://doi.org/10.1016/j.rse.2017.06.009

Koch, J., Elsgaard, L., Greve, M. H., Gyldenkærne, S., Hermansen, C., Levin, G., Wu, S., & Stisen, S. (2023). Water-table-driven greenhouse gas emission estimates guide peatland restoration at national scale. *Biogeosciences*, *20* (12), 2387–2403. https://doi.org/10.5194/bg-20-2387-2023

Kuhn, M. (2008). Building predictive models in *R* using the *caret* Package. *Journal of Statistical Software*, *28* (5). https://doi.org/10.18637/jss.v028.i05

Lees, K. J., Artz, R. R. E., Chandler, D., Aspinall, T., Boulton, C. A., Buxton, J., Cowie, N. R., & Lenton, T. M. (2021). Using remote sensing to assess peatland resilience by estimating soil surface moisture and drought recovery. *Science of The Total Environment*, *761*, 143312. https://doi.org/10.1016/j.scitotenv.2020.143312

Lees, K. J., Quaife, T., Artz, R. R. E., Khomik, M., & Clark, J. M. (2018). Potential for using remote sensing to estimate carbon fluxes across northern peatlands – A review. *Science of The Total Environment*, *615*, 857–874. https://doi.org/10.1016/j.scitotenv.2017.09.103

Liu, S., McGree, J., Ge, Z., & Xie, Y. (2016). Classification methods. In *Computational and Statistical Methods for Analysing Big Data with Applications* (pp. 7–28). Elsevier. https://doi.org/10.1016/B978-0-12-803732-4.00002-7

Liu, W., Fritz, C., van Belle, J., & Nonhebel, S. (2023). Production in peatlands: Comparing ecosystem services of different land use options following conventional farming. *Science of The Total Environment*, *875*, 162534. https://doi.org/10.1016/j.scitotenv.2023.162534

Ma, L., Zhu, G., Chen, B., Zhang, K., Niu, S., Wang, J., Ciais, P., & Zuo, H. (2022). A globally robust relationship between water table decline, subsidence rate, and carbon release from peatlands. *Communications Earth & Environment*, *3* (1), 254. https://doi.org/10.1038/s43247-022-00590-8

Marcot, B. G. (2012). Metrics for evaluating performance and uncertainty of Bayesian network models. *Ecological Modelling*, *230*, 50–62. https://doi.org/10.1016/j.ecolmodel.2012.01.013

Marcot, B. G., & Penman, T. D. (2019). Advances in Bayesian network modelling: Integration of modelling technologies. *Environmental Modelling & Software*, *111*, 386–393. https://doi.org/10.1016/j.envsoft.2018.09.016

Masegosa, A. R., Feelders, A. J., & Gaag, L. C. van der (2016). Learning from incomplete data in Bayesian networks with qualitative influences. *International Journal of Approximate Reasoning*, *69*, 18–34. https://doi.org/10.1016/j.ijar.2015.11.004

Millard, K., Thompson, D. K., Parisien, M.-A., & Richardson, M. (2018). Soil moisture monitoring in a temperate peatland using multi-sensor remote sensing and linear mixed effects. *Remote Sensing*, *10* (6), 903. https://doi.org/10.3390/rs10060903

Neapolitan, R. E. (2007). Learning Bayesian networks. *Proceedings of the 13th ACM SIGKDD International Conference on Knowledge Discovery and Data Mining*, *2007*, 1–1. https://doi.org/10.1145/1327942.1327961

Nielsen, C. K., Elsgaard, L., Jørgensen, U., & Lærke, P. E. (2023). Soil greenhouse gas emissions from drained and rewetted agricultural bare peat mesocosms are linked to geochemistry. *Science of The Total Environment*, *896*, 165083. https://doi.org/10.1016/j.scitotenv.2023.165083

Okruszko, H., & Byczkowski, A. (1996). Osuszanie mokradeł w Basenie Środkowym Biebrzy w ujęciu historycznym. *Zeszyty Problemowe Postępów Nauk Rolniczych*, *432*, 33–43.

Rao, M. B., & Rao, C. R. (2014). In M. B. Rao & C. R. Rao (Eds.), *Bayesian networks* (pp. 357–385). https://doi.org/10.1016/B978-0-444-63431-3.00010-3

Räsänen, A., Tolvanen, A., & Kareksela, S. (2022). Monitoring peatland water table depth with optical and radar satellite imagery. *International Journal of Applied Earth Observation and Geoinformation*, *112*, 102866. https://doi.org/10.1016/j.jag.2022.102866

R Core Team (2023). R: A language and environment for statistical computing. *R Foundation for Statistical Computing*. https://www.R-project.org/

Rohmer, J. (2020). Uncertainties in conditional probability tables of discrete Bayesian Belief Networks: A comprehensive review. *Engineering Applications of Artificial Intelligence*, *88*, 103384. https://doi.org/10.1016/j.engappai.2019.103384

Rositano, F., Piñeiro, G., Bert, F. E., & Ferraro, D. O. (2017). A comparison of two sensitivity analysis techniques based on four bayesian models representing ecosystem services provision in the Argentine Pampas. *Ecological Informatics*, *41*, 33–39. https://doi.org/10.1016/j.ecoinf.2017.07.005

Stachowicz, M., Venegas-Cordero, N., & Ghezelayagh, P. (in press). Two centuries of changes – revision of the hydrography of the Biebrza Valley, its transformation and probable ecohydrological challenges. *Ecohydrology & Hydrobiology*. https://doi.org/10.1016/j.ecohyd.2023.08.008

Tanneberger, F., Berghöfer, A., Brust, K., Hammerich, J., Holsten, B., Joosten, H., Michaelis, D., Moritz, F., Reichelt, F., Schäfer, A., Scheid, A., Trepel, M., Wahren, A., & Couwenberg, J. (2024). Quantifying ecosystem services of rewetted peatlands − the MoorFutures methodologies. *Ecological Indicators*, *163*, 112048. https://doi.org/10.1016/j.ecolind.2024.112048

Tiemeyer, B., Freibauer, A., Borraz, E. A., Augustin, J., Bechtold, M., Beetz, S., Beyer, C., Ebli, M., Eickenscheidt, T., Fiedler, S., Förster, C., Gensior, A., Giebels, M., Glatzel, S., Heinichen, J., Hoffmann, M., Höper, H., Jurasinski, G., Laggner, A., Leiber-Sauheitl, K., & Drösler, M. (2020). A new methodology for organic soils in national greenhouse gas inventories: Data synthesis, derivation and application. *Ecological Indicators*, *109*, 105838. https://doi.org/10.1016/j.ecolind.2019.105838

United Nations Environment Programme [UNEP]. (2022). *Global Peatlands Assessment – The State of the World's Peatlands: Evidence for action toward the conservation, restoration, and sustainable management of peatlands. Main Report. Global Peatlands Initiative.* United Nations Environment Programme.

Veci, L., Prats-Iraola, P., Scheiber, R., Collard, F., Fomferra, N., & Engdahl, M. (2014). The sentinel-1 toolbox. *IEEE International Geoscience and Remote Sensing Symposium (IGARSS)*, *2014*, 1–3.

Venegas-Cordero, N., Marcinkowski, P., Stachowicz, M., & Grygoruk, M. (in press). On the role of water balance as a prerequisite for aquatic and wetland ecosystems management: A case study of the Biebrza catchment, Poland. *Ecohydrology & Hydrobiology*. https://doi.org/10.1016/j.ecohyd.2024.08.001

Villaverde, A. F., Ross, J., Morán, F., & Banga, J. R. (2014). MIDER: Network Inference with Mutual Information Distance and Entropy Reduction. *PLoS ONE*, *9* (5), e96732. https://doi.org/10.1371/journal.pone.0096732

Villaverde, A. F., Ross, J., Morán, F., & Banga, J. R. (2014). MIDER: Network Inference with Mutual Information Distance and Entropy Reduction. PLoS ONE, 9 (5), e96732. https://doi.org/10.1371/journal.pone.0096732

Wickham, H. (2016). *ggplot2: Elegant Graphics for Data Analysis.* Springer International Publishing. https://doi.org/10.1371/journal.pone.0096732

Summary

Estimating mean groundwater levels in peatlands using a Bayesian belief network approach with remote sensing data. Large-scale management, protection, and restoration of wetlands require knowledge of their hydrology, i.e., the status and dynamics of the groundwater table, which determine the evolution of the wetland ecosystem, its conservation value, and possible economic use. Unfortunately, in many cases, hydrological monitoring data are unavailable, resulting in the search for a proxy for the average annual depth of the groundwater level (GWL). This study presents an approach to estimating the mean GWL in peatlands using a Bayesian belief network (BBN) model, leveraging long-term hydrological and remote sensing data in the Biebrza National Park in Poland. The remote sensing data employed includes the synthetic aperture radar (SAR) backscatter coefficient, peat subsidence, rate and distance to watercourses. The BBN model achieved a predictive accuracy of 83.3% and 73.1%, depending on the validation approach used. Among the remote sensing variables considered, the SAR backscatter coefficient was the most sensitive in predicting the GWL in the peatlands. However, the model presents multiple uncertainties resulting from limitations of the available remote sensing data, low variability of class combinations in the conditional probability table, and lack of upscaling to other regions performed. Despite these uncertainties, the developed BBN model remains a valuable next step in reaching the goal of efficient peatland monitoring and management.

Supplementary material – piezometers

TABLE 1. Piezometers within the Biebrza National Park used in the study

ID	Piezometer/Transect name	Start of measurement	End of measurement	Mean GWT [m]
1	–	2014	2022	0.001
2	–	2015	2022	−0.002
3	–	2014	2021	−0.004
4	–	2014	2021	−0.004
5	–	2015	2021	−0.003
6	–	2015	2021	−0.001
7	–	2015	2021	−0.004
8	–	2014	2021	−0.002
9	–	2015	2021	−0.001
10	–	2015	2021	−0.001
11	–	2017	2021	−0.001
12	–	2015	2021	−0.001
13	–	2011	2018	−0.001
14	Brzeziny Ciszewskie	1998	2022	−0.343
15	Brzeziny Ciszewskie	1998	2022	−0.320
16	Ciszewo	1994	2022	−0.351
17	Ciszewo	1994	2022	−0.267
18	Ciszewo	1994	2022	−0.380
19	Ciszewo	1994	2022	−0.247
20	Ciszewo	1994	2022	−0.314
21	Czerwone Bagno T	2008	2015	−0.062
22	Czerwone Bagno T	2008	2015	−0.039
23	Długa Luka	2009	2022	−0.023
24	Grobla Honczarowska	1998	2022	0.027
25	Grobla Honczarowska	1998	2022	0.089
26	Grobla Honczarowska	1998	2022	−0.010
27	Grzędy I	1996	2022	−0.385
28	Grzędy I	1996	2022	−0.498
29	Grzędy I	1996	2022	−0.363
30	Grzędy I	1996	2022	−0.381
31	Grzędy I	1996	2022	−0.330
32	Grzędy II	1996	2022	−0.514
33	Gugny	2009	2022	−0.123
34	Gugny	2009	2022	−0.095
35	Gugny II	2009	2022	−0.085
36	Gugny II	2009	2022	−0.125
37	Gugny II	2009	2022	−0.012
38	Jałowo	1998	2022	−0.302
39	Jałowo	1998	2022	−0.034
40	Kapice	2012	2021	−0.263
41	Kuligi	1994	2022	−0.314
42	Kuligi	1994	2022	−0.330
43	Kuligi	1994	2022	−0.369
44	Trójkąt I	1996	2022	−0.333
45	Trójkąt I	1996	2022	−0.338
46	Trójkąt I	1996	2022	−0.500
47	Trójkąt II	1996	2022	−0.275
48	Trójkąt II	1996	2022	−0.299
49	Trójkąt II	1996	2022	−0.304

Source: own work.

Scientific Review Engineering and Environmental Sciences (2024), 33 (4), 352–371

Sci. Rev. Eng. Env. Sci. (2024), 33 (4) https://srees.sggw.edu.pl

ISSN 1732-9353 (suspended) eISSN 2543-7496 DOI 10.22630/srees.9875

Received: 01.07.2024
Accepted: 22.10.2024

Muneer Ahmed RODENI[1]
Shahmir Ali KALHORO[1]
Altaf Hussain LAHORI[2]✉
Kashif Ali KUBAR[1]
Javed Ahmed MENGAL[3]
Khalid Hameed MENGAL[1]
Abdullah RAISANI[4]
Shabir AHMED[5]
Zain Ul Abidin KASI[6]
Siraj AHMED[6]
Bilal Ahmed ABABAKI[4]
Sher JAN[1]
Ghulam Haider ANGARIA[1]

[1] Lasbela University of Agriculture, Water, and Marine Sciences, Faculty of Agriculture, Department of Soil Science, Pakistan
[2] Sindh Madressatul Islam University, Department of Environmental Sciences, Pakistan
[3] Sindh Agriculture University Tando Jam, Faculty of Crop production, Department of Soil Science, Pakistan
[4] Agriculture Research Institute, Quetta, Pakistan
[5] Department of Agriculture Extension, Quetta, Pakistan
[6] Department of Forest and Wildlife, Quetta, Pakistan

Application of potassium co-amended with boron for improving the potassium, boron, growth and yield components of wheat under the dry climate condition of Lasbela Balochistan

Keywords: boron, potassium, wheat, biological yield, grain yield, dry climate

✉altaf@smiu.edu.pk

Introduction

Wheat (*Triticum aestivum* L.) is an important staple food crop of Pakistan and covers 8.79 million ha of the country with a total production of 25 million t (Panhwar et al., 2024). The national average yield of wheat is 2,639 kg·ha^{-1}, and this low yield of wheat may be due to biotic and abiotic factors, as well as imbalanced fertilization (Ali et al., 2019). The time of sowing and the planting density are significant and determine the proper establishment of the growing crop through balancing plant-to-plant competition and ultimately affecting the yield (Al-Ameri et al., 2019). Wheat is Pakistan's primary crop, accounting for 70% of Rabi's cropping area and 37% of the overall cropping area. Wheat is Pakistan's most important food grain, occupying the most land under cultivation and contributing 10.0% of value added agriculture and 2.1% of GDP, with rain-fed wheat accounting for 20% of Pakistan's land area. Balochistan agricultural output is approximately 871,300 t per year with about 382,940 ha under cultivation (Ali et al., 2019). Balochistan is Pakistan's largest but least populous province, challenged by water scarcity issues, meaning it is ecologically classified as a semi-arid to an arid desert zone (Ameer et al., 2023).

The goal of this research is to evaluate the effect of potassium and boron fertilizers that could improve the biological yield and grain yield of wheat. The goal is also to develop the optimum wheat genotype that can tolerate drought in the dry climate of Lasbela Balochistan.

Crops are often exposed to various types of stresses, including deficiencies during their lifetime due to the various roles of nutrients in plant cells, where their deficiency may lead to metabolic disorders. Micronutrient deficiency is widespread in many Asian countries due to the calcareous nature of the soils, high pH, low organic matter, salt stress, continuous drought, high bicarbonate content in irrigation water, and the imbalanced application of nitrogen-phosphorous--potassium (NPK) fertilizer (Narimani et al., 2010; Liza et al., 2021). Potassium is required for photosynthesis and plant metabolism (Wang et al., 2013; Cui et al., 2022). It is necessary for carbohydrate breakdown, which provides energy for plant development. Potassium also improves plant drought resilience and helps to reduce plant water loss (Hasanuzzaman et al., 2018; Rawat et al., 2022). Potassium assists in the conversion of nitrogen into proteins in plants, while grasses require potassium to counteract excessive nitrogen fertilizer rates. When potassium is deficient, some of the nitrogen remains as non-protein nitrogen. Potassium reacts strongly to any potassium applied to it. Some researchers have also observed the effects of using 40 kg·ha^{-1} boosted wheat and paddy yields by 21% and 35%, with significant studies having been undertaken in the North-West

Frontier Province to record the optimal amount of potash for wheat and rice, while diminutive research studies have been done on the percentage upturn in yield over control due to the direct residual and the reasons that cause potash in wheat (Hussan et al., 2022). Since any applied potassium is imprisoned in the clay lattice, and low potassium application rarely meets the soil, crops often fail to respond to the applied potassium, with production falling as the potash consumption rates drop. It does not become accessible to the plant when it is required or the plant is unable to rapidly absorb it through the soils to fulfill the potassium requirements. The limited reaction to the potassium foliar application to the soil of nitrogen and potassium sources was planned to determine how it affected the wheat crop (Hussan et al., 2022). Azeem et al. (2021) investigated the individual and combined effects of potassium nitrate at 4.5 $kg \cdot ha^{-1}$ and boron at 0.15 $kg \cdot ha^{-1}$ on the growth and yield of cotton under a salt stressed condition, where the combined application of potassium nitrate and boron showed the highest plant growth and productivity, even at higher salinities (12 $dS \cdot m^{-1}$). Ewais et al. (2022) assessed the impact of foliar application of boron and potassium amendments on the yield and quality of potatoes, and as a result the plant growth, yield and quality of potatoes were improved with the foliar application of boron and potassium. Madghash and Ali (2023) examined the potential of potassium humate and spraying with boron on the yield and its components of sesame crops, where the plant growth and yield was increased with the application potassium humate to the soil and spraying boron, under field conditions. Meena et al. (2024) applied potassium and boron at different application rates, related to the yield and economics of mustard greens (*Brassica juncea* L.), where as a result the plant growth and yield components of mustard crops were improved with the application of potassium at 40 $kg \cdot ha^{-1}$ and boron at 2 $kg \cdot ha^{-1}$, under field conditions.

To the best of our knowledge, the application of the sulfate of potash (SOP), muriate of potash (MOP), and boron, zarkhez plus (N 8%, P 23%, and K 18%), in the form of a solid and liquid/spray is a common practice in this area, but no attempt has been made to probe the co-application of potassium and boron on soil health, growth and yield under the arid climatic condition of Lasbela Balochistan. However, MOP is not good for the soils in Pakistan due to the presence of chloride--containing salt.

The present study aimed to examine the influence of the co-application of potassium and boron fertilizers at various stages of the growth and yield parameters of wheat under different doses, aiming to enhance plant height, leaf length, spike length, pedicel length, and the biological and grain yield parameters of wheat in the arid region of Lasbela Balochistan.

Material and methods

Study site description

The present study was conducted at the Lasbela University of Agriculture, Water, and Marine Sciences (LUAWMS) field experimental farm in Uthal (Fig. 1). This university commonly covers a coastal region of the district Lasbela Balochistan, is located 125 km away from Karachi and is widely known for the unique geographical surroundings of mountains and organic cotton cultivation, wheat, with a variety of vegetable cultivations, such as tomato, okra, etc. Winters are short, with dry and hot summers and an average annual rainfall of 169 mm.

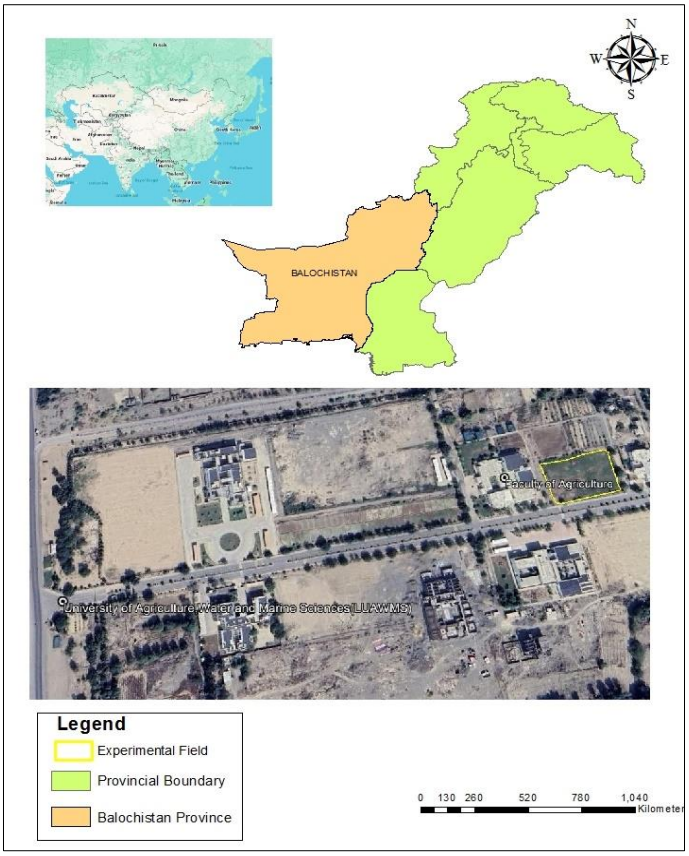

FIGURE 1. The geographical allocation of the field areas of the Lasbela University of Agriculture, Water, and Marine Sciences

Source: own work.

Rodeni, M. A., Kalhoro, S. A., Lahori, A. H., Kubar, K. A., Mengal, J. A., Mengal, K. H., Raisani, A., Ahmed, S., Kasi, Z. U. A., Ahmed, S., Ababaki, B. A., Jan, S., Angaria, G. H. (2024). Application of potassium co-amended with boron for improving the potassium, boron, growth and yield components of wheat under the dry climate condition of Lasbela Balochistan. *Sci. Rev. Eng. Env. Sci.*, *33* (4), 352–371. DOI 10.22630/srees.9875

Experimental design and crop management

The research study was conducted during 2020–2021 to estimate the effects of the combined applications of potassium and boron fertilizers on wheat growth and yield parameters. This study had the aim of comparing the outcomes of these applications with recommended applications of nitrogen and phosphorous, and to explore the potential for reducing the dependency on traditional nitrogen fertilizers. This is a widespread practice here in Pakistan, particularly in the study sites of Balochistan, where the local community only applies nitrogen and phosphorous fertilizers rather than other fertilizers that may be required.

The randomized complete block design (RCBD) using 6 × 5 m size plots was prepared, with triplicate application of both applications of fertilizers (potassium and boron) along with a control through the recommended doses of 70 kg·ha^{-1} and 120 kg·ha^{-1} of nitrogen and phosphorous fertilizers. The treatments were T_0 control, T_1 (70 kg·ha^{-1} and 0.6 kg·ha^{-1}, T_2 140 kg·ha^{-1} and 1.2 kg·ha^{-1}), T_3 (210 kg·ha^{-1} and 1.8 kg·ha^{-1}) of both the potassium and boron fertilizer applications respectively. The main purpose of this study was to estimate the effects of various treatments of both potassium and boron applications on wheat growth, yield parameters and co-related parameters of the soil physico-chemical properties which play a major role in the productivity of the crop. Before the sowing of seed, all physical and agronomical practices were carried out. This included the sowing of the TD1 100 kg·ha^{-1} wheat variety. Potassium was applied in two split doses, i.e. before the sowing of the seed and before the maturity of the plants. Boron was applied in three split doses, i.e. the time of sowing, the maturity of the plants, and the booting stage. All the agronomic observations were carried out in the required periods.

Data collection

The agronomic observations included plant height, leaf length, pedicel length, spike length, fresh and dry root biomass, thousand-grain weight (TWG), spike weight, and biological yield. Before harvesting at full maturity of the crop, five plants were selected randomly from each replication of the treatment of both fertilizer applications to estimate the effect of both fertilizers on vegetative growth, productivity, and the physiological characteristics of the wheat crop. The uniformly agronomic practices, such as hoeing, plant populations, irrigation, and plant protection measures for each treatment, were kept uniform and normal.

Soil sampling process and analysis

Before cultivation and after harvesting of the crop, separately from each plot, triplicate replication soil samples were collected, from the 0−10 cm and 10−20 cm soil depths, and finally composite samples were organized for the analysis of the soil basic properties. The collected soil samples were packed in well-labelled polyethylene bags and transported to the lab, all plant root material and stones were collected manually. Initially the soil samples were air-dried, and 2 mm sieved for further analysis. Soil extracts at a 1 : 2.5 ratio were prepared for the analysis of soil electrical conductivity (EC) [$dS \cdot m^{-1}$], pH, and organic matter content (SOM) [%], and were determined using a digital EC meter and pH meter, while the SOM was analyzed by wet oxidation (Walkley & Black, 1934), according to Jackson (2005). The available phosphorous and potassium were extracted by AB-DTPA (Soltanpour & Schwab, 1977) and the data was recorded using a spectrophotometer and flame photometer, according to Jackson (2005).

Statistical analysis

The collected data was subjected to a two-way analysis of variance (ANOVA) suggested by Gomes (1984). The mean of the three replicates of the treatments was calculated using MS Excel 2019. The least significant difference (LSD) test, at a 5% probability level, was achieved with the help of an IBM SPSS 20. The figures were organized by using a Sigma Plot 16 and OriginPro 21. The correlation matrix of the studied parameters was created using statistical tools for high-throughput data analysis.

Results

Soil basic properties

Before cultivation and after harvesting of the crop, a range of site soil samples were collected for the analysis of the basic soil properties, such as soil textural class, pH, EC [$dS \cdot m^{-1}$], SOM [%], available nitrogen [%], available phosphorous [$mg \cdot kg^{-1}$], available potassium [$mg \cdot kg^{-1}$] and boron. Table 1 and Figure 2 list the analysis results of the soil properties. Usually, there is no significant difference ($p < 0.05$) among the treatments before sowing, while after harvesting the results are significant ($p < 0.05$) due to the different applications of fertilization (Fig. 2). Maximum NPK and boron content were recorded in T_3 (0.068 ±0.0023%, 3.89 ±0.0153 $mg \cdot kg^{-1}$, 120 ±6.371 $mg \cdot kg^{-1}$, and 0.22 ±0.0121 $mg \cdot kg^{-1}$ respectively). In comparison to T_0

Rodeni, M. A., Kalhoro, S. A., Lahori, A. H., Kubar, K. A., Mengal, J. A., Mengal, K. H., Raisani, A., Ahmed, S., Kasi, Z. U. A., Ahmed, S., Ababaki, B. A., Jan, S., Angaria, G. H. (2024). Application of potassium co-amended with boron for improving the potassium, boron, growth and yield components of wheat under the dry climate condition of Lasbela Balochistan. *Sci. Rev. Eng. Env. Sci.*, *33* (4), 352–371. DOI 10.22630/srees.9875

TABLE 1. Soil basic characteristics before sowing seed

Parameter	Mean	*CV*	*LSD*	*p* value
Electrical conductivity [dS·m^{-1}]	0.49 ±0.02	5.74	0.02	0.47
pH	8.02 ±0.10	2.39	0.15	0.00
Organic matter [%]	0.29 ±0.04	3.18	5.10	0.02
Nitrogen [%]	0.07 ±0.01	1.14	5.95	0.00
Phosphorus [mg·kg^{-1}]	1.62 ±0.39	11.5	0.24	0.00
Potassium [mg·kg^{-1}]	87.6 ±4.12	0.57	0.39	0.00
Boron [mg·kg^{-1}]	0.16 ±0.01	6.17	0.02	0.00

The data for the soil basic properties before sowing of seed, soil EC, pH, organic matter, content of nitrogen, content of phosphorous, content of potassium and content of boron are presented in triplicate with the standard error (±), and the results do not differ significantly ($p < 0.05$).

Source: own work.

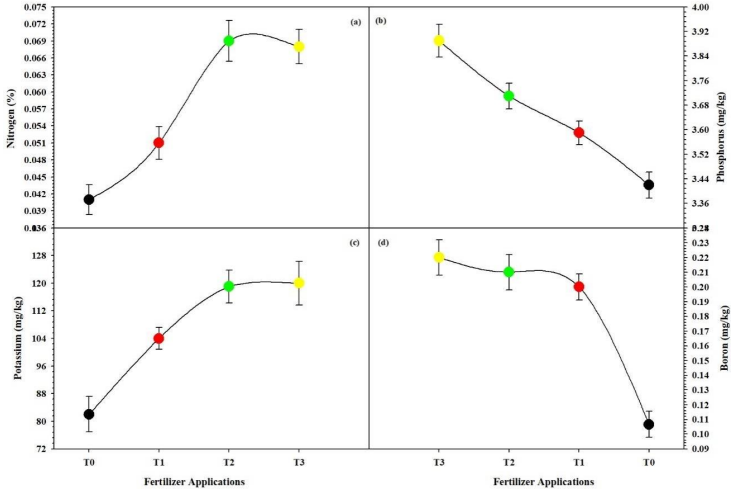

FIGURE 2. Triplicate means with the standard of nitrogen phosphorous and potassium in soil under different fertilizer applications and results are significantly different ($p \leq 0.05$)

Source: own work.

and T_1 (0.041 ±0.0103, 3.42 ±0.0265, 0.051 ±0.00323 and 3.59 ±0.0118), minor, non-significant differences ($p < 0.05$) were recorded in the nitrogen [%] and available phosphorous [mg·kg^{-1}], while the available potassium (82 ±5.131 mg·kg^{-1} and 104 ±3.214 mg·kg^{-1}) were significant ($p < 0.05$) – see Figure 2. Likewise, before sowing the results indicated that the soil was sandy loam in nature (sand 63.6%, silt 25.7%, and clay 10.7%), low to medium in alkaline, low to medium in SOM, adequate in exchangeable potassium, and low in both nitrogen and phosphorus nutrients.

Potassium and boron fertilization effect on growth parameters

The effect of both fertilization potassium and boron on the plant agronomic observations, i.e. plant height [cm], leaf length [cm], spike length [cm], and pedicel length [cm] were recorded 80−90 after sowing the seed, the analysis results demonstrating that there was significant differences ($p < 0.05$) among the different applications of both fertilizers (Fig. 2). The mean maximum data results of plant height [cm], leaf length [cm], spike length [cm], and pedicel length (cm) were recorded at T_3 (83.00 ±0.65, 11.77 ±0.08, 9.73 ±0.02, and 38.67 ±0.72) followed by T_2 (80.94 ±0.48, 11.51 ±0.152302, 9.65 ±0.023334 and 38.32 ±0.664809). Whereas mean minimum was recorded at T_0 (77.68 ±0.72, 10.32 ±0.21, 9.11 ±0.014 and 35.33 ±0.88) where no fertilizer was applied in either application of potassium or boron.

Moreover, spike length [cm], leaf length [cm], and pedicel length [cm] were the key factors for the wheat growth and yield, as such growth parameters play an important role in the formation of food through the process of photosynthesis, where wide and dense plant leaves prepare adequate amounts of food for growth of the plant. After 120 days from seed sowing, in a period known as wheat maturity, the effects of the foliar application of potassium and boron fertilizers under different levels were recorded. The analysis results showed that increasing the level of boron foliar application and potassium should improve the growth parameters of wheat (Fig. 3). The mean maximum was recorded for T_3 compared to the other treatments: T_0, T_1, and T_2, while the minimum was recorded at T_0 (Fig. 3). In the comparison of T_0, T_1, and T_3, significantly different ($p < 0.05$) amounts of the traits were recorded. However, in comparison to T_1 and T_2, the non-significant difference ($p < 0.05$) in the different amounts of treatment were also noted (Fig. 3).

Figure 4 shows that the application of potassium and boron effects the biological yield [kg·ha^{-1}] and grain yield [kg·ha^{-1}] of wheat. The mean maximum biological yield was observed in T_3 (19.186.7 ±10.9) compared to the other treatments: T_0, T_1, and T_2 (14.150 ±28.9, 17.161.7 ±31.13, 18.075 ±14.43) respectively, where 0 kg·ha^{-1}, 210 kg·ha^{-1} and 1.8 kg·ha^{-1} of potassium and boron fertilization were applied (Fig. 4). The mean minimum was recorded at T_1 (14.150 ±28.9). Overall the results are significant ($p < 0.05$) under the different applications of both fertilizers. Furthermore, the analysis results of the grain weight per spike and grain weight per TGW [kg·ha^{-1}] are presented in Figure 4, which show that the mean maximum was recorded for T_3 (3.00761 ±0.15); where the maximum application of both potassium and boron fertilizers were applied (210 kg·ha^{-1} and 1.8 kg·ha^{-1} respectively). The mean minimum was recorded for the control, T_0 (2.405 ±0.15),

Rodeni, M. A., Kalhoro, S. A., Lahori, A. H., Kubar, K. A., Mengal, J. A., Mengal, K. H., Raisani, A., Ahmed, S., Kasi, Z. U. A., Ahmed, S., Ababaki, B. A., Jan, S., Angaria, G. H. (2024). Application of potassium co-amended with boron for improving the potassium, boron, growth and yield components of wheat under the dry climate condition of Lasbela Balochistan. *Sci. Rev. Eng. Env. Sci.*, *33* (4), 352–371. DOI 10.22630/srees.9875

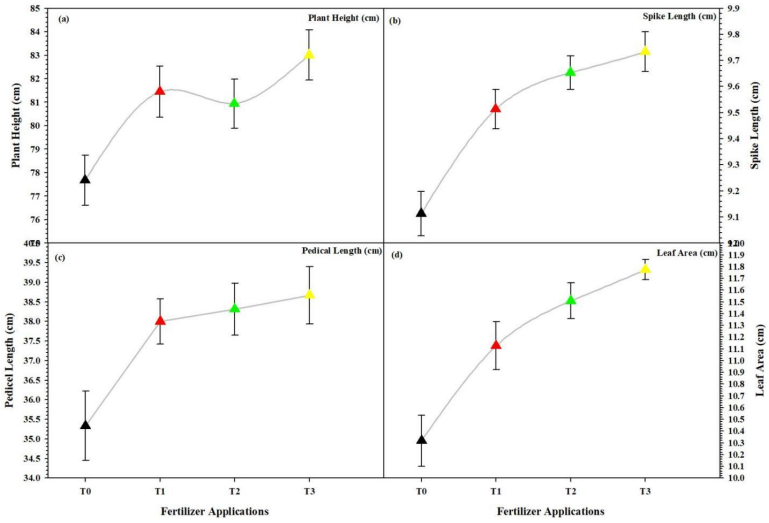

FIGURE 3. Triplicates mean that with the standard different plant growth characteristics (plant height [cm], spike length [cm], pedicel length [cm], and leaf area [cm]) under different applications of both fertilizers (potassium and boron) were significantly different ($p \leq 0.05$)

Source: own work.

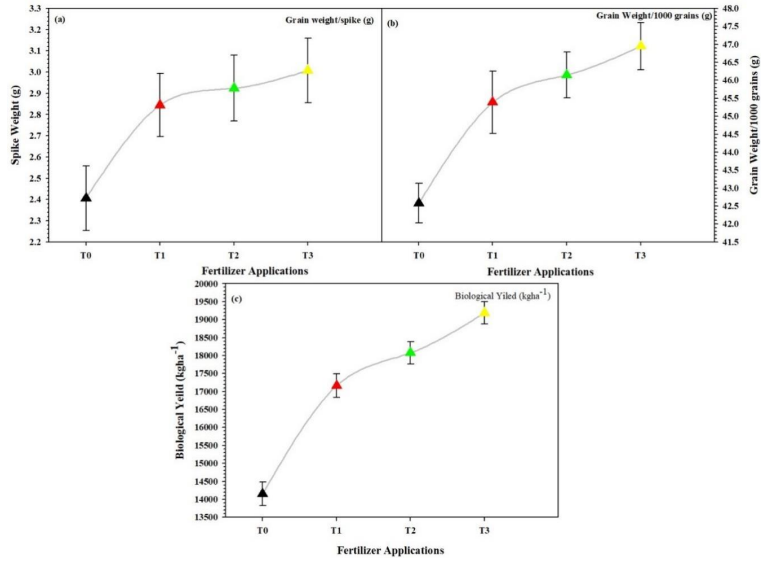

FIGURE 4. The triplicates mean that with the standard of different yield parameters: grain weight per spike weight [g], grain weight per thousand-grain weight [g], and biological yield [kg·ha^{-1}], the results are significant ($p \leq 0.05$) under different application of both fertilizers (potassium and boron)

Source: own work.

compared to the other treatments, T_0, T_1, and T_2 (2.84518 ±0.14, 2.92408 ±0.15 and 3.00761 ±0.15) respectively (Fig. 4). In comparison to T_2 and T_3, non-significant ($p < 0.05$) results were also recorded, although overall the results of grain weight per spike are significant under different applications of both fertilizers. Additionally, the analysis results of TGW showed that the mean maximum was recorded in T_3 (46.9487 ±0.65) compared to T_0, T_1, and T_2 (42.5787 ±0.55, 45.382 ±0.86 and 46.147 ±0.64) while the mean minimum was recorded in T_1 (42.5787 ±0.55). In a comparison between T_2 and T_3 (45.3892 ±0.86 and 46.1472 ±0.64), a non-significant ($p < 0.05$) difference was recorded; overall the results of biological yield [kg·ha^{-1}], grain weight per spike [g], and TGW are significant ($p < 0.05$) under different applications of both potassium and boron fertilizers (Fig. 4).

Nitrogen, phosphorous, potassium, and boron are up-taken by plants and affect the root biomass

Figure 5 presents the analysis results of nitrogen [%], available phosphorous [mg·kg^{-1}], available potassium [mg·kg^{-1}], and extractable boron [mg·kg^{-1}]. The results showed that the mean maximum of NPK content and extractable boron content were recorded for T_3 (1.642 ±0.0534, 0.5483 ±0.0164, 2.72 ±0.015 and 1.14 ±0.01) compared to other treatments, T_0, T_1, and T_2 respectively (Fig. 5), where the maximum application (210 kg·ha^{-1} and 1.8 kg·ha^{-1}) of potassium and boron fertilizers were applied (Fig. 5), with the mean minimum being recorded for control T_0 (1.173 ±0.044, 0.332 ±0.0029, 2.32 ±0.041 and 1.12 ±0.05).

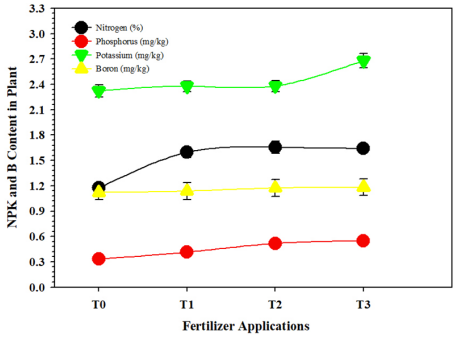

FIGURE 5. The triplicates mean that with the potassium and boron taken up by the plant under different applications of both fertilizers, the results are significantly different ($p \leq 0.05$) for the different applications of both fertilizers

Source: own work.

The treatments T_2 and T_3 (1.65 ±0.071, 1.64 ±0.053, 0.517 ±0.014, 0.548 ±0.016, 2.68 ±0.021, 2.72 ±0.015, 1.13 ±0.08, and 1.14 ±0.01) were non-significant ($p < 0.05$) under different applications of both fertilizers; whereas T_0 and T_3 (1.173 ±0.0442, 1.642 ±0.0534, 0.332 ±0.0029, 0.548 ±0.0164, 2.32 ±0.041, 2.72 ±0.015, 1.12 ±0.05 and 1.14 ±0.01) were significant ($p < 0.05$) under different applications of both fertilizers. Overall the results were significant ($p < 0.05$) under different applications of both fertilizers.

Fertilizer application effect on root biomass and soil organic content

The analysis results of the fresh and dry root biomass and soil organic matter results (Fig. 6) indicated that the mean maximum and significant ($p < 0.05$) results were recorded for both fresh and dry root biomass T_3 (6.932 g ±0.283) compared to all other treatments, T_0, T_1, T_2 and T_3 (4.616 g ±1.018, 5.357 g ±0.593, 5.0987 g ±0.7219 and 6.932 g ±0.283), whereas a minimum was recorded for the control, T_0 (4.616 g ±1.018).

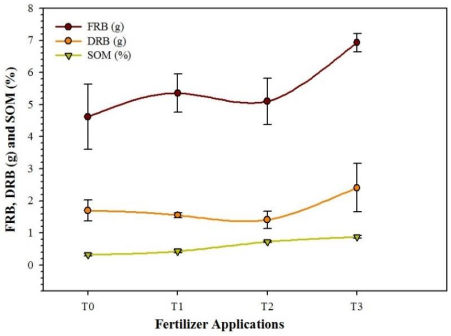

FIGURE 6. The triplicates mean that with the standard plant root biomass (fresh and dry) and under different applications of fertilizers, the results differ significantly ($p \leq 0.05$) under different applications of both fertilizers

Source: own work.

Moreover, in comparison to T_2 and T_3, a minor difference was also recorded although the results were non-significant ($p < 0.05$). The organic matter content in the soil increased 0.33–0.88% with T_4, in comparison to the control treatment.

Correlation matrix between soil properties, growth and yield parameters

As shown in Figure 7, the correlation matrix was performed for the soil properties, growth and yield parameters. The data revealed that the in-soil boron, grain weight, biological yield, leaf area and spike length were highly significant and correlated with the in-plant boron.

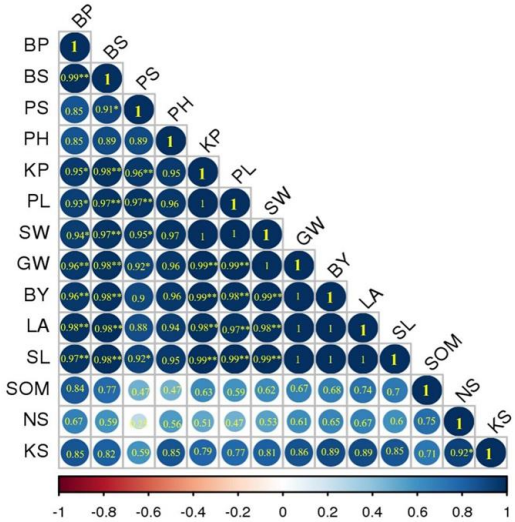

FIGURE 7. Correlation matrix among plant height (PH), pedicel length (PL), leaf area (LA), spike length (SL), biological yield (BY), spike weight (SW), grain weight (GW), in-plant potassium (KP), in-plant boron (BP), in-soil nitrogen (NS), in-soil phosphorus (PS), in-soil potassium (KS), in-soil boron (BS), and soil organic matter (SOM)

Source: own work.

Furthermore, the in-plant potassium, pedicel length and spike weight significantly correlated with the in-plant boron. It has been noted that in-soil phosphorus significantly correlated with the in-soil boron. Moreover, the in-plant potassium, pedicel length, spike weight, grain weight, biological yield, leaf area, and spike length were found to correlate highly significantly with the in-soil boron. The spike weight, grain weight and spike length positively correlated with the in-soil phosphorus. The grain weight, biological yield, leaf area and spike length were found to correlate highly significantly with the in-plant potassium and pedicel length. The biological yield, leaf area and spike length were found to be highly significantly associated with spike weight. The in-soil potassium positively correlated with the in-soil nitrogen.

Discussion

The present study was conducted to estimate the effect of the combined application of both potassium and boron fertilization on plant growth and the yield parameters of wheat. Our findings showed that increasing the levels of potassium fertilizer applications also increased the plant height, leaf length, spike length and pedicel length significantly ($p < 0.05$). Adequate amounts of potassium were also uptaken by the plant in comparison to the control, T_0 and T_1 (Fig. 5). Throughout the study, potassium and boron presented a noticeable impact on the different traits of wheat and increased the biological yield of wheat (Fig. 4), with similar findings also being recorded by Abbas et al. (2021), Mustafa et al., (2021) and Santos et al. (2021). The inadequate supply of nutrients and a dry environment commonly affect the growth of the plant at different stages, including the vegetative and grain and yield parameters, causing a 50% reduction in the production of the cultivated crops (Moghaddam et al., 2021; Wasaya et al., 2021; Pamungkas et al., 2022). The analysis results also showed that increasing the levels of potassium fertilizer applications should significantly increase plant height, leaf length, spike length and pedicel length ($p < 0.05$). Adequate amounts of potassium were also uptaken by the plant, as compared to the control, T_0 and T_1 (Fig. 5). Throughout this study, potassium and boron had a noticeable impact on the different traits of wheat and increased the biological yield of wheat (Fig. 4), with similar findings also recorded by Abbas et al. (2021), Mustafa et al. (2021) and Santos et al. (2021). Potassium enhances the fertility of soil, seed and fruit quality according to Brhane et al. (2017), and decreases the adverse effect of salinity in many fields of crop, including wheat (Rasool et al., 2008; Khan & Aziz, 2013; Al-Taher & Al-Naser, 2021). The observation of this research study concurred with Hossain et al. (2015), Rady and Mohamed (2018), and Hussan et al. (2022), through research on potassium in various wheat cultivars, where it was observed that increasing the level of potassium applications in wheat could enhance the growth and yield parameters.

Few studies (Ali et al., 2021; Akhtar et al., 2022) have reported that the combined application of both potassium and boron fertilizers enhanced the number of spikes per plant, TGW, and the biological yield and grain yield of wheat. Such findings may be due to an adequate supply of both of these mineral fertilizers. Likewise, the observation of this study also indicates that increased levels of potassium and boron fertilizers improve the number of spikes per plant, TGW, and the biological and grain yield of wheat. In comparison to the control, the findings of this study are significant in the TWG, biological yield, and grain yield (Fig. 4b and c). On the other hand, an adequate amount of boron fertilizer significantly affected

grain weight per spike since boron decreases infertility and helps the settlement of the grain seed of wheat (Akhtar et al., 2022). Ali et al. (2021) also recorded such a finding, indicating that different doses of boron fertilizer significantly increases the grain of rice and its yield attributes. The enhancement of the TWG of wheat may be due to the elevation of photosynthesis while the number of grains per spike was increased due to the nutrient-improved formation in the wheat plant.

Boron is an essential trace element for a variety of field, fruit, and vegetable crops, as it plays an important role in plant growth, including stability and the formation of the cell wall, the transformation of sugar and energy molecules to the different parts of the plant, and pollination seed settlement. A sufficient supply of boron is also important for nitrogen fixation in legume crops (Lima Filho & Malavolta, 1998). An adequate amount of boron application increases the boron concentration in the plant leaves and helps grain development (Rehman et al., 2018); an adequate supply of boron during entire growth stages could enhance the biological and grain yield of wheat grain (Günes & Alpaslan, 2000; Abou Seeda et al., 2021; Long & Peng, 2023). In-contrast, a boron deficiency results in low or empty pollen grains and a decreased number of flowers per plant (Vera-Maldonado et al., 2024). Likewise, the findings of this study indicated that an adequate supply of boron application could enhance the morphological characteristics of the wheat plant (Fig. 3). Furthermore, the uptake of phosphorous is also related to the up-take of boron, and, if boron is deficient, then the phosphate uptake may decrease with an untimely and significant effect on the biological and grain yield of wheat (Rasool et al., 2008; Zhao et al., 2020). Such results were also recorded in this study (Fig. 3), through the control with boron fertilization a significant difference was recorded. Enhancements in exchangeable potassium and available phosphorous and nitrogen in plants were also observed in the application of boron fertilization compared to the control (Fig. 5). These observations were also reported by Vera-Maldonado et al. (2024), who researched boron improvement in wheat bread and observed that an adequate supply of boron enhanced the NPK nutrients, and was also related to the up-take of phosphorous and potassium mineral nutrients in the soil rhizosphere (Al-Taher & Al-Naser, 2021; Vera-Maldonado et al., 2024). However, boron also assisted and adjusted the accessibility of other required nutrients from soil (Tariq & Mott, 2007). The hypothesis that boron and potassium in different fertilizer applications could improve the plant height, leaf length, number of spikes per plant, TGW, biological yield and grain yield of wheat (Fig. 3), with results being significantly different depending on the different applications of boron and potassium fertilization. The soil physical properties EC,

pH, and SOM did not have any significant effect on fertilization. However, total nitrogen, available phosphorous, and the available potassium were highly significant, with increased availability of the nitrogen, phosphorous, and potassium nutrients (Fig. 2) with increased applications of boron (Rawat et al., 2022). Root biomass and SOM increases in boron applications compared to the control since boric is a highly mobile nutrient in the soil (Robertson et al., 1981), and is easily up-taken by plant roots. Vera-Maldonado et al. (2024) reported that an adequate supply of boron improved the in-grain nitrogen content, co-related with protein, which may be due to the participation of boron in protein synthesis and nucleic acid metabolism (Robertson et al., 1981; Debnath & Ghosh, 2011; Ferdoush & Rahman, 2013; Ganie et al., 2014). Additionally, the positive and highly significant Pearson's co-relation ($p < 0.01$) among the different soil properties, growth, and yield parameters, such as plant height [cm], leaf length [cm], spike length [cm], pedicel length [cm], biological yield [kg·ha^{-1}], grain yield [kg·ha^{-1}], fresh root biomass, dry root biomass, and soil organic matter is indicated, in that the different application of both fertilizers, potassium and boron could, within split doses, improve the growth and yield of arid and semi-arid regions of the world and particularly the calcareous nature of Pakistan's soil. Likewise, findings were also recorded by Kalhoro et al. (2017), Kalhoro et al. (2018) and Kalhoro et al. (2019), that SOM and root biomass increased the activity of the micro-organisms directly affecting the soil properties and ultimately affecting the growth and yield parameters of the crop.

Conclusions

Based on the present study observations, a research study showed that both potassium and boron fertilizer applications have a significant effect on growth (plant height, pedicel length, leaf area, spike length, grain per spike, spike weight, grain weight, and biological yield) and the yield parameters of wheat. Potassium at a rate of 1.6 kg·ha^{-1} and boron at a rate of 220 kg·ha^{-1} of both fertilizations could enhance the growth and grain yield of wheat usually cultivated in hot and dry climatic conditions. However, studies are also required on diverse soil types and different land use systems with variable climatic conditions. Future studies should focus on the application of potassium and boron co-applied with biochar/modified biochar, nano-material, press mud compost, etc., to improve low fertile soil for sustainable agriculture.

Acknowledgments

The present study was conducted in the LUAWMS research experimental field Uthal. The authors thank LUAWMS fully for the use of the Department of Soil Science field and lab used to complete the research work.

References

Abbas, M., Abdel-Lattif, H., & Shahba, M. (2021). Ameliorative effects of calcium sprays on yield and grain nutritional composition of maize (*Zea mays* L.) cultivars under drought stress. *Agriculture*, *11* (4), 285. https://doi.org/10.3390/agriculture11040285

Abou Seeda, M. A., Abou El-Nour, E. A. A., Yassen, A. A., & Hammad, S. A. (2021). Boron, structure, functions, and its interaction with nutrients in plant physiology. A review. *Middle East Journal of Agriculture Research*, *10* (01), 117–179.

Akhtar, N., Ilyas, N., Arshad, M., Meraj, T. A., Hefft, D. I., Jan B. L., & Ahmad, P. (2022). The impact of calcium, potassium, and boron application on the growth and yield characteristics of durum wheat under drought conditions. *Agronomy*, *12* (8), 1917. https://doi.org/10.3390/agronomy12081917

Al-Ameri, B. H., Al-Saedi, S. A., & Razaq, I. B. (2019). Effect of Boron supplement on yield of wheat grown in calcareous soils of different textural classes under arid conditions. *Journal of Agricultural Science (Toronto)*, *11* (1), 112–117. https://doi.org/10.5539/jas.v11n1p112

Ali, A., Tariq, M., Rashid, M., Kalhoro, S. A., Maqbool, M., Ahmed, M., Narejo, M. N., & Marri, F. A. (2019). Fortified fertilizer application in wheat (*Triticum aestivum* L.) grown under water stress condition. *Pure and Applied Biology (PAB)*, 8 (1), 960–967. http://dx.doi.org/10.19045/bspab.2019.80037

Ali, S., Shah, S., & Arif, M. (2021). Agronomic biofortification with zinc and iron for the improvement of wheat phenology and yield. *Sarhad Journal of Agriculture*, *37* (3), 901–914. https://dx.doi.org/10.17582/journal.sja/2021/37.3.901.914

Al-Taher, F.M., & Al-Naser, H.H. (2021). The effect of different levels of potassium on the productivity of genotypes of wheat *Triticum aestivum* L. *IOP Conference Series: Earth and Environmental Science*, *923* (1), 012061. https://doi.org/10.1088/1755-1315/923/1/012061

Ameer, I., Kubar, K.A., Ali, Q., Ali, S., Khan, T., Shahzad, K., Riaz, M., Shah, Z. U. H., Rajpar, I., Ahmed, M., & Talpur, K. H. (2023). Land degradation resistance potential of a dry, semiarid region in relation to soil organic carbon stocks, carbon management index, and soil aggregate stability. *Land Degradation & Development*, *34* (3), 624–636. https://doi.org/10.1002/ldr.4480

Azeem, M., Shoujun, Y., Qasim, M., Abbasi, M. W., Ahmed, N., Hanif, T., Adnan, M. Y., Ahmad, R., & Dong, R. (2021). Foliar enrichment of potassium and boron overcomes salinity barriers to improve growth and yield potential of cotton (*Gossypium hirsutum* L.). *Journal of Plant Nutrition*, *44* (3), 438–454. https://doi.org/10.1080/01904167.2020.1845365

Brhane, H., Mamo, T., & Teka, K. (2017). Potassium fertilization and its level on wheat (*Triticum aestivum*) yield in shallow depth soils of Northern Ethiopia. *Journal of Fertilizers and Pesticides*, 8 (02), 8–10. https://doi.org/10.4172/2471-2728.1000182

Cui, M. H., Chen, X. Y., Yin, F. X., Xia, G. M., Yi, Y., Zhang, Y. B., Liu, S. W., & Li, F. (2022). Hybridization affects the structure and function of root microbiome by altering gene expression in roots of wheat introgression line under saline-alkali stress. *Science of The Total Environment*, *835*, 155467. https://doi.org/10.1016/j.scitotenv.2022.155467

Debnath, P., & Ghosh, S. K. (2011). Determination of critical limit of available boron for rice in terai zone soils of West Bengal. *Journal of the Indian Society of Soil Science*, *59* (1), 82–86.

Ewais, M. A., Abd El-Rahman, L. A., & Sayed, D. A. (2020). Effect of foliar application of boron and potassium sources on yield and quality of potato (*Solanum tuberosum* L.). *Middle East Journal of Applied Sciences*, *10* (1), 120–137. https://doi.org/10.36632/mejas/2020.10.1.15

Ferdoush, J. N., & Rahman, M. M. (2013). Effects of boron fertilization and sowing date on the grain protein content of wheat varieties. *Journal of Environmental Science and Natural Resources*, *6* (1), 41–45.

Gomes, M. I. (1984). Penultimate limiting forms in extreme value theory. *Annals of the Institute of Statistical Mathematics*, *36* (1), 71–85.

Günes, A., & Alpaslan, M. (2000). Boron uptake and toxicity in maize genotypes in relation to boron and phosphorus supply. *Journal of Plant Nutrition*, *23* (4), 541–550. https://doi.org/10.1080/01904160009382038

Hasanuzzaman, M., Bhuyan, M. B., Nahar, K., Hossain, M. S., Mahmud, J. A., Hossen, M. S., Masud, A. A. C., Moumita, & Fujita, M. (2018). Potassium: a vital regulator of plant responses and tolerance to abiotic stresses. *Agronomy*, 8 (3), 31. https://doi.org/10.3390/agronomy8030031

Hossain, A., Silva J. A. T. da, & Bodruzzaman, M. (2015). Rate and application methods of potassium in light soil for irrigated spring wheat. *Songklanakarin Journal of Science & Technology*, *37* (6), 635–642.

Hussan, M. U., Saleem, M. F., Hafeez, M. B., Khan, S., Hussain S., Ahmad, N., Ramzan, Y., & Nadeem, M. (2022). Impact of soil-applied humic acid, zinc and boron supplementation on the growth, yield and zinc translocation in wheat. *Asian Journal of Agriculture and Biology*, *1*, 1–8. https://doi.org/10.35495/ajab.2021.02

Jackson, M. L. (2005). *Soil chemical analysis. Advanced course: a manual of methods useful for instruction and research in soil chemistry, physical chemistry of soils, soil fertility, and soil genesis.* UW-Madison Libraries Parallel Press.

Kalhoro, S. A., Ding, K., Zhang, B., Chen, W., Hua, R., Shar, A. H., & Xu, X. (2019). Soil infiltration rate of forestland and grassland over different vegetation restoration periods at Loess Plateau in northern hilly areas of China. *Landscape and Ecological Engineering*, *15*, 91–99. https://doi.org/10.1007/s11355-018-0363-0

Kalhoro, S. A., Xu, X., Chen, W., Hua, R., Raza, S., & Ding, K. (2017). Effects of different land-use systems on soil aggregates: a case study of the Loess Plateau (Northern China). *Sustainability*, *9* (8), 1349. https://doi.org/10.3390/su9081349

Kalhoro, S. A., Xu, X., Ding, K., Chen, W., Shar, A. G., & Rashid, M. (2018). The effects of different land uses on soil hydraulic properties in the Loess Plateau, Northern China. *Land Degradation & Development*, *29* (11), 3907–3916. https://doi.org/10.1002/ldr.3138

Khan, A., & Aziz, M. (2013). Influence of foliar application of potassium on wheat (*Triticum aestivum* L.) under saline conditions. *Science Technology Division*, *32* (4), 285–289.

Lima Filho, O. F. de, & Malavolta, E. (1998). Evaluation of extraction procedures on determination of critical soil and foliar level of boron and zinc in coffee plants. *Communications in Soil Science and Plant Analysis*, *29* (7–8), 825–833. https://doi.org/10.1080/00103629809369988

Liza, M. M., Barman, A., Shome, S., & Rahman, M. E. (2021). Influence of coupled application of potassium and boron on growth and yield of late sown mungbean. *World Journal of Advanced Research and Reviews*, *11* (1), 256–264.

Long, Y., & Peng, J. (2023). Interaction between boron and other elements in plants. *Genes*, *14* (1), 130. https://doi.org/10.3390/genes14010130

Madghash, M. R., & Ali, O. N. (2023). Effect of potassium humate and spraying with boron on the yield and its components of sesame crop. *IOP Conference Series: Earth and Environmental Science*, *1225* (1), 012067. https://doi.org/10.1088/1755-1315/1225/1/012067

Meena, N., Sanathkumar, M., Nain, A., & Jat, S. (2024). Effect of potassium and boron on yield and economics of mustard (*Brassica juncea* L.). *International Journal of Advanced Biochemistry Research*, *8* (7), 1096–1099. https://doi.org/10.33545/26174693.2024.v8.i7n.1671

Moghaddam, M. S. H., Safaie, N., Soltani, J., & Hagh-Doust, N. (2021). Desert-adapted fungal endophytes induce salinity and drought stress resistance in model crops. *Plant Physiology and Biochemistry*, *160*, 225–238. https://doi.org/10.1016/j.plaphy.2021.01.022

Mustafa, H., Ilyas, N., Akhtar, N., Raja, N. I., Zainab, T., Shah T., Ahmad, A., & Ahmad, P. (2021). Biosynthesis and characterization of titanium dioxide nanoparticles and its effects along with calcium phosphate on physicochemical attributes of wheat under drought stress. *Ecotoxicology and Environmental Safety*, *223*, 112519. https://doi.org/10.1016/j.ecoenv.2021.112519

Narimani, H., Rahimi, M. M., Ahmadikhah A., & Vaezi, B. (2010). Study on the effects of foliar spray of micronutrient on yield and yield components of durum wheat. *Archives of Applied Science*, *2* (6), 168–176.

Pamungkas, S. S. T., Suwarto, Suprayogi, & Farid, N. (2022). Drought stress: responses and mechanism in plants. *Reviews in Agricultural Science*, *10*, 168–185. https://doi.org/10.7831/ras.10.0_168

Panhwar, N. A., Ahmed, S. R., Lahori, A. H., Mierzwa-Hersztek, M., Afzal, A., Vambol, V., Memon, A. H., Panhwar, S. A., Tunio, M., Buriro, S. A., & Vambol, S. (2024). Statistical analysis of association, heterosis, and inheritance of grain yield contributing quantitative traits in segregating lines of wheat (*Triticum aestivum* L.). *Journal of Environmental Accounting and Management*, *12* (01), 13–26. https://doi.org/10.5890/JEAM.2024.03.002

Rady, M. M., & Mohamed, G. F. (2018). Improving salt tolerance in *Triticum aestivum* (L.) plants irrigated with saline water by exogenously applied proline or potassium. *Advances in Plants & Agriculture Research*, 8 (2), 193–199. https://doi.org/10.15406/apar.2018.08.00312

Rasool, R., Kukal, S. S., & Hira, G. S. (2008). Soil organic carbon and physical properties as affected by long-term application of FYM and inorganic fertilizers in maize-wheat system. *Soil and Tillage Research*, *101*, 31–36. https://doi.org/10.1016/j.still.2008.05.015

Rawat, J., Pandey, N., & Saxena, J. (2022). Role of potassium in plant photosynthesis, transport, growth and yield. In N. Iqbal & S. Umar (Eds.), *Role of potassium in abiotic stress* (pp. 1–14). Springer. https://doi.org/10.1007/978-981-16-4461-0_1

Rehman, A. U., Farooq, M., Rashid, A., Nadeem, F., Stuerz, S., Asch, F., Bell, R. W., & Siddique, K. H. M. (2018). Boron nutrition of rice in different production systems. A review. *Agronomy for Sustainable Development*, *38* (3), 1–14. https://doi.org/10.1007/s13593-018-0504-8

Robertson, L. S., Lucas, R. E., & Christenson, D. R. (1981). *Boron: an essential plant micronutrient*. Cooperative Extension Bulletin.

Santos, E. F., Mateus, N. S., Rosário, M. O., Garcez, T. B., Mazzafera P., & Lavres, J. (2021). Enhancing potassium content in leaves and stems improves drought tolerance of eucalyptus clones. *Physiologia Plantarum*, *172* (2), 552–563. https://doi.org/10.1111/ppl.13228

Soltanpour, P. N., & Schwab, A. P. (1977). A new soil test for simultaneous extraction of macro-micro nutrients in alkaline soils. *Communications in Soil Science and Plant Analysis*, *8* (3), 195–207. https://doi.org/10.1080/00103627709366714

Tariq, M., & Mott, C. J. B. (2007). Effect of boron on the behavior of nutrients in soil-plant systems-a review. *Asian Journal of Plant Sciences*, *6* (1) 195–202.

Vera-Maldonado, P., Aquea, F., Reyes-Díaz, M., Cárcamo-Fincheira, P., Soto-Cerda, B., Nunes-Nesi, A., & Inostroza-Blancheteau, C. (2024). Role of boron and its interaction with other elements in plants. *Frontiers in Plant Science*, *15*, 1332459. https://doi.org/10.3389/fpls.2024.1332459

Walkley, A. & Black, I. A. (1934). An examination of the Degtjareff method for determining soil organic matter, and a proposed modification of the chromic acid titration method. *Soil Science*, *37* (1), 29–38.

Wang, M., Zheng, Q., Shen, Q., & Guo, S. (2013). The critical role of potassium in plant stress response. *International Journal of Molecular Sciences*, *14* (4), 7370–7390. https://doi.org/10.3390/ijms14047370

Wasaya, A., Abbas, T., Yasir, T. A., Sarwar, N., Aziz, A., Javaid, M. M., & Akram, S. (2021). Mitigating drought stress in sunflower (*Helianthus annuus* L.) through exogenous application of β-aminobutyric acid. *Journal of Soil Science and Plant Nutrition*, *21*, 936–948. https://doi.org/10.1007/s42729-021-00412-4

Zhao, Z., Wang, S., White, P. J., Wang, Y., Shi, L., & Xu, F. (2020). Boron and phosphorus act synergistically to modulate absorption and distribution of phosphorus and growth of *Brassica napus*. *Journal of Agricultural and Food Chemistry*, *68* (30), 7830–7838. https://doi.org/10.1021/acs.jafc.0c02522

Summary

Application of potassium co-amended with boron for improving the potassium, boron, growth and yield components of wheat under the dry climate condition of Lasbela Balochistan. A field experiment was performed to assess the impact of potassium co-amended with boron at different application rates on organic matter, nitrogen, phosphorus, potassium and boron in the soil, also in terms of plant height, spike length, pedicel length, leaf area, spike weight, grain weight, biological yield, fresh biomass and dry biomass of wheat under the dry climate of Uthal. Randomized complete block design (RCBD) was used with the combined application of both K and B fertilizers with a replicate of three times, treatments were T_0 control, T_1 70 K kg·ha^{-1} and 0.6 B kg·ha^{-1}, T_2 140 K and 1.2 B kg·ha^{-1}, T_3 210 K and 1.8 B kg·ha^{-1} of potassium and boron respectively. Furthermore, boron was applied in three split doses (time of sowing, maturity of plant, and booting stage); whereas potassium was used in two split doses (before sowing and maturity). The obtained results demonstrated that plant height was increased, ranging from 77.68 to 83.00 cm, with T_3, biological yield 14,150.0–19,186.67 kg·ha^{-1} with T_3, in-soil N 0.04–0.069% with T_3, in-soil P 3.42–3.89 mg·kg^{-1} with T_3, in-soil K 82.00–120.00 mg·kg^{-1} with T_3, in-soil B 0.11–0.22 mg·kg^{-1} with T_3 than control treatment. The uptake NPK, and B by the wheat plant was increased, ranging from 1.17–1.66% with T_3, 0.33–0.54 mg·kg^{-1} with T_3, 2.32–2.72 mg·kg^{-1} with T_3, and 1.12–1.14 mg·kg^{-1} with T_3 as compared with the control treatment. The plant fresh and dry biomasses and soil organic matter were increased at T_3 over that of the control soil. Overall, the findings of this study indicated that the co-application of potassium and boron at 210 and 1.8 kg·ha^{-1} doses can be successfully used to enhance grain and yield parameters of wheat, particularly those cultivated in dry climatic conditions.

Scientific Review Engineering and Environmental Sciences (2024), 33 (4), 372–387

Sci. Rev. Eng. Env. Sci. (2024), 33 (4) https://srees.sggw.edu.pl

ISSN 1732-9353 (suspended) eISSN 2543-7496 DOI 10.22630/srees.9917

Received: 18.06.2024
Accepted: 10.09.2024

Hary Yanto FENDI✉

Sebelas Maret University, Faculty of Vocational School, Indonesia
Sebelas Maret University, Appropriate Structure Research Group, Associate's Degree Program in Civil Engineering, Indonesia
Sebelas Maret University, Disaster Research Center, Indonesia

The impact of utilizing red brick powder and plastic pellets as fine particles on the compressive strength and absorption of water in paving blocks

Keywords: compressive strength, paving block, plastic pellets, red brick powder, water absorption

Introduction

Indonesia, a nation with significant potential across various sectors, is on the cusp of a civil engineering revolution, particularly in the development of physical infrastructure. The emergence of numerous innovations – especially in using alternative materials for paved roads – is a testament to this promising future. The potential of this research to contribute to these innovations and the development of physical infrastructure in Indonesia is engaging and exciting (Junkes et al., 2024).

Concrete bricks, commonly called paving blocks, are a construction material that offers more than meets the eye. These blocks represent a marvel of engineering as they are composed of a unique blend of water, aggregate, and portland cement

✉fendi@staff.uns.ac.id

or similar hydraulic adhesive, with or without additional components (National Standardization Agency [NSA], 1996). Renowned for their ability to withstand heavy loads and ease of maintenance, paving blocks are used for road surfaces, sidewalks, parks, and parking areas, showcasing their versatility and superiority within civil engineering and leaving a lasting impression.

Every day, our environment is burdened by various types of waste, including plastic. In Indonesia, the issue of plastic waste has reached alarming proportions, posing a severe threat to the environment and public health. However, the community's endeavors to combat this issue through the replacement, reduction and refinement principle (called the 3R approach), are inspiring and crucial. The 3R approach is significant as it can substantially mitigate the negative impact of plastic waste, fostering hope for a cleaner and healthier future (Garcia et al., 2024).

Research conducted by university academics has centered on discovering innovative ways to repurpose plastic waste for utilization in construction. For instance, plastic waste has been investigated for enhancing soil properties, road pavement, concrete, and paving blocks. Muzaidi et al. discovered that incorporating 3% of 10 × 10 mm and 10 × 5 mm plastic waste fragments improved the soil's compressive strength and shear-strength angle (Muzaidi et al., 2022). Handayasari demonstrated that substituting 5% sand with mineral water packaging waste increased concrete compressive strength to 22.741 MPa (Handayasari, 2017). Awoyera and Adesina (2020), and Wendimu et al. (2021) concluded that low-density polyethylene (LDPE) enhanced the compressive strength of bricks compared to clay. Arulrajah et al. (2017) used various types of plastic waste, such as linear low-density polyethylene filled with calcium carbonate (LDCAL), high-density polyethylene (HDPE), and LDPE for road pavement. Khatib et al. (2019) found that replacing coarse aggregate with bottle cap waste did not significantly reduce the flexural strength of concrete blocks. Gour et al. (2022) and Gopinath et al. (2023) suggested substituting aggregate with polypropylene (PP) waste in concrete, which could be used for brickwork, partitions, panels, and canal linings. Iduwin et al. (2023) and Ahmad et al. (2023) showed that using PP for aggregate substitution slightly increased the compressive strength of bricks.

Saxena et al. (2020) and Guo et al. (2024) observed that the compressive strength, flexural strength, and elastic modulus of concrete decreased with increased plastic waste percentage, but abrasion resistance increased. Dadzie et al. (2020) and Haigh (2024) demonstrated that using plastic bottles for walls helped maintain room temperature and reduce energy costs. Soni et al. (2022), Tempa et al. (2022), and Kakerissa and Latuheru (2023) used PP plastic waste mixed with gravel to manufacture paving blocks. They found that a composition of 70% plastic waste and

Fendi, H. Y. (2024). The impact of utilizing red brick powder and plastic pellets as fine particles on the compressive strength and absorption of water in paving blocks. *Sci. Rev. Eng. Env. Sci.*, *33* (4), 372–387. DOI 10.22630/srees.9917

30% sand produced D-quality paving blocks recommended for mass production due to their significant waste utilization (Widiyono et al., 2024). Krasna et al. (2019) stated that replacing 40% of sand with plastic increased the compressive strength of paving by 30%. There was a decrease in the compressive strength of the red brick in the sample with the percentage of addition of 10% and 15% (Candra et al., 2022; Paikun et al., 2023; Umar & Mustafa, 2023; Dary et al., 2024).

From the description above, this final assignment is interested in testing paving blocks with the innovative use of red brick powder and waste polypropylene plastic with processing to become plastic pellets, which is a key component in the research. The plastic pellet, when used in variations of 10%, 15%, 25%, and 25% red brick powder, is expected to reduce water absorption. The red brick powder, with pozzolanic characteristics, can unite aggregate in making paving blocks to produce suitable products, according to Indonesian standard SNI 03-0691-1996 (NSA, 1996).

Material and methods

According to SNI 03-0691-1996 (NSA, 1996), paving blocks are made of a mixture of portland cement (or similar hydraulic adhesives), water, and aggregates, with or without other additives. Four quality categories are used to group this mixture: Quality A for roads, Quality B for parking lots, Quality C for pedestrian facilities, and Quality D for parks and other uses. Table 1 shows the values of the physical properties of each quality.

TABLE 1. Physical properties of paving blocks

Quality	Size [mm]	Compressive strength [MPa]		Wear resistance [mm·min^{-1}]		Maximum average water absorption [%]
		AVG	min	AVG	min	
A	210 × 105 × 50	40.0	35.0	0.090	0.103	3
B	210 × 105 × 50	20.0	17.0	0.130	0.149	6
C	210 × 105 × 50	15.0	12.5	0.160	0.184	8
D	210 × 105 × 50	10.0	8.5	0.219	0.251	10

Source: own work.

The plastic used in processing processes to become plastic pellets was sourced from Cv. Hraltara in Buran, Tasikmadu District, Karanganyar Regency, as shown in Figure 1. The material added to the aggregate was red brick waste in a fine powder form and was obtained from homes of researchers in Ngawi City and Kos Sebastian 2 Jebres District, Surakarta.

FIGURE 1. Plastic pellets
Source: own work.

The research methodology used in this study follows a flowchart, as depicted in Figure 2. The entire research includes four main stages, which were carried out according to the following procedure:

1. Material testing (aggregate analysis):
   - Aggregate analysis:
     - Sieve analysis was conducted to determine the particle size distribution.
     - Specific gravity testing was performed to measure the density of the aggregates.
     - Absorption testing was carried out to assess the water absorption capacity of the aggregates.
     - Mud content testing was implemented to evaluate the amount of fine particles in the aggregates.
2. Specimen preparation:
   - Paving block specimens were fabricated using a cement-to-sand ratio of 1 : 4.
   - Various formulations were tested with different proportions of plastic pellets and red brick powder (10%, 15%, and 25% plastic pellets, and 25% red brick powder).
3. Specimen testing:
   - Compressive strength evaluation: Specimens were subjected to compressive strength testing for 28 days.
   - Water absorption measurement: Specimens were immersed in water for 24 h, and their water absorption was measured.

Fendi, H. Y. (2024). The impact of utilizing red brick powder and plastic pellets as fine particles on the compressive strength and absorption of water in paving blocks. *Sci. Rev. Eng. Env. Sci.*, *33* (4), 372–387. DOI 10.22630/srees.9917

4. Data analysis and discussion:
   – The test results were analyzed to evaluate the influence of plastic pellets and red brick powder on the paving blocks' compressive strength and water absorption.
   – The findings were compared against the requirements outlined in SNI 03-0691-1996.

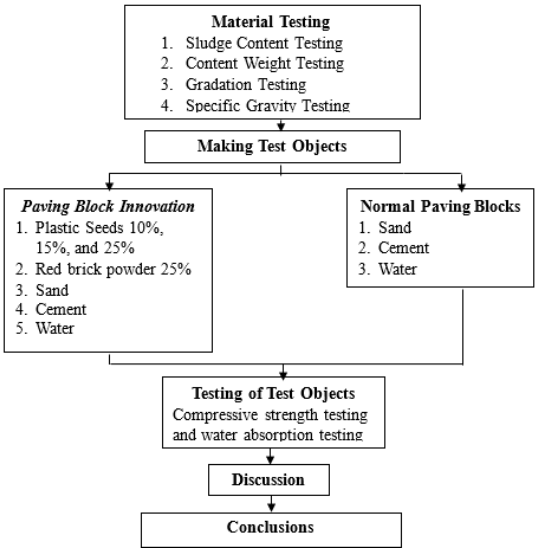

FIGURE 2. The flowchart of the research methodology
Source: own work.

The preparation of concrete paving block materials was checked according to material standards, which involve a series of tests and evaluations to ensure the materials meet the required quality and specifications. Aggregate testing was completed using sieve, absorption, density, and mud content analysis.

The research uses plastic pellets in variations of 10%, 15%, and 25%, and 25% red brick powder. Test specimens are made with a mixture using a cement-to-sand ratio of 1 : 4. Some essential equipment used are compressive strength testing machines with an accuracy of 1 kN, as well as dial gauges. The test specimen was made with dimensions of 21 × 10.5 × 5 cm. After the test specimen hardens, it is cut with a cutting tool from the initial size to a size of 5 × 5 × 5 cm. Testing the robustness and compressive strength of block paving is carried out over 28 days. It is intended to influence the usage of plastic pellets and red brick powder to improve compressive strength, absorb water, and make cost-effective paving blocks.

Results and discussion

Table 2 presents the overall content weight of the components in the paving block samples. A mud content test was conducted to determine the mud content in the sand intended for making paving blocks. The test aimed to ascertain the percentage of mud present in the sand. According to SNI 7656:2012 (NSA, 2012), the permissible mud content in the sand should not exceed 5%. However, the results of the test revealed a mud content of 9.4%. This indicates that the sand only meets the requirement of less than 5% mud, a finding of significant concern. The findings suggest that if the mud content exceeds 5%, the sand should be washed correctly before being used in the mixture.

TABLE 2. Content weight test results

Material	Aggregate weight [g]	Container volume [cm^3]	Unit weight [$g \cdot cm^{-3}$]
Sand	1 090	0.001	1.09
Red brick powder	1 060	0.001	1.06
Plastic pellets	540	0.001	0.54

Source: own work.

Following the testing of sand gradation, it was determined that the acceptable modulus value of the sand is 2.45, which falls within the specified range ($1.5 < MK < 3.8$) outlined in SNI 7656:2012 (NSA, 2012). However, during testing, there was a percentage weight loss of 1.25%. This suggests that the aggregate samples are unsuitable for concrete building materials or paving blocks due to excessive weight loss. The detailed gradation test results for sand can be observed in Figure 3.

Furthermore, the red brick powder gradation testing indicated an acceptable modulus value of 2.7, which aligns with the specified fineness modulus range. Similar to the sand testing, there was a 1.25% weight loss during testing, highlighting the inadequacy of the red brick powder for concrete or paving block production. The comprehensive gradation test results for red brick powder can be found in Figure 4.

In contrast, the testing of plastic pellet gradation showcased an acceptable modulus value of 4.7, meeting the provisions of SNI 7656:2012 (NSA, 2012), which stipulate a fineness modulus range of $1.5 < MK < 3.8$. Moreover, the weight loss percentage during testing was only 0.25%, well below the permitted maximum of 1%. This points to the suitability of the plastic pellets for inclusion in concrete and paving blocks utilized as building materials. The detailed test result gradation for plastic pellets is visually depicted in Figure 5, further corroborating its appropriateness for the project.

Fendi, H. Y. (2024). The impact of utilizing red brick powder and plastic pellets as fine particles on the compressive strength and absorption of water in paving blocks. *Sci. Rev. Eng. Env. Sci.*, *33* (4), 372–387. DOI 10.22630/srees.9917

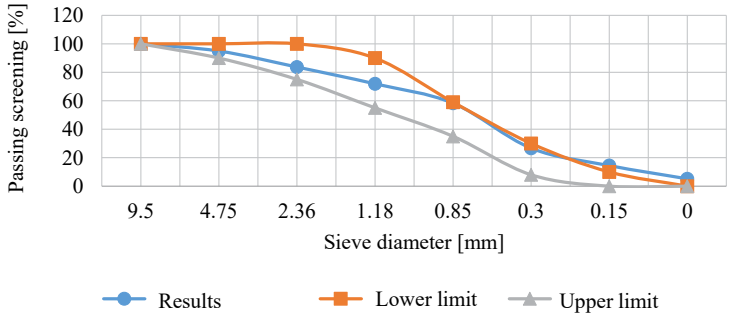

FIGURE 3. Sand gradation chart
Source: own work.

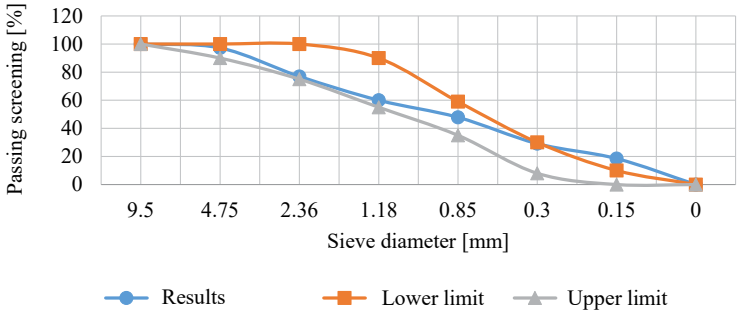

FIGURE 4. Red brick powder gradation chart
Source: own work.

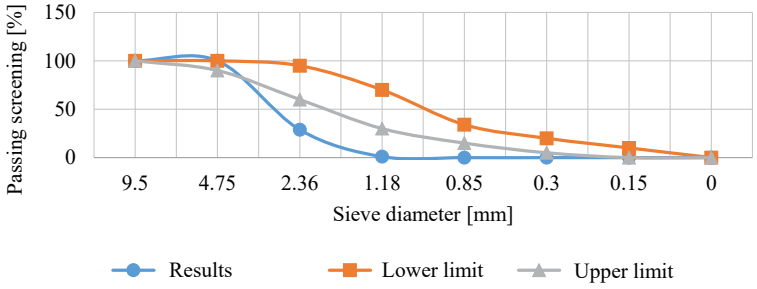

FIGURE 5. Plastic pellet gradation chart
Source: own work.

The test results for sand show that the bulk specific gravity is 2.3, the bulk SSD specific gravity is 2.38, the apparent specific gravity is 2.49, and the absorption is 3.1%. These values were compared to ASTM C33 specification requirements

(Taylor, 2004; Berney & Smith, 2008), which specify that bulk specific gravity, bulk SSD specific gravity, and apparent specific gravity should fall within the range of 1.6–3.3, and absorption should be less than 2%. Adhering to these standards is not just a formality but a crucial step in ensuring our analysis's quality and reliability.

Furthermore, the test results for red brick powder reveal a significant issue. The bulk specific gravity is 3.4, the bulk SSD specific gravity is 4, the apparent specific gravity is 8.5, and the absorption is 17.6%. Compared to ASTM C33 specification requirements, these results indicate that the red brick powder does not meet the required conditions for bulk specific gravity, bulk SSD specific gravity, apparent specific gravity, and absorption. This non-compliance is an urgent matter that needs to be addressed.

Following the 28-day aging period, a comprehensive evaluation was conducted to assess the strength of the paving blocks, involving meticulous testing of three distinct variations. The detailed findings from the substantial compressive strength test for the paving blocks are meticulously documented in Table 3. Each variation was rigorously marked and precisely compressed by the calculations outlined in the tables. Notably, all variations consistently demonstrated considerable strength in the testing summary. Further nuanced insights into the average compressive strength of the paving blocks are elucidated in Table 4.

TABLE 3. Comparison of the compressive strength values from testing paving blocks

Test	Normal	Compressive strength [MPa]	Innovation	Compressive strength [MPa]	Deviation [MPa]
1	V0 A	10.69	V1 A	6.57	–4.12
2	V0 B	10.21	V1 B	7.58	–2.63
3	V0 C	7.33	V1 C	3.72	–3.61
4	V0 A	10.69	V2 A	3.57	–7.12
5	V0 B	10.21	V2 B	3.08	–7.13
6	V0 C	7.33	V2 C	3.68	–3.65
7	V0 A	10.69	V3 A	12.19	+1.50
8	V0 B	10.21	V3 B	12.36	+0.15
9	V0 C	7.33	V3 C	9.73	+2.40

Note: V0 = 0% plastic pellets + 0% red brick powder, V1 = 10% plastic pellets + 25% red brick powder, V2 = 15% plastic pellets + 25% red brick powder, V3 = 25% plastic pellets + 25% red brick powder.

Source: own work.

Fendi, H. Y. (2024). The impact of utilizing red brick powder and plastic pellets as fine particles on the compressive strength and absorption of water in paving blocks. *Sci. Rev. Eng. Env. Sci.*, *33* (4), 372–387. DOI 10.22630/srees.9917

TABLE 4. A summary of test results for average compressive strength values of paving blocks

Test specimen	Additional material		Average compressive strength [MPa]
	Plastic pellets [%]	Red brick powder [%]	
V0 A, V0 B, V0 C	0	0	9.41
V1 A, V1 B, V1 C	10	25	5.95
V2 A, V2 B, V2 C	15	25	3.44
V3 A, V3 B, V3 C	25	25	11.43

Note: V0 = 0% plastic pellets + 0% red brick powder, V1 = 10% plastic pellets + 25% red brick powder, V2 = 15% plastic pellets + 25% red brick powder, V3 = 25% plastic pellets + 25% red brick powder.

Source: own work.

Moreover, Figure 6 visually articulates the profound impact of integrating additional plastic pellets and red brick powder materials, which served as partial sand substitutes, on the paving blocks' robustness. Noteworthy is the revelation that while the highest average compressive strength was attained with the traditional mixture, a distinct concoction of cement and sand in a 1 : 4 ratio, enhanced with the supplementary materials at a concentration of 25% each, yielded an impressive average compressive strength of 9.09 MPa. Based on these comprehensive and intricate findings, it is evident that only the standard paving blocks and the select three variations can be unequivocally classified as D-quality paving blocks, rendering them eminently suitable for deployment within park environments.

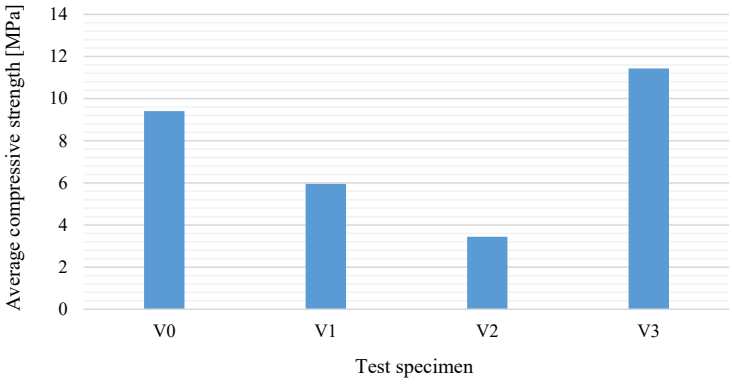

FIGURE 6. Average compressive strength values for paving blocks

Source: own work.

A comprehensive test was conducted to examine the absorption of water in paving blocks. The process involves immersing the paving block in water for a continuous period of 24 h, followed by subjecting the block to an extreme temperature by placing it in an oven at 110°C for an additional 24 h. This meticulous test is performed when the paving blocks have reached 28 days of age, utilizing three test specimens for each distinct variation. An illustrative example of this examination includes the calculation of absorption of water from a specific paving block test specimen denoted as V1 D. This calculation considers additional components, such as 10% plastic pellets and 25% red brick powder, incorporated with heavy sand.

The calculated results for the absorption of water from each variation of paving blocks are collated and documented comprehensively in Table 5, providing an intricate and detailed overview of the variation in absorption across different compositions. After the detailed calculations in the tables, the amassed data about the average water absorption of paving blocks is meticulously summarized and presented in Tables 6 and 7.

TABLE 5. Comparison of testing the water absorption value of paving blocks

No	Normal	Water absorption [%]	Innovation	Water absorption [%]	Deviation [%]
1	V0 A	11.70	V1 A	13.70	–2.00
2	V0 B	11.34	V1 B	15.18	–3.84
3	V0 C	11.18	V1 C	14.39	–3.21
4	V0 A	11.70	V2 A	14.21	–2.51
5	V0 B	11.34	V2 B	13.66	–2.32
6	V0 C	11.18	V2 C	16.38	–5.20
7	V0 A	11.70	V3 A	14.48	–2.78
8	V0 B	11.34	V3 B	15.14	–3.80
9	V0 C	11.18	V3 C	14.76	–3.58

Note: V0 = 0% plastic pellets + 0% red brick powder, V1 = 10% plastic pellets + 25% red brick powder, V2 = 15% plastic pellets + 25% red brick powder, V3 = 25% plastic pellets + 25% red brick powder.

Source: own work.

Fendi, H. Y. (2024). The impact of utilizing red brick powder and plastic pellets as fine particles on the compressive strength and absorption of water in paving blocks. *Sci. Rev. Eng. Env. Sci.*, *33* (4), 372–387. DOI 10.22630/srees.9917

TABLE 6. Summary of average water absorption test results for paving blocks

Test specimen	Additional material		Average water absorption [%]
	Plastic pellets [%]	Red brick powder [%]	
V0 A, V0 B, V0 C	0	0	11.40
V1 A, V1 B, V1 C	10	25	14.43
V2 A, V2 B, V2 C	15	25	14.75
V3 A, V3 B, V3 C	25	25	14.80

Note: V0 = 0% plastic pellets + 0% red brick powder, V1 = 10% plastic pellets + 25% red brick powder, V2 = 15% plastic pellets + 25% red brick powder, V3 = 25% plastic pellets + 25% red brick powder.

Source: own work.

TABLE 7. Summary of test results for the optimal average water absorption capacity of paving blocks

Test object	Additional material		Average compressive strength [MPa]
	Plastic pellets [%]	Red brick powder [%]	
1	0	0	9.41
4	25	25	11.43

Source: own work.

Moreover, Figure 7 presents a detailed graphical representation illustrating the intricate nuances of the increases and decreases in water absorption from paving blocks. This representation provides a visual insight into the variations in water absorption across different compositions and further adds a layer of detailed analysis to the results.

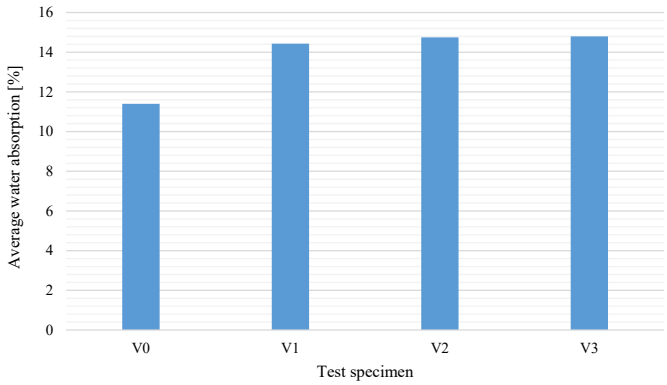

FIGURE 7. Average water absorption value of paving blocks

Source: own work.

Upon thorough examination of Figure 7, it is evident that the absorption of water consistently demonstrates an ascending trend with each variation. Notably, the highest average water absorption value from the paving blocks is obtained when utilizing a specific mixture of cement and sand at a precise ratio of 1 : 4, coupled with additional materials comprising 25% plastic pellets and 25% red brick powder, resulting in a substantial average water absorption of 14.80%. These comprehensive and detailed findings lead to the significant conclusion that all variations of paving blocks hold the classification of being of high quality, thereby rendering them suitably applicable to diverse park requirements.

Using red brick powder and plastic pellets as fine particles in paving blocks significantly affects their compressive strength and water absorption characteristics. Adding these additives can improve the compressive strength of paving blocks, as evidenced by studies showing that certain mixtures can meet or exceed the standards required for load-bearing applications (Silva et al., 2023). In this study, the addition of 25% plastic pellets has been shown to meet the compressive strength requirements, indicating that the same proportion of red brick powder and plastic pellets can produce beneficial results. In addition, using additives such as red brick powder and plastic pellets increases the strength and affects the durability of paving blocks. Durability testing, including water absorption testing, revealed that the right combination of materials can lower water absorption rates, thereby increasing the life of paving blocks under environmental stress (Widiyono et al., 2024). The interaction between these additives and the base materials, such as cement and aggregate, is critical to optimizing mechanical properties and resistance to water infiltration (Folorunsho et al., 2023). Thus, strategically using red brick powder and plastic pellets can produce strong and durable paving blocks that meet critical performance criteria in construction applications.

Conclusions

This study explored the potential of incorporating waste red brick powder and polypropylene (PP) plastic pellets as alternative aggregates in paving block production. The results demonstrated that the innovative paving block formulations achieved compressive strength values comparable to traditional blocks, particularly those containing 25% red brick powder and 25% plastic pellets. While this formulation met the minimum requirements for category D paving blocks according to SNI 03-0691-1996, it exhibited slightly lower compressive strength than previous findings. Regarding water absorption, the study revealed that adding

red brick powder and plastic pellets generally increased water absorption compared to traditional paving blocks. The formulation with 25% red brick powder and 25% plastic pellets exhibited the highest water absorption, exceeding the maximum allowed limit of 10% as per SNI 03-0691-1996.

In conclusion, this study provides valuable insights into the feasibility of utilizing recycled materials in paving block production. The results suggest that these materials can be successfully integrated to create sustainable and durable construction products. Future research should focus on fine-tuning the material composition and production processes to optimize the balance between compressive strength and water absorption, ensuring that the paving blocks meet the specific requirements of various applications while promoting environmental sustainability.

References

Ahmad, S., Dawood, O., Lashin, M. M. A., Khattak, S. U., Javed, M. F., Aslam, F., Khan, M. I., Elkotb, M. A., & Alaboud, T. M. (2023). Effect of coconut fiber on low-density polyethylene plastic-sand paver blocks. *Ain Shams Engineering Journal*, *14* (8), 101982. https://doi.org/10.1016/j.asej.2022.101982

Arulrajah, A., Yaghoubi, E., Wong, Y., & Horpibulsuk, S. (2017). Recycled plastic granules and demolition wastes as construction materials: Resilient moduli and strength characteristics. *Construction and Building Materials*, *147*, 639–647. https://doi.org/10.1016/j.conbuildmat.2017.04.178

Awoyera, P. O., & Adesina, A. (2020). Plastic wastes to construction products: Status, limitations and future perspective. *Case Studies in Construction Materials*, *12*, e00330. https://doi.org/10.1016/j.cscm.2020.e00330

Berney, E. S., & Smith, D. M. (2008). *Mechanical and physical properties of ASTM C33 sand.* U.S. Army Corps of Engineers.

Candra, A. I., Romadhon, F., Azhari, F. M., & Hidiyati, E. F. (2022). Increasing compressive strength of the red brick with fly ash and rice husk ash. *Jurnal Teknik Sipil dan Perencanaan*, *24* (2), 107–117. https://doi.org/10.15294/jtsp.v24i2.35855

Dadzie, D., Kaliluthin, A., & Kumar, D. (2020). Exploration of Waste Plastic Bottles Use in Construction. *Civil Engineering Journal*, *6* (11), 2262–2272. https://doi.org/10.28991/cej-2020-03091616

Dary, R. W., Oktaviani, T., Putri, W. N., & Putra, H. (2024). Effect of compressive strength of red brick with the aaddition of carrageenan. *International Journal of Research in Vocational Studies (IJRVOCAS)*, *3* (4), 144–149. https://doi.org/10.53893/ijrvocas.v3i4.82

Folorunsho, O. W., Suleiman, T. M., Amadi, A. N., Hassan, A., & Hakeem, O. A. (2023). Comparative studies on the compressive strength of pavement blocks made from different geological materials with plastic waste additives and cement pavement for use in road construction. *Fudma Journal of Sciences*, *7* (6), 191–199. https://doi.org/10.33003/fjs-2023-0706-2185

Garcia, N., Molina, D., Torres, Y., & de Almeida, L. (2023). The proposes for the use of the cleaner production tool (P+L) in the hope plastic solid waste recycling process. *Angolan Industry and Chemical Engineering Journal*, *3* (3), 29–36. https://www.aincej.com.angolaonline.net/index.php/home/article/view/21/12

Gopinath, M., Abimaniu, P., Dharsan Rishi, C., Pravinkumar, K., & Tejeshwar, P. G. (2023). Experimental investigation on waste plastic fibre concrete with partial replacement of coarse aggregate by recycled coarse aggregate. *Materials Today: Proceedings*. https://doi.org/10.1016/j.matpr.2023.04.573

Gour, M., Sharma, S., Garg, N., Das, S., & Kumar, S. (2022). Utilization of Plastic Waste as a Partial Replacement of Coarse Aggregates in Concrete. *IOP Conference Series: Earth and Environmental Science*, *1086* (1), 12047. https://doi.org/10.1088/1755-1315/1086/1/012047

Guo, Z., Sun, Q., Zhou, L., Jiang, T., Dong, C., & Zhang, Q. (2024). Mechanical properties, durability and life-cycle assessment of waste plastic fiber reinforced sustainable recycled aggregate self-compacting concrete. *Journal of Building Engineering*, *91*, 109683. https://doi.org/10.1016/j.jobe.2024.109683

Haigh, R. (2024). The mechanical behaviour of waste plastic milk bottle fibres with surface modification using silica fume to supplement 10% cement in concrete materials. *Construction and Building Materials*, *416*, 135215. https://doi.org/10.1016/j.conbuildmat.2024.135215

Handayasari, I. (2017). Studi Alternatif Bahan Konstruksi Ramah Lingkungan Dengan Pemanfaatan Limbah Plastik Kemasan Air Mineral Pada Campuran Beton. *Poli-Teknologi*, *16* (1), 159366. https://doi.org/10.32722/pt.v16i1.865

Iduwin, T., Hadiwardoyo, S. P., Rifai, A. I., & Lumingkewas, R. H. (2023). Contribution of Plastic Waste in Recycles Concrete Aggregate Paving Block. *Journal of Advanced Research in Applied Mechanics*, *110* (1), 1–10. https://doi.org/10.37934/aram.110.1.110

Junkes, V. H., Fuziki, M. E. K., Tusset, A. M., Rodrigues, P. H., & Lenzi, G. G. (2024). Environmentally friendly concrete block production: valorization of civil construction and chemical industry waste. *Environmental Science and Pollution Research*, *31* (12), 17788–17803. https://doi.org/10.1007/s11356-023-31706-y

Kakerissa, Y., & Latuheru, R. (2023). Utilization of plastic waste as a substitutional material for paving block manufacturing. *Engineering and Technology Journal*, *8* (3). https://doi.org/10.47191/etj/v8i3.07

Khatib, J., Jahami, A., Elkordi, A., & Baalbaki, O. (2019). Structural performance of reinforced concrete beams containing plastic waste caps. *Magazine of Civil Engineering*, *7* (91), 73–79. https://doi.org/10.18720/MCE.91.7

Krasna, W., Noor, R., & Ramadani, D. (2019). Utilization of plastic waste polyethylene terephthalate (PET) as a coarse aggregate alternative in paving block. *MATEC Web of Conferences*, *280*, 4007. https://doi.org/10.1051/matecconf/201928004007

Muzaidi, I., Anggarini, E., & Hardiani, D. (2022). Solidifikasi Struktur Tanah Lempung Lunak Banjarmasin Dengan Limbah Plastik Pet (Polyethylene Terephthalate). *EXTRAPOLASI*, *19*, 1–8. https://doi.org/10.30996/ep.v19i01.5520

National Standardization Agency [NSA], (1996). *Paving block (SNI 03-0691-1996)*. National Standardization Agency. https://spada.uns.ac.id/pluginfile.php/110917/mod_resource/content/1/sni-03-0691-1996-paving-block.pdf

National Standardization Agency [NSA], (2012). *Procedures for selecting mixtures for normal concrete, heavy concrete and mass concrete (SNI 7656:2012)*. National Standardization Agency. https://app.box.com/s/efw1el9wf9l79bnryqpq7sujoht816ok

Paikun, P., Amdani, S. A., Susanto, D. A., & Saepurrahman, D. (2023). Analysis of the compressive strength of concrete from brick wall waste as a concrete mixture. *ASTONJADRO*, *12* (1), 150–162. https://doi.org/10.32832/astonjadro.v12i1.8145

Saxena, R., Gupta, T., Sharma, R. K., Chaudhary, S., & Jain, A. (2020). Assessment of mechanical and durability properties of concrete containing PET waste. *Scientia Iranica*, *27* (1), 1–9. https://doi.org/10.24200/SCI.2018.20334

Silva, W. B. C., Barroso, S. H. A., Cabral, A. E. B., Stefanutti, R., & Picado-Santos, L. G. (2023). Assessment of concrete road paving blocks with coal bottom ash: physical and mechanical characterization. *Case Studies in Construction Materials*, *18*, e02094. https://doi.org/10.1016/j.cscm.2023.e02094

Soni, A., Rajput, T., Sahu, K., & Rajak, S. (2022). Utilization of waste plastic in manufacturing of paver blocks. *International Journal for Research in Applied Science and Engineering Technology*, *10* (2), 939–942. https://doi.org/10.22214/ijraset.2022.40410

Taylor, M. (2004). *Proposed changes to ASTM C33*. https://citeseerx.ist.psu.edu/document?repid=rep1&type=pdf&doi=d556f92f31a600f2442ddbfc4a378f32611c835d

Tempa, K., Chettri, N., Thapa, G., Phurba, Gyeltshen, C., Norbu, D., Gurung, D., & Wangchuk, U. (2022). An experimental study and sustainability assessment of plastic waste as a binding material for producing economical cement-less paver blocks. *Engineering Science and Technology, an International Journal*, *26*, 101008. https://doi.org/10.1016/j.jestch.2021.05.012

Umar, M. Z., & Mustafa, A. F. (2023). The performance optimization of concrete bricks using a sagu fiber. *SINERGI*, *27* (1), 7–14. https://doi.org/10.2241/sinergi.2023.1.002

Wendimu, T. B., Furgasa, B. N., & Hajji, B. M. (2021). Suitability and utilization study on waste plastic brick as alternative construction material. *Journal of Civil, Construction and Environmental Engineering*, *6* (1), 9–12. https://doi.org/10.11648/j.jccee.20210601.12

Widiyono, A., Saputro, Y. A., Pambudi, F. B. S., Hermawan, A. B. B. H., & Mahardika, M. A. (2024). Assistance in utilization of plastic waste through eco-paving blocks at Adiwiyata Elementary School, Demak Regency. *Warta Pengabdian Andalas*, *31* (2), 368–376. https://doi.org/10.25077/jwa.31.2.368-376.2024

Summary

The impact of utilizing red brick powder and plastic pellets as fine particles on the compressive strength and absorption of water in paving blocks. The construction industry faces increasing pressure to reduce its environmental impact. Traditional paving block production often relies on non-renewable materials and contributes to waste generation. The need for sustainable and durable paving block alternatives is evident. This study investigated the potential of incorporating waste red brick powder and polypropylene (PP) plastic pellets as a fine aggregate in paving block production. Various formulations were tested, with varying percentages of these materials. The resulting paving blocks' compressive strength and water absorption were evaluated against SNI 03-0691-1996 standards. The results indicate that the innovative paving block formulation incorporating 25% plastic pellets and 25% red brick powder achieved a maximum compressive strength of 12.19 MPa. In comparison, a mixture containing 15% plastic pellets and 25% red brick powder exhibited a minimum compressive strength of 3.08 MPa. The average water absorption for all formulations was 14.80%. These findings highlight the potential of waste materials as viable alternatives in construction, promoting a more sustainable approach to urban infrastructure.

Scientific Review Engineering and Environmental Sciences (2024), 33 (4), 388–400

Sci. Rev. Eng. Env. Sci. (2024), 33 (4) https://srees.sggw.edu.pl

ISSN 1732-9353 (suspended) eISSN 2543-7496 DOI 10.22630/srees.9953

Received: 06.09.2024
Accepted: 04.11.2024

Olena VOLOSHKINA
Tetiana TKACHENKO✉
Illia SVIATOHOROV
Yuliia BEREZNYTSKA

Kyiv National University of Construction and Architecture, Faculty of Engineering Systems and Ecology, Ukraine

The influence of urban building orientation on the risk of heat stress from being in the courtyard area during the peak summer period

Keywords: orientation of urban buildings, temperature, shading percentage, surface heating

Introduction

At the stage of designing and choosing the orientation of the location of a building, an extremely important aspect is the analysis of the degree of shading of the territory at different times of the day to ensure it is comfortable for anyone who is there. The general level of thermal comfort is closely related to the meteorological indicators and morphological features of the city. A number of scientific articles by foreign authors have been devoted to the study of this issue, with a direct reference to the area in which they live (Gulyás et al., 2006; Bourbia & Boucheriba, 2010; Heusinkveld et al., 2014). In this regard, the obtained research

✉tkachenkoknuba@gmail.com

results may be relevant only for a specific geographical location (Zeng & Dong, 2015; Kedissa et al., 2016; Smith et al., 2019). The impact of climate change on the health of the population in terms of the varying orientations of buildings in an area and the component of solar radiation at different times of the day in Ukraine has not been sufficiently studied.

In the work by Willett and Sherwood (2012), the forecasting levels of exceeding the threshold values in summer were established, based on a fixed distribution of anomalies with respect to the average seasonal value according to the wet bulb globe temperature (WBGT) indicator. Forecasting the impact of the regional temperature rise and the level of risk for the population was described in a paper by Fischer et al. (2012). Many scientific studies are devoted to increasing the size of the thermal dome in urbanized areas and the comfort of residents staying in open spaces in the summer months of the year (Steeneveld et al., 2011).

Based on the example of the city of Kyiv, in Sviatohorov (2024), the long-term changes in heat stress depending on global climatic changes were studied. Based on the study of average monthly long-term climate data in the city of Kyiv using the Copernicus Climate Change Service (Boris Sreznevsky Central Geophysical Observatory, 2024) and the data of the Borys Sreznevsky Central Geophysical Observatory, the author obtained the dependence of the value of the heat index (HI) from the value of temperature and air humidity for observations in different periods. This index combines the air temperature and the relative humidity in the shade to determine the human-perceptible equivalent temperature.

Taking into account the trends of increasing temperature indicators as a result of global warming in matters of urban planning (Balcerak, 2014; Luo & Lau, 2018; Li & Zhang, 2021), significant attention has recently been paid to "green construction" technologies, which, at the same time as using innovative materials and landscaping technologies, should also take into account the orientation of the building (Prasad et al., 2017) with respect to the sides of the world, in order to increase the percentage of shading from direct solar radiation.

The purpose of these studies is to determine and compare the dependence of the heating of facade surfaces along the perimeter of the courtyard and the underfloor surface of the courtyard of a residential building on the percentage of surface shading at different orientations relative to the cardinal points. This will make it possible to assess the potential risk of thermal stress for the residents in this future residential area during the design stage when initially planning the territory.

Voloshkina, O., Tkachenko, T., Sviatohorov, I., Bereznytska, Y. (2024). The influence of urban building orientation on the risk of heat stress from being in the courtyard area during the peak summer period. *Sci. Rev. Eng. Env. Sci.*, *33* (4), 388–400. DOI 10.22630/srees.9953

These studies were conducted for Ukraine's first climatic zone and, even at the design stage, allowed the reduction of the risk of heat stress in the adjacent territory during the operation of the buildings in the future.

Material and methods

For the assessment of the impact of thermal stress on the human body, which is based on the WBGT indicator as well as the interpretation of human thermal comfort, then the normative documents of the ISO series devoted to these calculations can be used, such as ISO 7243 (International Organization for Standardization [ISO], 2017).

The area of the residential area depends on the location of the building blocks, and has a different percentage of shading and heating of the surface depending on the amount of direct solar radiation falling on it at different times of the day.

For the study, a U-shaped construction scheme was selected, involving a five-section, nine-story residential building, typical for the city of Kyiv and the Kyiv region (the first climate zone). The total area of each section in the plan is about 550 m^2, with the area of the underlying surface of the yard measuring 2,200 m^2. This configuration of blocking sections creates the effect of self-shading of the facades and partial shading of the courtyard, which has a positive effect on the overall temperature of the surfaces. The influence of the surrounding buildings has been excluded from the calculation. It was decided to make the underlying surface free of trees and bushes to exclude the influence of unpredictable shading.

The calculation of the amount of solar radiation was conducted by the authors using the specialized TownScope program (Teller & Azar, 2001). At the beginning of the work, the authors prepared a corresponding 3D model of the building and exported it to the 3Ds format (Fig. 1).

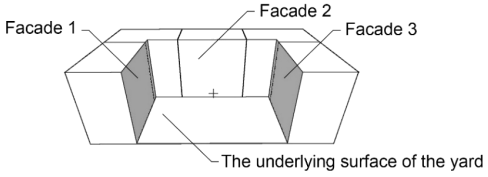

FIGURE 1. Scheme of blocking sections of a residential building (studied surfaces)
Source: own work.

The monitoring data of the Borys Sreznevsky Central Geophysical Observatory for July 2021 was also used for the study, with an average air temperature of 24.6°C. The choice of the calculation period was based on the purpose of investigating the changes in the heating of the subfloor surface and facade surfaces in the peak summer period, which corresponds to the month of July in the first climatic zone of Ukraine. Since the average air temperature for July was taken, the research was conducted based on the example of one daylight day during this month.

In the first stage, using the TownScope program, the amount of direct solar radiation in $W \cdot m^{-2}$ was calculated for each considered surface of the facades and the plane of the courtyard. Using the schemes obtained in the TownScope program, the percentage of shading of the surfaces of the residential building and the adjacent territory was determined graphically, with different orientations being used with respect to the cardinal points. The surfaces of the facades adjacent to the courtyard of the residential building were considered, as well as the underlying surface of the courtyard.

To determine the amount of direct solar radiation hitting a horizontal surface, depending on the orientation with respect to the sides of the world and considering shading, a separate unified element of the area was selected, which we take as a square with an area of S_i.

We have two variables that depend on time:

1. Intensity of direct solar radiation on a separate unified element of the area:

$$R = f(t, A_i) = A_i(t)S_1, \tag{1}$$

where: A_i – the hourly amount of direct solar radiation per 1 m^2, depending on the orientation of the block of the building under consideration, was determined based on the tabular form used in the regulatory documents.

2. Surface area of the element, considering shading:

$$S_1 = f(t, \beta). \tag{2}$$

The effectiveness of shading is determined by the formula:

$$\Delta R = [A_i(t) - A_{i+1}(t)] \sum S_1 i = A_i(t) \cdot (1 - \beta) \cdot \sum S_1 i, \tag{3}$$

where: β – coefficient that characterizes the percentage of shading, which should be taken according to the values that were calculated separately in accordance with

the current regulatory documents, $\sum S_1 i$ – the total area of the residential territory under consideration, i – the module number with areas S_1, $i = 1, 2, 3, \ldots, n$.

Thus, we can present any area of the residential area featuring different locations of the building. The total areas of the surfaces were calculated on the basis of the 3D model of the residential building.

The average heating temperature of the surfaces of the building facades and the underlying surface from solar radiation during one hour of daylight can be determined according to the formula of A.M. Shklover (Korkina et al., 2023), which gives a good correlation between the calculated and experimental data:

$$t_{\text{cal}} = t_{\text{out}} + \frac{R \cdot \alpha_{S,c}}{\alpha_{\text{out}}}, \tag{4}$$

where: t_{out} – outside air temperature [°C], R – direct solar radiation that reaches the surface during the studied period of time [W·m^{-2}], $\alpha_{S,c}$ – coefficient of absorption of solar radiation by the surface of the facade, which is determined according to Clause 11.3 of DSTU 9190-2022 (Ukrainian Scientific Research and Training Center for Standardization, Certification and Quality Problems [UkrNDNC], 2022), and α_{out} – heat exchange coefficient of the facade surface, calculated according to the empirical formula (Ratushniak & Popova, 2004; Korkina et al., 2023):

$$\alpha_{\text{out}} = 1.16 \cdot (5 + 10\sqrt{v}), \tag{5}$$

where: ν – wind speed [m·s^{-1}].

The surface of the residential area also receives heat from neighboring buildings, and as a result the heat index on the residential area will increase. In this case, the expression of the balance of the specific heat flow for the surface of the facade, which receives radiation heat, is calculated under the following assumptions:

- there is no multiple reflection and absorption between building facades and the underlying surface,
- the temperature of the outer surface does not depend on the temperature of the indoor air,
- calculations are made for a thin surface layer of the facade in one hour, so it is considered that the thin layer has a constant temperature that corresponds to the end of the time interval,
- the considered surfaces of the facades do not have skylights,
- the influence of the atmosphere is not considered.

The heating temperature of the underlying surface of the courtyard is calculated considering the percentage of shading per hour and the average value is determined during the calculated hours. At the same time, we accept the coefficient of absorption of solar radiation by the surface of the yard in accordance with EN ISO 7730 (European Committee for Standardization [CEN], 2005), $\alpha_{S,c} = 0.7$, for the paving of the surface of the yard with clinker bricks, and 0.7 for the facade facing bricks. The coefficient of heat exchange of the surface is accepted according to Formula (5) for Kyiv, according to the average statistical reference data (Boris Sreznevsky Central Geophysical Observatory).

Results and discussion

The percentage of shading of the facade surfaces and the amount of direct solar radiation falling on the investigated surfaces are presented in Table 1.

TABLE 1. Calculation of the total amount of direct solar radiation on the horizontal surface and on the surface of the facades, depending on the orientation with respect to the sides of the world, considering shading during a day in July 2021 having an average monthly temperature of 24.6°C

Surface name	Surface area [m^2]	Shading [%]							
		S	SE	SW	NE	NW	N	W	E
Facade 1	1 050	48.8	61.5	42.7	80.4	36.0	54.2	28.8	80.9
Facade 2	1 900	31.1	40.7	40.7	70.6	70.6	86.8	50.4	50.4
Facade 3	1 050	48.9	42.5	61.5	31.6	80.2	54.4	80.7	28.9
Underlying surface of the yard	2 200	42.5	36.5	36.5	53.0	53.0	62.8	41.4	41.4
Total shading [%]	1 050	48.8	61.5	42.7	80.4	36.0	54.2	28.8	80.9
×	×	Direct solar radiation [$W \cdot m^{-2}$]							
		S	SE	SW	NE	NW	N	W	E
Facade 1	1 050	4 230	2 792	4 033	4 127	5 411	6 608	3 446	640
Facade 2	1 900	3 821	4 145	5 174	2 737	4 667	1 150	6 473	4 309
Facade 3	1 050	6 123	4 899	4 761	4 125	2 538	4 381	367	3 377
Underlying surface of the yard	2 200	7 393	6 527	7 078	5 924	6 720	6 555	6 712	5 566

Source: own work.

The analysis of the obtained data, taking into account the percentage of shading, made it possible to plot the graphs of the dependence of the total amount of direct solar radiation during daylight for each hour over the entire area of the courtyard at different orientations with respect to the cardinal points (Fig. 2).

Voloshkina, O., Tkachenko, T., Sviatohorov, I., Bereznytska, Y. (2024). The influence of urban building orientation on the risk of heat stress from being in the courtyard area during the peak summer period. *Sci. Rev. Eng. Env. Sci.*, *33* (4), 388–400. DOI 10.22630/srees.9953

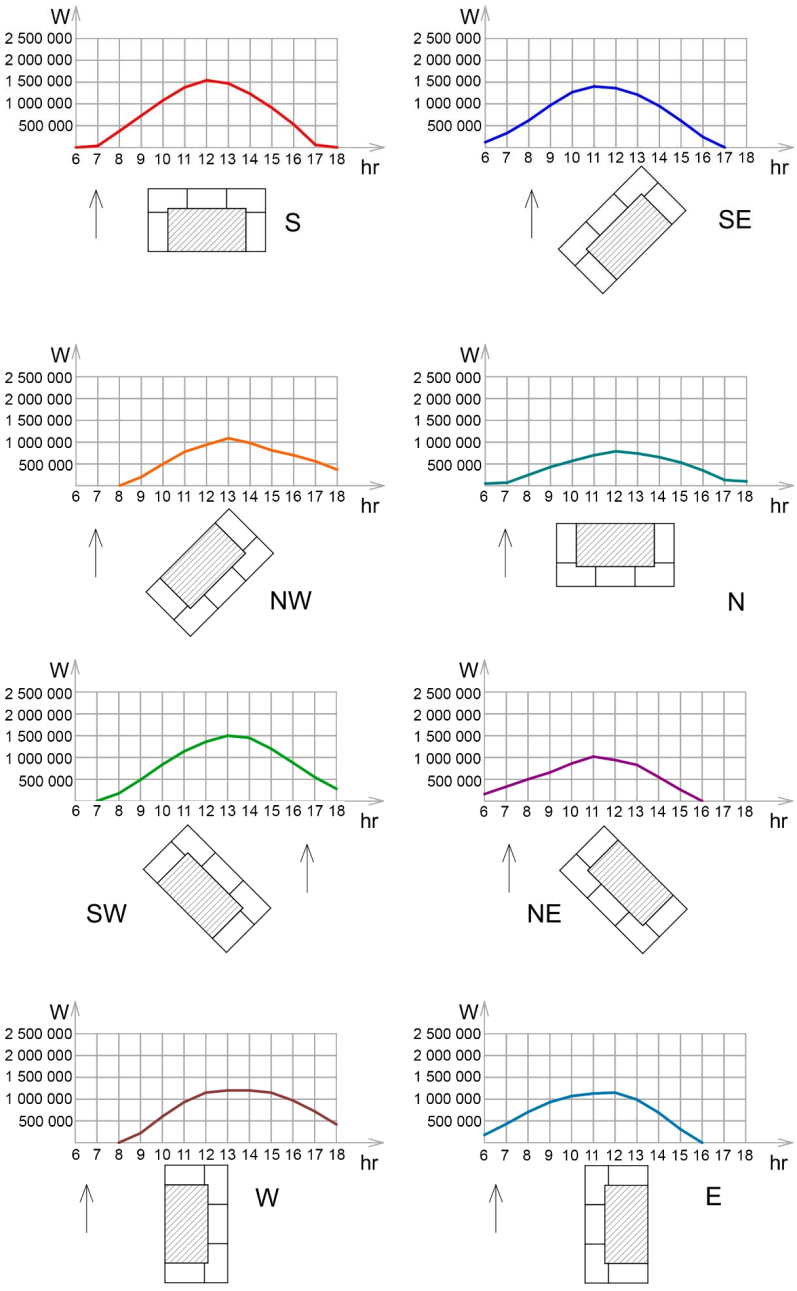

FIGURE 2. The amount of direct solar radiation hitting the horizontal surface of the yard, depending on the orientation with respect to the cardinal points, considering the shading

Source: own work.

The heating temperature of the underlying surface of the courtyard was calculated considering the percentage of shading per hour, with the average value being determined during the calculated hours (Table 2).

TABLE 2. Average heating temperature of the facades during daylight hours adjacent to the courtyard, July 2021, Kyiv, with an average monthly temperature of 24.6°C

Surface name	Surface area [m^2]	S *t* [°C]	SE *t* [°C]	SW *t* [°C]	NE *t* [°C]	NW *t* [°C]	N *t* [°C]	W *t* [°C]	E *t* [°C]
Facade 1	1 050	29.7	27.1	31.0	25.8	29.8	29.2	28.3	24.8
Facade 2	1 900	30.8	30.3	31.8	25.8	26.7	24.8	29.4	27.8
Facade 3	1 050	31.9	31.2	28.9	28.6	25.4	27.6	24.7	28.2
Underlying surface of the yard	2 200	34.6	34.3	35.1	28.8	29.4	28.3	30.5	29.8

Source: own work.

According to Table 2, in all orientation options, the underfloor surface heats up more than the surface of the facades. This plane has the greatest impact on the risk of heat stress.

For effective evaluation of the obtained results, presented in Tables 1 and 2, two schemes were created (Figs 3 and 4). Figure 3 illustrates the relationship of the shading coefficient with respect to the average temperature of the understory surface of the inner yard at different orientations relative to the cardinal points. Figure 4 illustrates the relationship between the total amount of direct solar radiation falling on the underlying surface of the yard and the average temperature of this surface.

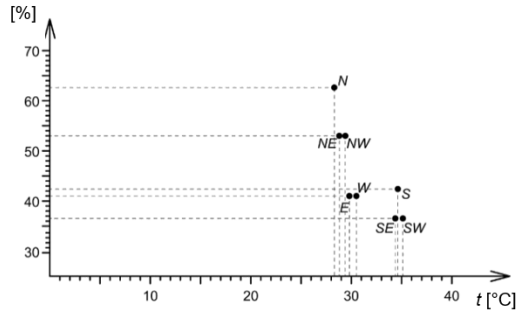

FIGURE 3. The scheme of the relationship between the shading coefficient and the average temperature of the underfloor surface of the courtyard of a residential building at different orientations with respect to the cardinal points

Source: own work.

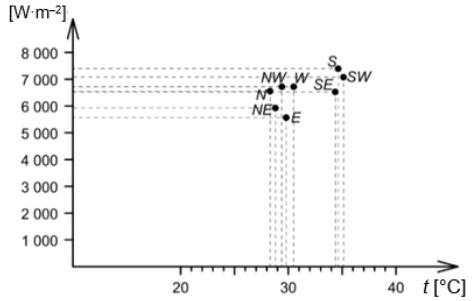

FIGURE 4. The scheme of the relationship of the total amount of direct solar radiation falling on the underfloor surface of the yard to the average temperature of the surface of the yard of a residential building at different orientations with respect to the sides of the world

Source: own work.

In analyzing the data of the scheme (Fig. 3), the lowest average temperature of the underfloor surface during the day was observed when the courtyard was oriented to the north, giving a temperature of 28.3°C. With this orientation, the largest percentage of shading of the courtyard surface was obtained at 62.8%. However, it should be considered that the orientation of the U-shaped yard to the north may become problematic when designing housing, due to the need to observe the standardized insolation of the yard sites.

The north-eastern (28.8°C) and north-western (29.4°C) orientations differ by heating the latter surface by 0.6°C in favor of the former. The shading coefficients were 59.4 and 60.1, respectively, which is less than with the northern orientation by 3.4% and 2.7%. Orientations to these directions are favorable from the point of view of limiting the heating of the underlying surface of the inner yard.

The average heating temperature of the underfloor surface in the eastern and western orientation of the courtyard of the U-shaped residential building is 29.8°C and 30.5°C. These are also satisfactory indicators within the limits of variability when designing this configuration of a sectional residential building.

The south, southeast and southwest orientations of the yard are the most unfavorable. The results differ from the average heating temperature of the surface of the northern orientation of the yard in the direction of growth by 6.8°C, 6.3°C and 6.0°C. The shading coefficient is lower by 20.3%, 26.3% and 26.3%, respectively.

Figure 2 makes it possible to compare the ratios of the total amount of direct solar radiation falling on the horizontal surface of the yard at different orientations. Thus, allows the pre-assessment of the effectiveness of the decisions taken during the design, in terms of reducing the risk of thermal stress of the population. Graphs are created for convenient demonstration of the results and can be used

in the project work. This graphic material has a correlation with the obtained temperature indicators of the surface heating, presented in Tables 1 and 2.

The heating temperatures were obtained for all the considered surfaces. To achieve a more precise statement of the problem related to determining the air temperature in the courtyard, it is necessary to use the Stefan–Boltzmann formula, considering the angular radiation coefficient and consistently determining the additional heat flow obtained by the radiant heat exchange of the receiving surface having an area of 2,200 m^2 from each of the adjacent facade surfaces.

Preliminary estimation calculations of the heating temperature of the inner courtyard surfaces in the peak summer period indicate the possibility of considering, at an early stage, the methods of designing the green building technologies based on passive methods of cooling the urban surfaces. This work can be useful for designers of residential buildings in order to regulate the temperature regime in microdistricts.

Conclusions

Considering the projected increase in average annual temperatures in Ukraine, particularly the situation for Kyiv and the Kyiv region, which are in the first climatic zone of Ukraine, a comprehensive solution to the issues of reducing the temperature indicators and increasing the degree of cooling of the surrounding area should be provided. One of the measures of "green building" technologies should be the adaptive orientation of urban buildings in relation to which direction they face in the world to prevent overheating of the courtyard surfaces.

Research has proven that the amount of solar energy reaching urban surfaces directly depends on the orientation of the residential structure. The underfloor surface of the U-shaped multi-section residential building considered in the work, given the shading, is the least prone to overheating when oriented towards the West, Northwest, North, Northeast, and East. Based on the results of the research, it should be recommended that during the design of a U-shaped residential structure, the orientation of the yard area should be laid out to have the angular values of East–North–West. That is, by designing the yard of a residential building in any degree between these directions. The greatest overheating of the underlying surface occurs in the Southwest–South–Southeast orientation. This placement of the volume of the U-shaped residential building is the most unfavorable from the point of view of the risk of heat stress in people in the yard. Surface shading coefficients are also much smaller. Heat exchanges

between the surfaces of the facades and the sub-floor surface will take longer, which will negatively affect the average temperature of the yard. With such orientations, the courtyard needs additional measures of green construction to reduce the temperatures.

In further works, the authors plan to consider other typical urban residential structures, and to identify the most effective model of residential formation from the point of view of reducing the surface temperature of the inner yard.

This study may be useful to architects when planning the territories for new microdistricts on the outskirts of the city in areas free from existing buildings. The orientation of residential quarters, considering the heating of adjacent areas and facades of the surfaces, should improve the microclimate of the future residential environment and reduce the risk of heat stress for the population.

Acknowledgments

The publication was prepared in the framework of the project: "Multilevel Local, National and Regionwide Education and Training in Climate Services, Climate Change Adaptation and Mitigation 619285-EPP-1-2020-1-FI-EPPKA2-CBHE-JP" The European Commission's support for the production of this publication does not constitute an endorsement of the contents, which reflect the views only of the authors, and the European Commission cannot be held responsible for any use which may be made of the information contained therein.

References

Balcerak, E. (2014). Statistical analysis describes urban heat island effect in Europe. *Eos, Transactions American Geophysical Union*, *95* (6), 60. https://doi.org/10.1002/2014EO060010

Boris Sreznevsky Central Geophysical Observatory (2024). *Climate data for the city of Kyiv*. http://cgo-sreznevskyi.kyiv.ua/uk/diialnist/klimatolohichna/klimatychni-dani-po-kyievu

Bourbia, F., & Boucheriba, F. (2010). Impact of street design on urban microclimate for semi arid climate (Constantine). *Renewable Energy*, *35* (2), 343–347. https://doi.org/10.1016/j.renene.2009.07.017

European Committee for Standardization [CEN]. (2005). *Ergonomics of the thermal environment – analytical determination and interpretation of thermal comfort using calculation of the PMV and PPD indices and local thermal comfort criteria* (EN ISO 7730).

Fischer, E. M., Oleson, K. W., & Lawrence, D. M. (2012). Contrasting urban and rural heat stress responses to climate change. *Geophysical Research Letters*, *39* (3), 1–8. https://doi.org/10.1029/2011GL050576

Gulyás, Á., Unger, J., & Matzarakis, A. (2006). Assessment of the microclimatic and human comfort conditions in a complex urban environment: modelling and measurements. *Building and Environment*, *41* (12), 1713–1722. https://doi.org/10.1016/j.buildenv.2005.07.001

Heusinkveld, B. G., Steeneveld, G. V., Hove, L. W. A. van, Jacobs, C. M. J., & Holtslag, A. A. M. (2014). Spatial variability of the Rotterdam urban heat island as influenced by urban land use. *Journal of Geophysical Research: Atmospheres*, *119* (2), 677–692. https://doi.org/10.1002/2012JD019399

International Organization for Standardization [ISO]. (2017). *Ergonomics of the thermal environment – assessment of heat stress using the WBGT (wet bulb globe temperature) index* (ISO 7243:2017).

Kedissa, C., Outtas, S., & Belarbi, R. (2016). The impact of height/width ratio on the microclimate and thermal comfort levels of urban courtyards. *International Journal of Sustainable Building Technology and Urban Development*, 7 (3–4), 174–183. https://doi.org/10.1080/2093761X.2017.1302830

Korkina, E. V., Gorbarenko, E. V., Voitovich, E. V., Tyulenev, M. D., & Kozhukhova, N. I. (2023). Temperature Evaluation of a Building Facade with a Thin Plaster Layer under Various Degrees of Cloudiness. *Energies*, *16* (15), 5783. https://doi.org/10.3390/en16155783

Li, C., & Zhang, N. (2021). Analysis of the daytime urban heat island mechanism in East China. *Journal of Geophysical Research: Atmospheres*, *126* (12), e2020JD034066. https://doi.org/10.1029/2020JD034066

Luo, M., & Lau, N. C. (2018). Increasing heat stress in urban areas of eastern China: Acceleration by urbanization. *Geophysical Research Letters*, *45* (23), 13,060–13,069. https://doi.org/10.1029/2018GL080306

Prasad, K., Anchan, S. S., Kamath, S., & Akella, V. (2017). Impact of building orientation on energy consumption in the design of green building. *International Journal of Emerging Research in Management & Technology*, *6* (2), 8–11. Retrieved from: https://www.researchgate.net/publication/326478143

Ratushniak, H. S., & Popova, H. S. (2004). *Building thermal physics*. VNTU.

Smith, P., Lamarca, C., & Henríquez, C. (2019). A comparative study of thermal comfort in public spaces in the cities of Concepción and Chillán, Chile. In C. Henríquez & H. Romero (Eds), *Urban Climates in Latin America* (pp. 111–134). Springer International Publishing. https://doi.org/10.1007/978-3-319-97013-4_6

Steeneveld, G. J., Koopmans, S., Heusinkveld, B. G., Van Hove, L. W. A., & Holtslag, A. A. M. (2011). Quantifying urban heat island effects and human comfort for cities of variable size and urban morphology in the Netherlands. *Journal of Geophysical Research: Atmospheres*, *116*, D20129. https://doi.org/10.1029/2011JD015988

Sviatohorov, I. O. (2024). Increased heat stress for the population of urbanized areas against the background of global climate change. *Environmental Safety and Natural Resources*, *49* (1), 49–59. https://doi.org/10.32347/2411-4049.2024.1.49-59

Teller, J., & Azar, S. (2001). Townscope II – A computer system to support solar access decision-making. *Solar Energy*, *70* (3), 187–200. https://doi.org/10.1016/S0038-092X(00)00097-9

Ukrainian Scientific-Research and Training Center of Standardization, Certification and Quality Problems [UkrNDNC]. (2022). *Enerhetychna efektyvnist budivel. Metod rozrakhunku enerhospozhyvannya pid chas opalennya, okholodzhennya, ventylyatsiyi, osvitlennya ta haryachoho vodopostachannya* [*Energy efficiency of buildings. Method for calculating energy consumption during heating, cooling, ventilation, lighting and hot water supply*] (DSTU 9190).

Willett, K. M., & Sherwood, S. (2012). Exceedance of heat index thresholds for 15 regions under a warming climate using the wet-bulb globe temperature. *International Journal of Climatology*, *32* (2), 161–177. https://doi.org/10.1002/joc.2257

Zeng, Y., & Dong, L. (2015). Thermal human biometeorological conditions and subjective thermal sensation in pedestrian streets in Chengdu, China. *International Journal of Biometeorology*, *59*, 99–108. https://doi.org/10.1007/s00484-014-0883-8

Summary

The influence of urban building orientation on the risk of heat stress from being in the courtyard area during the peak summer period. The research assesses the risk of heat stress and improvements related to the comfort of being outdoors for an urban population. The specialized TownScope program, banks of monitoring data of the Copernicus Climate Change Service and the Borys Sreznevsky Central Geophysical Observatory were all used for the calculations. The calculations were made for the 1st climatic zone of Ukraine. On the example of the city of Kyiv and the Kyiv region, a widespread U-shaped construction scheme of a five-section, nine-story residential building was chosen. In the calculations, the influence of the surrounding buildings was excluded, and the surface of the courtyard was free of trees and bushes to exclude the influence of unpredictable shading in the calculations. To obtain the calculation data, the authors prepared a corresponding 3D model of the building and exported it in the 3Ds format. The temperature of the facades and the courtyard at different orientations with respect to the cardinal points was calculated. Graphs of the dependence of the amount of direct solar radiation falling on the surface per hour during daylight hours were plotted. The heating temperature of the surfaces of building facades and the underlying surface from solar radiation during one hour of daylight was determined according to the formula by A.M. Shklover. This study makes it possible to apply relevant innovative technologies of "green construction", both at the design stage and during the operation of an existing building.

Scientific Review Engineering and Environmental Sciences (2024), 33 (4), 401–418

Sci. Rev. Eng. Env. Sci. (2024), 33 (4) https://srees.sggw.edu.pl

ISSN 1732-9353 (suspended) eISSN 2543-7496 DOI 10.22630/srees.9956

Received: 10.09.2024
Accepted: 17.10.2024

Sergii SURKOV[1]
Volodymyr KRAVCHENKO[3]
Iryna KORDUBA[2]
Andrii GOLOVCHENKO[3]
Oleksandr BUTENKO[1]
Serhii TSYBYTOVSKYI[2]✉
Yuliia TRACH[4]

[1] Odesa Polytechnic National University, Institute of Distance and Correspondence Education, Ukraine
[2] Kyiv National University of Construction and Architecture, Department of Environmental Protection Technologies and Labor Protection, Ukraine
[3] Odesa Polytechnic National University, Nuclear Power Plants Department, Ukraine
[4] Warsaw University of Life Sciences – SGGW, Institute of Civil Engineering, Poland
National University of Water and Environmental Engineering, Institute of Agroecology and Land Management, Ukraine

Use of an ejector to reduce the time of air injection during testing of the containment system at nuclear power plants

Keywords: airtight enclosure system, air injection time, optimal ejector design

Introduction

The further development of nuclear energy is based on three main principles: safety, cost-effectiveness, and public attitude (Shirokov, 1997). All these principles are interrelated. To ensure safe operation, nuclear power plants (NPPs) are

✉serhii.uaror@gmail.com

Surkov, S., Kravchenko, V., Korduba, I., Golovchenko, A., Butenko, O., Tsybytovskyi, S., Trach, Y. (2024). Use of an ejector to reduce the time of air injection during testing of the containment system at nuclear power plants. *Sci. Rev. Eng. Env. Sci.*, *33* (4), 401–418. DOI 10.22630/srees.9956

equipped with the necessary safety systems that prevent accidents and are designed to keep equipment from being destroyed in the case of accidents. Localizing safety systems are designed to contain radioactive substances within the unit and prevent their release into the environment. Of course, the availability of safety systems affects both the cost and operational performance of a nuclear power plant.

In ensuring the required level of safety, the cost performance of power plants is crucial when deciding on the choice of an energy source. Therefore, nuclear power is always in competition with other energy sources; recently it was gas power plants while today it is renewable energy sources, as these already have specific capital investments at the level of nuclear power plants or less. However, today they are losing in terms of cost and unstable electricity production. It should be noted that the development of electricity storage solves the latter drawback and makes wind and solar power plants more popular, as they do not pose a nuclear threat. Thus, it should be emphasized that only the economic advantages of NPPs make them more acceptable in the market today.

Thus, during the NPP operation, great attention is paid to the safety systems that serve to maintain the integrity of the safety barriers. The latter are designed to prevent the release of radioactive fission products into the environment in the event of an accident. The containment system is the last system to prevent fission products from being released to the environment in the event of a severe accident. To confirm the readiness of this system to perform its functions in the event of an accident, appropriate leakage tests are performed after each repair.

The "absolute pressure" method is used to test the level of sealing of the containment system and elements of the accident localization system at Ukrainian NPPs. According to this method, the mass of air available in the CSA is determined by measuring the pressure, temperature and humidity according to the Mendeleev–Clapeyron equation. The tests consist of five stages: vacuuming; air injection to achieve the required pressure of 1.72 kg·cm^{-2}; stabilization of the parameters; measurement; and pressure release, as well as lasting more than 25 h. No work is carried out in the CSO during the tests. A compressor is used to provide the overpressure in the CSF and, given the large volume of the CSF, it takes a relatively long time to inject the air, which affects the economic performance of the NPP (Kravchenko et al., 2023).

Literature review and problem statement

In Kravchenko et al. (2022), it was proposed to use an ejector, the working medium for which is air after the compressor, to reduce the time of air injection. In this case, the ejector was calculated, its characteristic constructed, and the injection

time determined. A number of assumptions were made in the calculations, which is why the results were obtained with a corresponding error. It should be noted that equipment for cleaning the air of dust and moisture is installed directly after the compressor. Accordingly, when using the ejector, the air that is drawn into the ejector must also be cleaned of dust and moisture. The availability of this equipment was not considered on paper by Kravchenko et al. (2022). The presence of additional resistance at the inlet of the air drawn into the ejector should lead to a decrease in the air flow at the outlet of the ejector and an increase in the time of air injection to the required pressure in the CSO.

The aim of this study is to clarify the results obtained in a paper by Kravchenko et al. (2022), regarding minimizing the time for air injection into the CSU during leakage tests. To achieve this goal, the following tasks were performed:

- An algorithm for calculating the gas ejector was developed, adapted to the case when the full pressures in all nozzles are set.
- The dynamics of air injection into the CSO under variable pressure were then calculated and the injection time determined.
- The dynamics of air injection into the CSO under variable pressure were then calculated and the injection time determined.
- The design and operational factors that affect this time were determined.
- The ejector design was optimized with respect to the minimum air injection time.

Compressor operation without an ejector

Before starting the calculation of the ejector itself, it is necessary to build a characteristic for the gas compressor that injects the working air flow.

To solve this problem, the first step is to obtain the compressor characteristic in the form of the flow versus the backpressure at the outlet. In addition, it is advisable to immediately convert the volume flow rate to a mass flow rate, given that the 'normal cubic meters' are calculated at an air temperature of 0°C. In this case, the mass air supply is calculated as follows:

$$G = \rho Q = \frac{p_{\text{abc}} Q}{\text{RT}}, \tag{1}$$

where: G – mass air supply [kg·s^{-1}], ρ – air density [kg·m^{-3}], Q – volume flow rate [m^3·s^{-1}]; p_{abc} – absolute pressure (p = 101,325) [Pa], R – specific gas constant (R_{air} = 287) [J·kg^{-1}·K^{-1}], and T – absolute thermodynamic temperature (T = 273.15) [K].

Surkov, S., Kravchenko, V., Korduba, I., Golovchenko, A., Butenko, O., Tsybytovskyi, S., Trach, Y. (2024). Use of an ejector to reduce the time of air injection during testing of the containment system at nuclear power plants. *Sci. Rev. Eng. Env. Sci.*, *33* (4), 401–418. DOI 10.22630/srees.9956

Figure 1 shows the characteristic of the TsK-35/8 centrifugal compressor.

In the AB section, at an overpressure of $p \leq 4.73$ bar, it is convenient to approximate the characteristic by the linear dependence:

$$G = 3.44669 - 0.04554p, \tag{2}$$

where: G – mass flow rate [kg·s^{-1}], p – overpressure at the compressor outlet [bar].

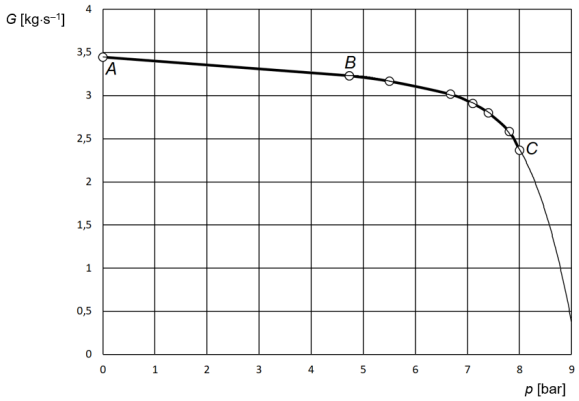

FIGURE 1. Approximation of the characteristics of the TsK-135/8 compressor
Source: own work.

In section BC, at an overpressure of $p > 4.73$ bar, a fourth-degree polynomial approximation is used:

$$G = -0.02774 \cdot p^4 + 0.6588 \cdot p^3 - 5.85566 \cdot p^2 + 22.94649 \cdot p - 30.13195.$$

This approximation provides a high value of the coefficient of agreement, $R^2 = 0.9987$. In addition, this approximation allows the characterization to be extended to the right of point C by extrapolation.

Since the overpressure in the CSO does not exceed 0.7 bar, the compressor characteristics in this range are described by a linear relationship. The fill time can then be determined analytically.

The differential equation describing the filling process can be represented as:

$$\frac{dm}{dt} = G(m), \tag{3}$$

where: m – mass of air inside the SGU [kg], $G(m)$ – mass flow rate of the air entering the SGU [kg·s^{-1}].

Hence:

$$dt = \frac{dm}{G(m)}. \tag{4}$$

This allows the calculation of certain integral:

$$t = \int_{m_1}^{m_2} \frac{dm}{G(m)}, \tag{5}$$

where: m_1 and m_2 – masses of air inside the containment at the beginning and end of the filling process.

The mass of air in the containment vessel is determined using a gas equation (Mendeleev–Clapeyron):

$$m = \frac{pv}{\mathrm{RT}}, \tag{6}$$

where: V – volume of air in the SGO [m^3].

We get m_1 = 72.260 kg and m_2 = 121.235 kg.

Absolute pressure is related to mass:

$$p_{\mathrm{abc}} = \frac{m\mathrm{RT}}{v}. \tag{7}$$

But the compressor characteristic (2) uses an overpressure expressed in bars. We can define it by the formula

$$p = \frac{p_{\mathrm{abc}} - 101{,}325}{100{,}000} = \frac{m\mathrm{RT}}{100{,}000 \cdot v} - 1.01325 \text{ [bar]}.$$

Then the dependence of the compressor supply on the mass of air in the CSO is described by the equation:

$$G(m) = 3.44669 - 0.045543\left(1.40223 \cdot 10^{-5} m - 1.01325\right) = 3.40054 - 6.38619 \cdot 10^{-7} m. \tag{8}$$

Surkov, S., Kravchenko, V., Korduba, I., Golovchenko, A., Butenko, O., Tsybytovskyi, S., Trach, Y. (2024). Use of an ejector to reduce the time of air injection during testing of the containment system at nuclear power plants. *Sci. Rev. Eng. Env. Sci.*, *33* (4), 401–418. DOI 10.22630/srees.9956

Integrating (5), we obtain the time for filling the CSO:

$$t = \int_{m_1}^{m_2} \frac{dm}{3.40054 - 6.38619 \cdot 10^{-7} m} = \frac{\ln\left(3.40054 - 6.38619 \cdot 10^{-7} m\right)}{-6.38619 \cdot 10^{-7}} \Big|_{m_1}^{m_2}. \quad (9)$$

The time is equal to 14,274 s or 3.965 h. The result obtained analytically is the same as the result of the numerical integration.

Calculation of a gas ejector (jet compressor)

Although gas ejectors have long been known and are widely used in various industries, research on ejectors continues. Their typical use is in the oil and gas industries (Carpenter, 2020; Ping & Macdonald, 2020; Bernat et al., 2023), and in the energy industry (Sammak et al., 2021).

A number of studies have been devoted to optimizing the geometry of ejectors. For this, 1D models (Wang et al., 2021; Van den Berghe et al., 2022) and 3D models are used (Butenko & Smyk, 2015; Shi et al., 2024), as well as neural networks (Gupta et al., 2021).

Further improvement of the ejectors is possible due to the use of pulse ejectors (Voropaiev et al., 2021), gas-wave ejectors (Li et al., 2024), and vortex separation ejectors (Novruzova & Qadashova, 2020).

The peculiarity of our calculation is that we need to minimize the time of increasing the air pressure in the CSA by means of the ejector, considering the fact that the pressure inside the CSA is continuously changing. This led to the need to change the sequence of calculations within the classical mathematical model of the ejector.

Figure 2 shows the design scheme of an ejector with a cylindrical mixing chamber. The figure shows the parameters of the working, ejected and mixed flow, as well as the main sections for which the equations are drawn up.

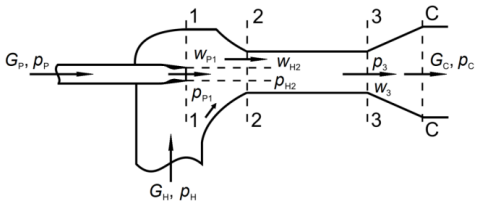

FIGURE 2. Design scheme of the gas ejector

Source: own work.

The equations describing the operation of the ejector include the continuity equations:

$$G_p + G_H = G_c. \tag{10}$$

As well as the equation of conservation of momentum of the quantity of motion:

$$\varphi_2 \left(G_p w_{p_2} + G_H w_{H_2} \right) - \left(G_p + G_H \right) w_3 = \left(p_3 + p_{p_2} \right) f_{p_2} + \left(p_3 + p_{H_2} \right) f_{H_2}, \tag{11}$$

where: φ_2 – velocity coefficient of the mixing chamber, w_i – gas velocities in the corresponding sections [m·s^{-1}], p_i – absolute gas pressures of gas velocities in the corresponding sections [Pa], and f_i – cross-sectional areas [m^2].

The usual assumption of pressure equality is used:

$$p_{p_2} = p_{p_1} = p_H. \tag{12}$$

The presence of energy losses in different parts of the ejector is considered using velocity coefficients. The following values of speed coefficients are recommended:
- working nozzle: $\varphi_1 = 0.95$,
- mixing chamber (MC): $\varphi_2 = 0.975$,
- diffuser: $\varphi_3 = 0.9$,
- inlet section of the CP: $\varphi_4 = 0.925$.

The peculiarity of supersonic gas ejector calculations is that they consider the compressibility of gases. In this case, the speed of the working flow usually exceeds the speed of sound. Traditionally, gas-dynamic functions are used in the calculated-reduced pressure:

$$\Pi(\lambda) = \left(1 - \frac{k-1}{k+1} \lambda^2 \right)^{\frac{k}{k-1}} \tag{13}$$

and reduced mass velocity

$$q(\lambda) = \left(\frac{k+1}{2} \right)^{\frac{k}{k-1}} \lambda \left(1 - \frac{k-1}{k+1} \lambda^2 \right)^{\frac{k}{k-1}}, \tag{14}$$

where: λ – reduced velocity, k – adiabatic index.

Surkov, S., Kravchenko, V., Korduba, I., Golovchenko, A., Butenko, O., Tsybytovskyi, S., Trach, Y. (2024). Use of an ejector to reduce the time of air injection during testing of the containment system at nuclear power plants. *Sci. Rev. Eng. Env. Sci.*, *33* (4), 401–418. DOI 10.22630/srees.9956

We assume that the main geometric parameter, the ejector module, is given:

$$M = \frac{f_3}{f_{p^*}}, \tag{15}$$

where: f_3 – cross-sectional area of the cylindrical mixing chamber [m^2], f_{p^*} – critical cross-sectional area of the working air nozzle [m^2].

The total pressure in all three nozzles is also given, and therefore the air compression ratio:

$$\varepsilon = \frac{p_c}{p_H}. \tag{16}$$

It is necessary to determine the air flow rate in all nozzles and the ejection coefficient: $u = \frac{G_H}{G_p}$.

Working flow

First of all, the parameters of the working flow can be calculated since it does not depend on the ejection ratio. The working air flow rate is set based on the compressor capacity.
The gas-dynamic function is calculated as follows:

$$\Pi_{p_2} = \frac{p_H}{p_p}. \tag{17}$$

Using (6), the reduced velocity can be determined analytically:

$$\lambda_{p_2} = \sqrt{\frac{k+1}{k-1}\left[1 - \Pi_{p_2}^{\frac{k-1}{k}}\right]}. \tag{18}$$

It should be borne in mind that the velocity at the outlet of the working nozzle is usually supercritical, i.e., $\lambda_{p_2} > 1$. The reduced mass velocity q_{p_2} is calculated using (18). Next, the outlet cross-sectional area of the nozzle is calculated:

$$f_{p_2} = \frac{f_{p^*}}{q_{p_2}}. \tag{19}$$

The cross-sectional area of the ejected flow is 2-2:

$$f_{H_2} = f_3 - f_{p_2} v. \tag{20}$$

Critical speed at a given air temperature:

$$a_* = \sqrt{\frac{2k}{k+1}}\mathrm{RT}. \tag{21}$$

Working fluid velocity at the nozzle outlet

$$w_{p_2} = \varphi_1 a_* \lambda_{p_2}. \tag{22}$$

In most literature, when calculating the ejector characteristics, the ejection coefficient u is set and the compression ratio ε is calculated. However, with this calculation sequence, it is difficult to determine the maximum value of the ejection coefficient, which significantly reduces the accuracy of calculating the filling time of the CSO.

In the course of the work, the calculation methodology was improved and it was proposed to set the compression ratio ε and calculate the ejection coefficient. In this case, the convergence of the results is significantly improved.

The calculation of the ejector characteristic is performed under the assumption that the air movement is adiabatic. In this case, the characteristic would have the form ABC (Fig. 3). It should be noted that on the ABC line, each value of the ejection coefficient corresponds to two values of the compression coefficient, which led to poor convergence of the iterative process using the Gauss–Seidel method.

It is known from experiments that when the speed of sound reaches Section 3-3, the so-called flow closure occurs. In this case, despite changes in pressure, the air velocity in the critical section remains constant and equal to the local speed of sound. This phenomenon corresponds to the vertical section BD in Figure 3, and the real characteristic of the ejector is ABD.

In addition, it is theoretically possible to close the flow in Sections 1-1 and 2-2, but these critical modes are not realized under the studied parameters.

Surkov, S., Kravchenko, V., Korduba, I., Golovchenko, A., Butenko, O., Tsybytovskyi, S., Trach, Y. (2024). Use of an ejector to reduce the time of air injection during testing of the containment system at nuclear power plants. *Sci. Rev. Eng. Env. Sci.*, *33* (4), 401–418. DOI 10.22630/srees.9956

Mixed flow

At each step, the value of λ_{c_3} is set in the range from 0 to 1. The condition λ_{c_3} ensures that the mixed flow velocity is subsonic.

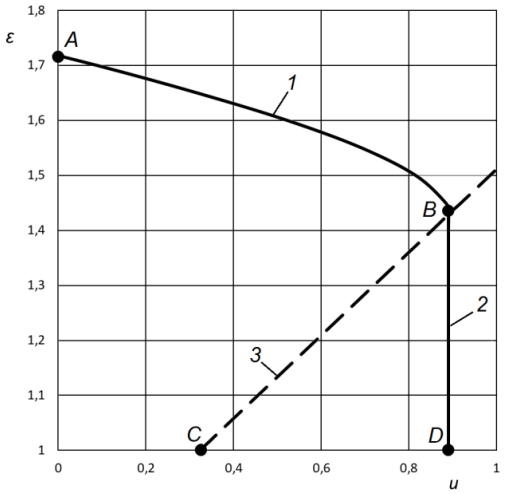

FIGURE 3. Calculated characteristic of the ejector at $M = 8.6$ (1 – adiabatic characteristic, 2 – short-circuit mode in Section 3-3, 3 – critical mode limit in Section 3-3)

Source: own work.

For a given value of λ_{c_3}, we determine the values of the gas-dynamic functions λ_{c_3} and q_{c_3} pressure at the outlet of the mixing chamber:

$$p_3 = \Pi_{c_3}. \tag{23}$$

Mixed flow velocity in Section 3-3 is calculated as follows:

$$w_3 = \frac{a_* \lambda_{c_3}}{\varphi_3}, \tag{24}$$

where: φ_3 – diffuser velocity coefficient.

Since the modulus of the ejector is given, we determine the cross-sectional area of the CS:

$$f_3 = M f_{p*} \tag{25}$$

and then the mixed flow rate:

$$G_c = \frac{k\Pi_* p_c q_{c_3} f_3}{a_*}. \tag{26}$$

Therefore, the flow is ejected.

From the mass conservation equation, we determine the mass flow rate:

$$G_H = G_c - G_p. \tag{27}$$

In the case of a cylindrical mixing chamber:

$$f_{H_2} = f_3 - f_{p_2}. \tag{28}$$

The reduced mass velocity of the ejected flow in Section 2-2:

$$q_{H_2} = \frac{G_H a_*}{k_H \Pi_{H*} p_H f_{H_2}}. \tag{29}$$

Knowing q_{H_2}, it is impossible to determine the reduced velocity λ_{H_2} analytically, so it is determined by the numerical method. After that, Π_{H_2} is determined.

Ejected flow velocity in Section 2-2 is calculated as follows:

$$w_{H_2} = \varphi_4 a_* \lambda_{H_2}, \tag{30}$$

Then the pressure of the ejected flow in Section 2-2:

$$p_{H_2} = \Pi_{H_2} p_H. \tag{31}$$

All the found values are substituted into the momentum balance equation (11) and the inviscidity is calculated, i.e., the difference in the total momentum from zero.

The subroutine for determining the root of a nonlinear algebraic equation automatically changes the value of λ_{c_3} in a given range until this inviscidity becomes zero with a given permissible error. Thus, at a given pressure p_c the value of λ_{c_3} is determined such that the law of mass conservation (5) and the law of momentum conservation (11) are fulfilled. After specifying λ_{c_3}, the ejection coefficient u can be determined. Figure 4 shows the dependence of the flow compression ratio ε as a function of the ejection coefficient *u* at three values of the ejector module.

Surkov, S., Kravchenko, V., Korduba, I., Golovchenko, A., Butenko, O., Tsybytovskyi, S., Trach, Y. (2024). Use of an ejector to reduce the time of air injection during testing of the containment system at nuclear power plants. *Sci. Rev. Eng. Env. Sci.*, *33* (4), 401–418. DOI 10.22630/srees.9956

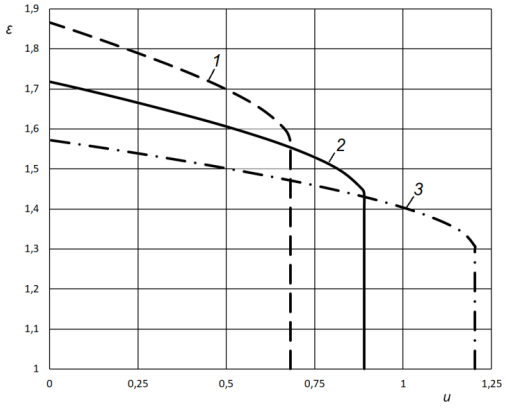

FIGURE 4. Dependence of the flow compression ratio ε to the ejection coefficient *u*
Source: own work.

Characteristics of ejectors at different modulus values:

$$1 - M = 7.0;\ 2 - M = 8.6;\ 3 - M = 11.0 \tag{32}$$

Figure 4 shows that ejectors that provide high ejection rates have a limited compression ratio. Our goal is to find an ejector module that provides an optimal balance between these indicators.

Based on the obtained characteristics, the next step is to model the dynamics of air injection into the CSO to determine the optimal ejector module.

Dynamics of the process of air injection into the CSU

The pressure in the CSA is related to the mass of the gas contained there, based on the equation of the state of gas or the Mendeleev–Clapeyron equation. The dependence of air mass on time is expressed by the differential equation (3). The calculation of the dynamics of filling the containment is reduced to the numerical solution of the differential equation (3). The solution was performed using the Runge–Kutta–Felberg method of the fourth order or fifth of accuracy with automatic selection of the integration step.

The dependence of the pressure in the zones on time at different ejector modules is shown in Figure 5.

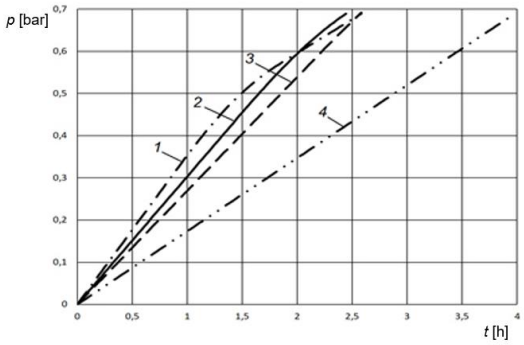

FIGURE 5. Dynamics of pressure change in the SG at different ejector modules (1 – M = 7.0; 2 – M = 8.6; 3 – M = 11.0; 4 – compressor without ejector)

Source: own work.

Curve 4 in Figure 5 shows the filling of the storage tank directly from the compressor without the use of an ejector. The figure shows that in this case, the filling time is maximum and is approximately 4 h. Curve 3 shows the dynamics of filling the storage tank with an ejector module of 7.0. The filling rate remains at the approximately constant, albeit low. Curve 1 corresponds to a module of 11.0. At the beginning the filling rate is high, but in the upper part of the graph the ejection ratio decreases, and in fact one compressor is working. Finally, Curve 2 corresponds to a modulus of 8.6, which ensures the shortest possible filling time.

Figure 6 shows the dependence of the charge time on the ejector module.

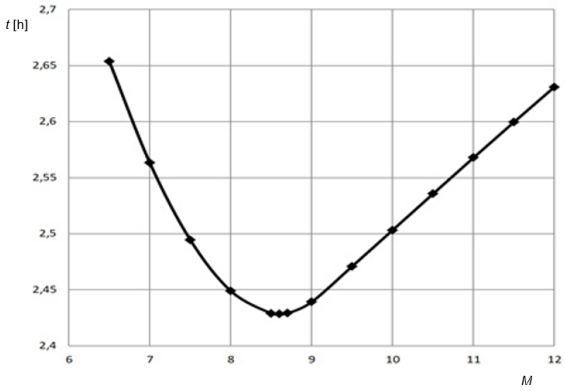

FIGURE 6. Dependence of the time of filling of the ZO on the ejector module

Source: own work.

Surkov, S., Kravchenko, V., Korduba, I., Golovchenko, A., Butenko, O., Tsybytovskyi, S., Trach, Y. (2024). Use of an ejector to reduce the time of air injection during testing of the containment system at nuclear power plants. *Sci. Rev. Eng. Env. Sci.*, *33* (4), 401–418. DOI 10.22630/srees.9956

Figure 6 shows that the shortest filling time is achieved with a module of 8.6 and is approximately 2.43 h. This means that the use of an ejector reduces the filling time by 38.8%.

Figure 7 shows the dependence of the filling time of the ash container on the overpressure in front of the working nozzle.

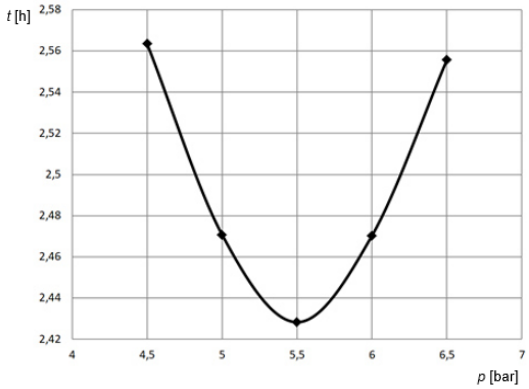

FIGURE 7. Dependence of the filling time of the nozzle on the pressure before the nozzle
Source: own work.

Figure 7 shows that the optimal overpressure is 5.5 bar. The fact is that at high compressor outlet pressures, the compressor flow rate decreases. In this case, despite the high ejection coefficients, the total flow rate at the ejector outlet decreases.

Effect of additional resistances

When calculating the air injection to the cooling zone, it is necessary to consider the effect of the air filters, which represent an additional hydraulic resistance.

The preliminary calculation uses the velocity coefficients φ, which are related to loss coefficients ζ by the ratio:

$$\zeta = \frac{1}{\varphi^2}. \tag{33}$$

The additional drag coefficient (ζ_D) affects the velocity coefficient as follows:

$$\varphi = \frac{1}{\sqrt{\zeta + \zeta_D}}. \tag{34}$$

There is currently no reliable information on the loss factor. The data sheet of the dust filter installed at the compressor outlet shows that its aerodynamic resistance is 0.1 bar. If we assume that the resistance of the moisture separator will be equal to 0.1 bar, then we note that the total resistance of the two filters that must be additionally installed at the inlet of the air drawn into the ejector will be equal to Δp = 0.2 bar with a filter nozzle diameter of D = 0.15 m. To determine the appropriate loss factor, we can perform the calculation under the conditions of installation directly behind the compressor.

– for volume flow to the compressor:

$$Q = \frac{G}{\rho} = \frac{3.4}{1.2} = 2.83 \text{ m} \cdot \text{s}^{-1}, \tag{35}$$

– for air velocity:

$$w = \frac{4Q}{\pi D^2} = \frac{4 \cdot 2.83}{\pi \cdot 0.15^2} = 160 \text{ m} \cdot \text{s}^{-1}, \tag{36}$$

– then the additional loss factor:

$$\zeta_D = \frac{2\Delta p}{\rho w^2} = \frac{2 \cdot 20{,}000}{1.2 \cdot 160^2} = 1.3. \tag{37}$$

According to Equation 34, we obtain φ_4 = 0.636. The calculated characteristic of the ejector with this value of the speed coefficient is shown in Figure 8.

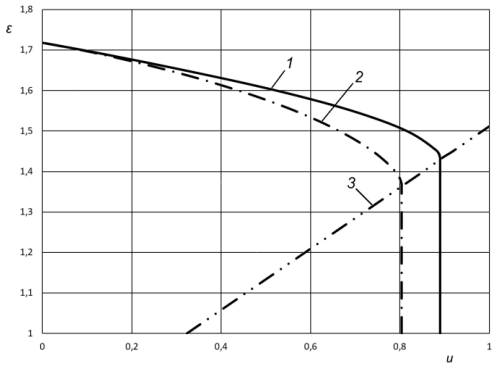

FIGURE 8. Effect of additional resistance on the ejector characteristic: 1 – φ_4 = 0.925 (standard settings), 2 – φ_4 = 0.636 (filter at the input), 3 – critical mode limit in Section 3-3

Source: own work.

The calculations of the dynamics of the process of filling the CSO show that, in the presence of additional resistances, the useful effect of the ejector decreases. When a filter is installed at the inlet of the suction flow, the estimated time for filling the CSG is 2.56 h. That is, the reduction in filling time due to the ejector is 35.5%.

Although the installation of the filter somewhat reduces the useful effect of using the ejector, the reduction in air injection time by 35.5% is significant. The installation of the ejector can be recommended for practical implementation.

Conclusions

In this work, we have developed an algorithm for calculating a gas ejector, which differs from the classical algorithm in the sequence of calculations and uses modern numerical methods. The modeling of the process of filling the gas ejector was performed by numerical solution of the differential equation. The air injection time is optimized by two parameters – the ejector module and the compressor outlet pressure.

The calculation shows that the ejector can reduce the time of filling the CSA by 38.8%, which will reduce the total test time.

The presence of a filter at the inlet of the ejected air reduces the effect of using the ejector: the reduction in discharge time will be equal to 35.5%.

Further theoretical and experimental studies are needed to clarify the results obtained.

References

Bernat, M., Nagy, S., & Smulski, R. (2023). Use of a New Gas Ejector for a TEG/TREG Natural Gas Dehydration System. *Energies*, *16* (13), 5011. https://doi.org/10.3390/en16135011

Butenko, O. G., & Smyk, S. Y. (2015). Improvement of the central ejector efficiency under nonoptimal operating modes. *Scientific Bulletin of National Mining University*, *2*, 57–61.

Carpenter, C. (2020). Installation of gas ejector provides boost to low-pressure gas well. *Journal of Petroleum Technology*, *72* (11), 69–70. https://doi.org/10.2118/1120-0069-JPT

Gupta, P., Kumar, P., & Rao, S. M. (2022). Artificial neural network model for single-phase real gas ejectors. *Applied Thermal Engineering*, *201* (Part A), 117615. https://doi.org/10.1016/j.applthermaleng.2021.117615

Kravchenko, V. P., Vlasov, A. P., Holovchenko, A. M., Mazurenko, A. S., Dubkovsky, V. O., & Chulkin, O. O. (2023). Status and prospects of testing the hermetic enclosure system of the reactor plant with VVER-1000 for tightness. *Nuclear and Radiation Safety*, *2* (98), 53–60.

Kravchenko, V., Vlasov, A., Andryuschenko, A., Vlasov, D., Golovchenko, A., & Gavrilov, P. (2022). Reduced air injection time during containment testing due to the use of an ejector. *Proceedings of Odessa Polytechnic University*, *1* (65), 62–69.

Li, H., Zhao, Y. & Hu, D. (2024). Simulation and analysis of pressure waves in flow channels of axial and radial gas wave ejectors. *Recent Patents on Engineering* (in press). http://dx.doi.org/10.2174/0118722121321712240724075604

Novruzova, S. G., & Qadashova, E. V. (2020). Possibility of vortex separation ejector application in the collection and separation of gas. *News of the Academy of Sciences of the Republic of Kazakhstan, Series of Geology and Technical Sciences*, *5* (443), 150–155. https://doi.org/10.32014/2020.2518-170X.115

Ping, W. & Macdonald, B. (2020, October 25). *Giving a boost to low pressure gas well by installing gas ejector* [Conference session]. SPE/IATMI Asia Pacific Oil & Gas Conference and Exhibition, Bali, Indonesia. https://doi.org/10.2118/196440-MS

Sammak, M., Ho, C., Dawood, A., & Khalidi, A. (2021). Improving combined cycle part load performance by using exhaust gas recirculation through an ejector. *Turbo Expo: Power for Land, Sea, and Air*, *84966*, V004T06A012. https://doi.org/10.1115/GT2021-59358

Shi, H., Wang, R., Xiao, Y., Zhu, X., Zheng, R., Song, C., & Liu, Z. (2024). Optimization of exhaust ejector with lobed nozzle for marine gas turbine. *Brodogradnja*, *75* (3), 75303. http://dx.doi.org/10.21278/brod75303

Shirokov, S. V. (1997). *Yadernyye energeticheskiye reaktory* [*Nuclear power reactors*]. KPI.

Van den Berghe, J., Dias, B. R., Bartosiewicz, Y., & Mendez, M. A. (2023). A 1D model for the unsteady gas dynamics of ejectors. *Energy*, *267*, 126551. https://doi.org/10.1016/j.energy.2022.126551

Voropaiev, G. O., Zagumennyi, I. V., & Rozumnyuk, N. V. (2021). Modeling of gas – dynamic processes in the elements of impulse ejector. *Journal of Numerical and Applied Mathematics*, *1* (135), 66–72. https://doi.org/10.17721/2706-9699.2021.1.08

Wang, Z., Wang, S., Li, Y., Chen, L., & Zhang, H. (2021). Design and numerical investigation of ejector for gas pressurization. *Asia-Pacific Journal of Chemical Engineering*, *16* (3), e2625. https://doi.org/10.1002/apj.2625

Summary

Use of an ejector to reduce the time of air injection during testing of the containment system at nuclear power plants. The containment system (CS) is the last barrier to the release of radioactive substances into the environment in the event of a nuclear accident. After each overload, this system is tested for its ability to perform its functions by determining the integral leakage, which should not exceed a certain value. The tests are

Surkov, S., Kravchenko, V., Korduba, I., Golovchenko, A., Butenko, O., Tsybytovskyi, S., Trach, Y. (2024). Use of an ejector to reduce the time of air injection during testing of the containment system at nuclear power plants. *Sci. Rev. Eng. Env. Sci.*, *33* (4), 401–418. DOI 10.22630/srees.9956

performed at an overpressure in the CS of 0.72 kg·cm^{-2}, which is achieved by injecting air with a compressor. The paper considers the use of an ejector to accelerate the injection process, which has a positive effect on the technical and economic performance of a nuclear power plant (NPP) power unit by increasing the amount of electricity generated, which is very important today, when the NPPs provide the maximum share of electricity generated in the country. Previous studies have evaluated the use of an ejector for this purpose, but they did not consider the need to install filters on the intake air stream. In addition, they used numerical methods that generate an error. The present work uses a mathematical apparatus that provides a more accurate result. The obtained calculated compressor injection time coincides with the actual injection time for the Rivne NPP power units. The design of the ejector ensures the minimum injection time is determined. The optimal ejector module is equal to 8.6 (the ratio of the cross-sectional area of the cylindrical mixing chamber to the critical cross-sectional area of the working air nozzle). This reduces the injection time by 38.8%. The suction air must be free of dust and moisture. Suitable filters have a total aerodynamic resistance of 0.2 bar. Taking these air filters into account slightly reduces the efficiency of the ejector. The final time of air injection using the ejector is 2.56 h, which reduces the time of air injection for testing by 35.5%.

Scientific Review Engineering and Environmental Sciences (2024), 33 (4), 419–442

Sci. Rev. Eng. Env. Sci. (2024), 33 (4) https://srees.sggw.edu.pl

ISSN 1732-9353 (suspended) eISSN 2543-7496 DOI 10.22630/srees.9760

Received: 07.04.2024
Accepted: 13.08.2024

AGUSTAN[1]✉

Usman RIANSE[2]

Endro SUKOTJO[3]

Arman FASLIH[4]

[1] Universitas Halu Oleo, Faculty of Engineering, Department of Civil Engineering, Indonesia
[2] Universitas Halu Oleo, Faculty of Agriculture, of Agriculture, Indonesia
[3] Universitas Halu Oleo, Faculty of Economics and Business, Department of Economics, Indonesia
[4] Universitas Halu Oleo, Faculty of Engineering, Department of Architecture, Indonesia

Exploration and implementation of a smart tourism destination with the 6As framework & TOPSIS (case study: Wakatobi, Indonesia)

Keywords: Wakatobi, tourism destination, 6As framework, TOPSIS, tourism assessment, smart tourism

Introduction

The tourist industry is a lucrative sector that plays a significant role in the economic development of numerous emerging nations. The provision of government support demonstrates a commitment to further enhance the growth of the tourism industry (Jan & Chaudhry, 2024). The government's endeavors to enhance and broaden tourism offerings are being closely monitored to draw a larger number of both domestic and foreign tourists. A wider range of tourist attractions

✉agustan08edu@uho.ac.id

in an area will create more prospects for increased visitation, benefiting not only the attractions themselves but also the entire region (Khairi & Darmawan, 2021). Management of tourism destinations and suppliers is becoming a top priority and a big challenge (Shen et al., 2020). The tourist business is widely recognized as one of the largest and most rapidly expanding industries globally, exerting a significant impact on the economy. In this sector, progress is contingent upon the choice to visit tourist destinations and the frequency of visitor visits (Sinambela, 2021).

Destinations serve as central hubs for tourist activity and, as a result, are significant areas of focus for the examination of tourism. Nevertheless, they are widely recognized as being challenging to handle because of their intricate networks of parties (Xu et al., 2024). The intricate nature of destinations suggests that they are influenced by a diverse array of factors in both their internal and external surroundings (Fyall & Garrod, 2020). Destination management organizations (DMOs) in heritage tourism prioritize the sustainable growth of tourism. Proponents of smart tourism argue that the use of technology may assist DMOs in maximizing tourist growth by tackling concerns such as the maximum number of visitors a destination can handle, effectively managing the interests of many stakeholders, and promoting community participation (Mandić & Kennell, 2021). A smart tourism destination (STD) is a response to the requirements of modern tourism development and is closely linked to the utilization of information communication and technology (ICT) applications. The intelligent destination is constructed around four primary pillars: technology, innovation, accessibility, and sustainability (Damanik et al., 2022).

Several previous researchers have tried to put forward a definition of a tourism destination, including Goeldner and Ritchie (2003). According to their authoritative textbook, a "tourism destination" refers to a specific geographic area where visitors can engage in different forms of travel experiences. Framke (2010), in his article, sees destinations as units and content. Destinations are perceived as entities at various geographical scales, lacking clear geographical demarcations, and are formed through social activities. Furthermore, the content of the destination is perceived as both a collection of attractions and services, as well as a vibrant collection of attractions, culture, events, landscapes, and services. Finally, United Nations World Tourism Organization defines tourism destination as a tangible area, with or without specific administrative or analytical limits, where a visitor can stay overnight (UNWTO, 2019). A tourist cluster refers to the grouping or co-location of products, services, activities, and experiences along the value chain of tourism. It is considered the fundamental unit of study in the field of tourism. A destination comprises multiple stakeholders and can connect and expand into

larger destinations. Additionally, its image and identity, which are intangible, can impact its market competitiveness (Risty, 2024).

According to Andrianto and Sugiama (2014), for a location to be transformed into a tourist destination, it must satisfy four essential components of tourism known as the 4As: attractions, accessibility, amenities, and ancillary services. Firstly, Goeldner and Ritchie (2003) see attractions as the primary factors that influence prospective visitors in their choice of one destination over another. The attractions were classified and categorized distinctly into five main groups: culture, nature, event, recreation, and entertainment. Then, Leask (2016) also expressed that an attraction is the pivotal matter of the destination appeal and the driver to visit a destination. Secondly, accessibility, according to the explanation by Tamin (1997) that accessibility is how easy or difficult it is to reach a location. It can be used as a performance measure of distance, travel time, or cost. Thirdly, Goeldner and Ritchie (2003) explain in their books that amenities refer to goods and services that are special to a particular place or region, and that enhance the appeal of that location for living and working. The presence of opposing elements and disadvantages renders places unappealing. Natural amenities refer to environmental factors, such as climate, that are primarily unaffected by human influence or intervention. On the other hand, human amenities encompass cultural aspects that are shaped and created by people. Finally, Nichols (n.d.), in her article, explains that ancillary services in the tourism business are supplementary products and services provided to enhance the principal service or product. These services are specifically developed to improve the entire customer experience and offer additional benefits to travelers (Kalaivani et al., 2023).

Buhalis (2000) presents six frameworks that can be used to analyze tourism locations. The six components consist of many types of attractions, including natural, man-made (or purpose-built), heritage, and special events. Accessibility refers to the overall transportation system, which includes routes, terminals, and vehicles. The amenities include hotel and catering facilities, commerce, other tourist services, and offered packages (prearranged packages by intermediaries and principals). Activities refer to the various options and experiences that are offered at a particular destination, which consumers can engage in during their visit. Ancillary services refer to the additional services that are utilized by tourists, such as banking facilities, telephones, postal services, newsagents, hospitals, and so on. The two additional components, namely available packages and activities, can still be calculated separately in the field and can be separated from the previous four main components. Of course, this will make it easier for field assessors to collect data. These 6As frameworks have become one of the core conceptual models of

smart, accessible destinations (Lin et al., 2022). This means that carrying out an independent assessment using the 6As framework in each tourist geographic area has become a necessity in efforts and steps to fulfill smart destination qualifications for visitor satisfaction. As explained by Buhalis and Amaranggana (2014), smart tourism destinations employ systems to enhance the tourism experience and optimize resource management. This is done to maximize both the competitiveness of the destination and the satisfaction of consumers, while also demonstrating sustainability over a long period. These destination services have been tested by Um and Chung (2019) in three tourist destination cities in South Korea and have had a positive effect on tourist satisfaction.

Sequentially, the research carried out in Venice and Salzburg (Buonincontri & Micera, 2016) stated that the 6As framework by Buhalis (2000) is useful and relevant for smart cities chosen as destinations and also for cloud computing services to connect all the 6As of the destination. A year later, Spanish researchers firmly stated the new $(SA)^6$ framework of STDs in their methodology (Tran et al., 2017). However, the six main frameworks still use Buhalis' 6As framework. They managed to decipher it into each of them, which was concretized in 57 total specific indicators in the table, including the addition of the word "smart" to each of the 6A elements. Huertas et al. (2019) in their work tried to arrange it in the form of a hierarchical diagram and give percentage weights to the results published by Tran et al. (2017) in which a total of 57 indicators from the 6A elements with percentage weights: smart attractions (27.27%), smart accessibility (27.27%), smart amenities (13.64%), smart ancillary (13.64%), smart activities (9.09%), and smart available packages (9.09%) bringing the total to 100%. This hierarchy and weighting will help the researchers even though it is not binding. Arif et al. (2020) also implemented the 6As framework in the city of Batu in East Java Province, Indonesia. The research used data from 11 destinations around the city and its surroundings. The next researcher, Grzunov (2022), who examined the last two years in Bosnia and Herzegovina also uses the $(SA)^6$ framework compiled by Huertas et al. (2019), and also prioritizes destinations in many cities in Croatia. However, Grzunov's (2022) research collects data using the online questionnaire method, which was distributed online via email directly to the mayor (mayor's office) of each city ($N = 127$) and head (head's office) of every municipality ($N = 429$) in Croatia. The results of this research are very subjective because they depend on the knowledge and opinions of the respondents, but this research is very useful for the Croatian government and adds to the richness of the methodological experiment.

Each country or region has different geographical characteristics of tourism destinations (Komilova et al., 2021). To attract tourists and satisfy visitor satisfaction,

this statement can also be turned into a question: Why are so few tourists coming? Is visitor satisfaction fulfilled? What components must be implemented, improved, and added to the managed destination environment? – and many other basic and important questions. Of course, this will be scary and very dangerous if visitors return with an unpleasant impression of the destination and its community. So, every tourism area must compete to immediately carry out an assessment, especially destinations that are still in development planning, so that all resources owned by stakeholders, especially the local government, can be more effective and efficient; therefore, the 6As framework assessment is one of the best solutions at the moment (Klepers & Ābols, 2023).

All the research previously mentioned was carried out in urban destination areas, thus opening up discussions that began to intersect smart cities and STDs. However, research that takes an island perspective has not yet been obtained. Meanwhile, this research tries to test it not only in urban areas but also in island destination areas. Therefore, this research aims to explore tourism resources and implement the 6As framework in the Wakatobi archipelago destination area, which is one of the island districts in Southeast Sulawesi province, Indonesia. This research also tries to combine the 6As framework with the Technique for Order Preference by Similarity to Ideal Solution (TOPSIS), considering the local government's interest in supporting decisions regarding priority needs for destination development.

Material and methods

Exploration of tourism resources

In this exploration process, we try to investigate the sources of tourist attractions into three categories: natural resources, cultural resources, and man-made resources. The exploration method involves several steps (Zhang & Long, 2023):

1. Field observation: extensively on four main islands (Wangi-Wangi, Kaledupa, Tomia, and Binongko). The attractions of each island were observed, carefully recorded, collected, and focused on tourism potential. Team members from residents were certainly involved.
2. Secondary data collection: local archives, tourism brochures, and local government reports.
3. Online databases and websites, such as United Nations Educational, Scientific and Cultural Organization (UNESCO) and national tourism portals, were reviewed to complement our field data with existing literature and digital records.

The focus of this exploration is how many items can be obtained that can be categorized as one attraction or destination point according to category and all kinds of facilities around.

Implementation of the 6As framework

A conceptual framework based on research visualizes the complex subject (Put van den Beemt & Smith, 2016) for analyzing tourism destinations (Buhalis, 2000). The primary determinants of international tourist flow are mostly associated with demand factors in the regions where tourists originate and supply factors in the places they visit (Gidebo, 2021), so field assessment is becoming very urgent.

These six frameworks include: attractions, accessibility, amenities, available packages, activities, and ancillary services. The steps involved in this assessment are as follows:

1. Assessment criteria: For each component of the 6As framework, specific variables and indicators are identified and assessed based on natural landscapes, cultural sites, or man-made attractions.
2. A score is assigned to each variable, with a score of the potential of that location reflecting the quantity and significance of its tourism resources.
3. Data collection involves a systematic survey of each identified tourism site. The survey is conducted by trained research assistants using a predetermined assessment form to ensure accuracy and consistency.
4. The data collected is analyzed quantitatively, and a score for each variable is calculated. For example, attractions (A1): the various characteristics of the natural landscape's charm in the scope of the designated area ($A1_1$), including man-made attractions ($A1_2$), cultural tourism ($A1_3$), and special events ($A1_4$) are added up. Likewise, the following example for amenities (A3): how many lodgings and hotels ($A3_1$), restaurants ($A3_2$), public facilities ($A3_3$), shopping locations including malls, shops, minimarkets, etc. are available ($A3_4$), then add them all up again, and so on until all six components are complete.
5. The scores for each island are combined to provide a comprehensive assessment of its tourism potential across the six components of the 6As framework (Withanage et al., 2024).

As explained by Buhalis (2000), the 6As consist of attractions with four indicators, accessibility with four indicators, amenities with four indicators, available packages at the destination, activities that can be carried out within the destination, and ancillary services with five indicators that can support visitor satisfaction.

The arrangement of symbols and equations from A1 to A6 is the work of Arif et al. (2020). In this research, several previous narratives are all combined in Table 1, so that the methodology is easier to duplicate or has the character of a template that can be developed at any time without changing the core components. TD1, TD2, and TDn are several tourist destinations in geographic characteristic areas. Lines from A1 to A6 are ready to be filled in from the field inspection results.

TABLE 1. 6As framework assessment of tourism destinations (TD)

No	Component	Variable/Indicator	Score TD1	Score TD2	Score TDn
1	Attractions	natural landscapes	$A1_1$	–	–
	$A1 = A1_1 + A1_2 + A1_3 + A1_4$	man-made attractions	$A1_2$	–	–
		cultural tourism	$A1_3$	–	–
		special events	$A1_4$	–	–
2	Accessibility	transportation routes	$A2_1$	–	–
	$A2 = A2_1 + A2_2 + A2_3 + A2_4$	terminals	$A2_2$	–	–
		public transportation inside	$A2_3$	–	–
		public transportation outside	$A2_4$	–	–
3	Amenities	lodging and hotels	$A3_1$	–	–
	$A3 = A3_1 + A3_2 + A3_3 + A3_4$	restaurants	$A3_2$	–	–
		public facilities	$A3_3$	–	–
		shopping centers	$A3_4$	–	–
4	Available packages	The offered options include guide services, prearranged travel packages, and tours tailored to specific interests.	A4	–	–
	A4 Represents the total count of packages provided to tourists at a specific travel destination.				
5	Activities	Every tourism destination typically offers a range of activities for visitors to enjoy.	A5	–	–
	A5 Visitor engagement refers to the total number of activities that tourists participate in at a tourist site.	The activities include sightseeing, swimming, outbound excursions, leisure activities, shooting photographs, and several other things.			
6	Ancillary services	communication channels	$A6_1$	–	–
	$A6 = A6_1 + A6_2 + A6_3 + A6_4 + A6_5$	Internet services	$A6_2$	–	–
		ATM or bank branch	$A6_3$	–	–
		medical services	$A6_4$	–	–
		postal services	$A6_5$	–	–

Source: own work.

Agustan, Rianse, U., Sukotjo, E., Faslih, A. (2024). Exploration and implementation of a smart tourism destination with the 6As framework & TOPSIS (case study: Wakatobi, Indonesia). *Sci. Rev. Eng. Env. Sci.*, *33* (4), 419–442. DOI 10.22630/srees.9760

Technique for Order Preference by Similarly to Ideal Solution (TOPSIS)

TOPSIS was designed to solve a multiple objective decision-making problem (Lai et al., 1994). The TOPSIS method operates on the principle that the optimal solution is characterized by its proximity to the positive-ideal solution and its distance from the negative-ideal solution. Based on this, alternatives are ranked (Chakraborty, 2022). This technique is used to rank tourist destinations based on their overall performance across the 6A components. The detailed steps for implementing TOPSIS (Madanchian & Taherdoost, 2023) are as follows:

Stage 1: Calculate the normalized performance ratings:

$$y_{ij} = \frac{x_{ij}}{\sqrt{\Sigma_{i=1}^{i} x_{ij}^2}}. \tag{1}$$

Stage 2: Integrate weights with the ratings:

$$v_{ij} = w_j \, y_{ij}. \tag{2}$$

Stage 3: Find positive and negative ideal solutions:

$$A^+ = (v_1^+, v_2^+, \ldots, v_n^+),$$

$$A^- = (v_1^-, v_2^-, \ldots, v_n^-). \tag{3}$$

Stage 4: Obtain the separation values:

$$S_i^+ = \sqrt{\Sigma_{j=1}^{j} \left(v_{ij} - v_j^+ \right)^2},$$

$$S_i^- = \sqrt{\Sigma_{j=1}^{j} \left(v_{ij} - v_j^- \right)^2}, \tag{4}$$

Stage 5: Calculate the overall preference score:

$$v_i = \frac{S_i^-}{S_i^- + S_i^+}. \tag{5}$$

Stage 6: The remaining alternatives are ranked based on higher V_i values.

Research study location

The location shown in Figure 1 is Wakatobi Regency, which is one of the districts in the province of Southeast Sulawesi, Indonesia. The capital of this district is located in the Wangi-Wangi sub-district, formed based on the Law of the Republic of Indonesia Number 29 of 2003, dated 18 December 2003 (Winfield, 2024). Previously, Wakatobi was part of the Buton Regency. The area of Wakatobi Regency is around 13,900 km², consisting of a land area of ±473.62 km² or only 3% and an area of water (sea) of ±13,426 km² or amounting to 97% of the area of Wakatobi Regency (Hardi et al., 2024). It consists of four main islands that form the Wakatobi archipelago: Wangi-Wangi, Kaledupa, Tomia, and Binongko.

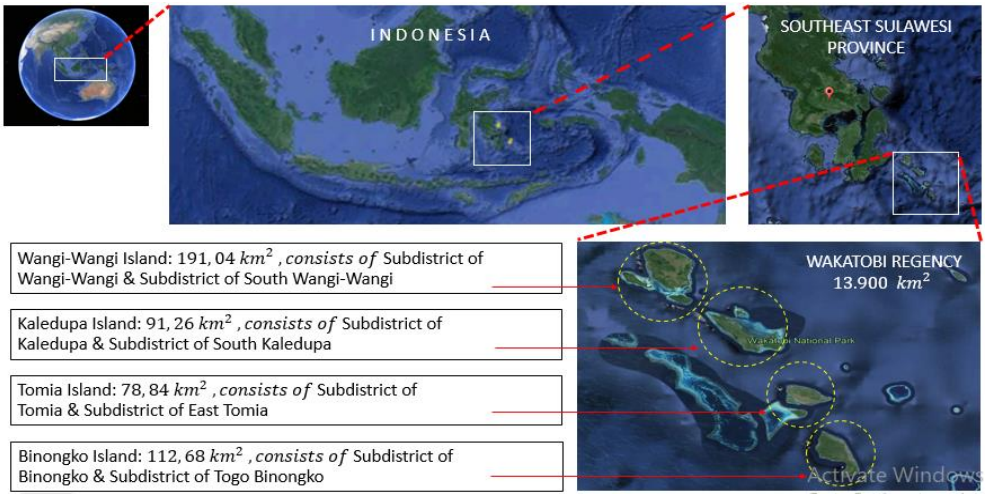

FIGURE 1. Wakatobi Regency (research location)
Source: own work.

Results and discussion

The exploration of tourism resources of the Wakatobi identified several opportunities to classify them by type: natural, cultural, and man-made resources.

Natural resources: Wakatobi is famous for its natural beauty: beautiful sandy beaches that are suitable for human activities, beautiful corals, and marine resources of a type that is difficult to find in many other parts of the world. These natural attractions are anchored by the Wakatobi National Park. The beauty of the islands

Agustan, Rianse, U., Sukotjo, E., Faslih, A. (2024). Exploration and implementation of a smart tourism destination with the 6As framework & TOPSIS (case study: Wakatobi, Indonesia). *Sci. Rev. Eng. Env. Sci.*, *33* (4), 419–442. DOI 10.22630/srees.9760

is also enriched by numerous caves, mangrove forests, and coasts, which create a perfect place for ecotourism and marine activities.

Cultural resources: Another social benefit is cultural, which includes celebrations, historical spots, and local artifacts of Wakatobi. Local cultural festivals like the Wakatobi Wave Festival and the Blacksmith Festival in Binongko introduce tourists to the people's typical ways of living. Most cultural attractions, such as the historical architectural features of the area, consisting of forts and traditional villages, help explore more of the island and its development, but they also help to maintain and popularize cultural heritages.

Man-made resources: The purpose-built attractions in Wakatobi include various resorts, dive centers, and cultural parks. These amenities also remain a factor in the tourism experience since such facilities are considered necessary in a vacation destination. In the past, when the islands provided very limited accommodation and restaurants, there were few facilities to attract tourists. However, facilities such as airports and ferry terminals have become key assets to the islands, boosting tourist traffic. Search results for several man-made destinations are generally located in resort environments with a high level of privacy. The government also created a cultural park aimed at accommodating community social activities. The night market is an entertainment option, and the lighthouses on Wangi-Wangi and Binongko also function as educational points. Figure 2 illustrates some other potential destination spots.

Table 2 is an additional table that functions as basic information that describes the main characteristics of Wakatobi's attractions, namely the beach and the beauty of the surface and underwater colorful coral reefs. More than 30 names of beaches managed by residents plus landscape structures in the form of caves, coastal forests, mountains, hills, and the rest of the land activities from the cultural sector

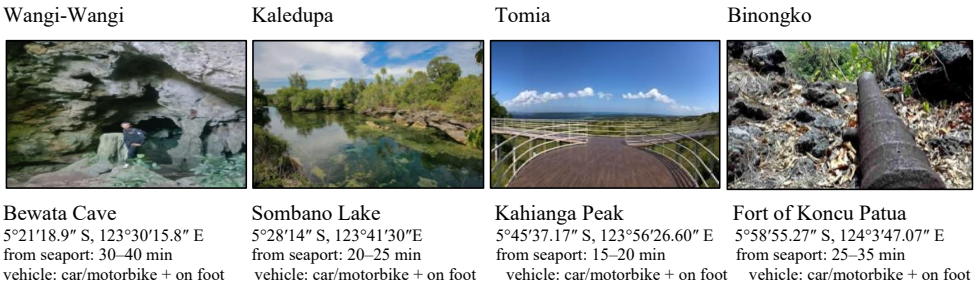

FIGURE 2. Some different potential destinations

Source: own work.

TABLE 2. Attractions in each tourist sub-district in Wakatobi

Sub-district	Attractions
Wangi-Wangi	**Nature:** Cemara Beach, Wambuliga Beach, Toliamba Peak, Waboe-Boe Peak, Moli'i Sahatu Beach, Jodoh Beach, Kaluku Beach, Sousu Beach, Waha Beach, Kombiy Garden, Tindoi Forest, Kontamale Cave, Kosapi Cave, Sara Longa Forest **Culture:** Wakatobi Wave, Kabuenga, Kari'a, Benteng Wabue-Bue, Goa Tofengka, Goa Wapia-Pia **Man-made:** Marina Togo Mowondu, Sombu Dive, Patuno Resort, Naya Matahora, Wanci Night Market, Tindoi Lighthouse
South Wangi-Wangi	**Nature:** Kapota Lake/Tailaronto'oge Lake, Molai One Beach, Sousu Beach, Waikesa Beach, Kapota Beach, Watu Kapala Tsore Site, Topa Mandati Springs (baths), Liya Togo and Liya Mawi Mangrove Forests, Lobu Cave, Kalelawar Cave (bat cave), Bewata Cave **Culture:** Bajo Mola, Liya Palace Fort Area, Watinti Fort, Togo Malengo Fort, Baluara Fort, Mandati Tonga Fort **Man-made:** Wakatobi Cultural Park
Kaledupa	**Nature:** Sombano Lake, Langira Beach, Sombano Beach, Hoga Beach, Sangia Wagugu Cave, Sangia Akka Kuri-Kuri Cave, Watu Meleu **Culture:** Bajo Mantigola, Bajo Juaraa, Barata Kahedupa, Laulua Village Site, Ollo Old Fort, Horuo Fort, Tapa'a Fort, Bente Mosque **Man-made:** none
South Kaledupa	**Nature:** Peropa Beach, panorama of Pangila Hills, One Mbiha Beach, Sangka'anukiye Natural Cave, Darawa Natural Cave **Culture:** Bajo Lohowa, village weaving craftsmen in Pajam, Lentea Village, Darawa Village, traditional village in Palea, traditional house in Kamali, Kamali Fort, La Donda Fort, Tobelo Fort, La Manungkira Fort, La Bohasi Fort **Man-made:** none
Tomia	**Nature:** Barakati Beach, Lakota Beach – Marimabuk, Tolandono Beach, **Culture:** Tomia Island Festival, Creative Lodge for Pandan Mat Craftsmen, Fort Patua **Man-made:** none
East Tomia	**Nature:** Kahianga Peak, Hu'untete Beach, Hongaha Beach, Tee Timu Beach, Puncak Waru Usuku, Liang Kuri-Kuri Cave, Telaga Tee Timu Cave **Culture:** Kulati Village Farm **Man-made:** Wakatobi Dive Resort
Binongko	**Nature:** Buku Beach, Palahidu Beach, Yoro Beach, Mbara-Mbara Beach, Wakarumende Beach, Haso Beach, Yoro Mangrove, Kapala Cliff, Tolutulua Hill Cliff, Koncu Kapala Peak, Lapungga Forest, Bongira Forest, Laloala Forest, Titi Makoro Cave, Lasikori Cave, Topa Mata (Bat) spring, Topa Labago **Culture:** Koncu Kapala traditional village, Fort Wali, Fort Watiua, Fort Palahidu, Fort Baluara, Fort Koncu Patua, Fort Loji, Tomb of Wa Ode Goa **Man-made:** none
Togo Binongko	**Nature:** Batu Park, One Malangka Beach, Belaa Beach, Wee Beach, Sowa Mangrove Forest, Onemelangka Mangrove, Kamento Mangrove, Lahandu Hill, Bharangka Tooha Forest, Tai Suappa (saltwater lake), Liameangi Cave, Liabheka Cave, Liangkondu Cave, Topa Haka (Cave Water), Mokia Tee, Palefungka Tee **Culture:** Blacksmith Craftsmen, Kau Rangka (Cempaka ecosystem), Oihu Fort, Pimpi Fort, Koto-Koto Fort **Man-made:** Tadhuna Lighthouse

Source: Field observation, hard and soft doc (Bauer, 2022), online version.

Agustan, Rianse, U., Sukotjo, E., Faslih, A. (2024). Exploration and implementation of a smart tourism destination with the 6As framework & TOPSIS (case study: Wakatobi, Indonesia). *Sci. Rev. Eng. Env. Sci.*, *33* (4), 419–442. DOI 10.22630/srees.9760

are records of human civilization such as forts, dances, local crafts, and others. The four main islands are divided into eight sub-district administrative areas. This is important to convey because attractions are the main core of a destination and are on the menu for enthusiasts who like underwater paradise tourism.

Figure 3 is a sample of panoramic spots above and below the sea on each of the islands under consideration. McMellor and Smith have tried to compare the species and generic richness of scleractinian corals in the Wakatobi National Park area with several regions in Indonesia. They state that Wakatobi National Park is located in the middle of the Coral Triangle area, which has the highest marine biodiversity in Southeast Asia. Their findings show that strict no-take-zones are effective in protecting fish and benthic assemblages associated with coral reefs in Wakatobi (McMellor & Smith, 2010).

FIGURE 3. Explore the natural panorama above and below the sea in Wakatobi
Source: Wakatobi Tourism Authority (2024).

Wakatobi has extraordinary marine tourism charm, beautiful underwater corals, and beaches with white sand, complementing the contrast of the clear blue sea. This tourist destination is still not completely touched by the modernity of development, so it can still be authentic and have a local feel. Wakatobi is mainly famous for its coral reefs, making it one of the diving destinations for divers, especially foreign divers. Apart from scuba divers, tourists can also explore the coral reef section of the shallow areas through snorkeling activities (Giglio et al., 2023). On several websites, there is information regarding Wakatobi as a snorkeling destination; the best-known location is Sombu on the west coast of Wangi-Wangi Island, which is also one of the favorite diving locations (Bauer, 2022). Wakatobi requires much traveling, often under basic conditions, but to quote Jacques-Yves Cousteau, it is an “underwater nirvana”, and de Vries (2019) also agrees.

Several traditions and cultures have the potential to become tourist attractions (Rahmawati et al., 2023). Holding a cultural festival is one of the activities usually carried out by the local tourism department, which includes the Tindoi Fort Festival in the Wangi-Wangi District, Koba Fort Festival in the South Wangi-Wangi District, Barata Kaledupa Festival in the Kaledupa District, Pajujudi Festival in the Tomia District, and Blacksmith Festival in the Binongko District. This festival is regularly held every year, but in 2020, it was not held due to COVID-19. In 2021, several cultural festivals will begin to be held again on the Wakatobi; this can be seen at the WAVE festival in Wangi-Wangi Island and the Micro, Small, and Medium-sized Enterprises Festival in the Tomia Islands (Bauer, 2022). Here are some pictures of events/festivals on the Wakatobi tourism agenda in Figure 4.

Wakatobi Wave (Wangi-Wangi) Date: December

Kahedupa Barata Festival (Kaledupa) Date: Aug.–Sept.

Island Maritime Festival (Tomia) Date: October

Blacksmith Island Festival (Binongko) Date: March

FIGURE 4. Tourism events as a reflection of culture in the Wakatobi
Source: Wakatobi Tourism Authority (2024).

The Indonesian government has decided to encourage economic growth by developing tourism as a key sector (Aida et al., 2024). To support this policy, the government has determined ten priority tourism destinations, of which six destinations are part of the national tourism strategic area (according to Government Regulation No 50 of 2011 concerning the National Tourism Development Master Plan), and the other four destinations are included in the special economic zone (Hamzah et al., 2023). While efforts continue, five new destination areas have been added as a super priority, including Wakatobi (Taali et al., 2024). Again, in 2012, Wakatobi was designated as a UNESCO global biosphere reserve, which aims to preserve local wisdom and create a sustainable economy and sustainable livelihoods for local communities. With the establishment of a biosphere reserve at Wakatobi National Park, Indonesia has eight biosphere reserves, and to date, there are 598 biosphere reserve units throughout the world spread across 117 countries. Wakatobi boasts a wide range of ecosystems (Hawati et al., 2024), including several marine and coastal habitats that support a rich array of seagrass, coral reefs, commercially valuable fish, sea birds, turtles, cetaceans, and mangroves.

Around 590 species of fish, 396 species of coral reef, 22 major species and 11 associate species of mangrove, and 9 out of the 12 species of seagrass can be discovered in Wakatobi (UNESCO, 2019).

Implementation of the 6As framework

The results of the search on the four islands have provided an overview of the characteristics of the attractive force they have. Therefore, the application of the 6As framework by Buhalis, which has been prepared in Table 2, is presented in the following series of tables. Tables 3, 4, and 5 each have four variable components assessed from the field survey results. Table 3 is a table of attractiveness scores. This is the most important component because it is the force of attractiveness for visitors (Thu & Lee, 2022).

TABLE 3. Attractions scores

No	Tourism Destination	$A1_1$	$A1_2$	$A1_3$	$A1_4$	Score
1	Wangi-Wangi	14	6	6	4	30
2	South Wangi-Wangi	10	1	6	3	20
3	Kaledupa	7	0	8	3	18
4	South Kaledupa	5	0	10	3	18
5	Tomia	3	0	3	3	9
6	East Tomia	7	1	1	3	12
7	Binongko	17	0	8	3	28
8	Togo Binongko	16	1	5	3	25
					Number of forms of attraction	160

Source: own work.

As seen in Table 3, the Wangi-Wangi sub-district has the highest score. It has 14 natural landscape attractions, six cultural attractions, six man-made attractions, and four main events, namely (Wakatobi Wave, the Republic of Indonesia's birthday, Wakatobi's anniversary, and year-end events), while the Tomia sub-district has the lowest score influenced by it being the smallest island so that the variety of natural landscapes is limited in quantity but in terms of quality it is no less competitive as proven by the Wakatobi Dive Resort in Tomia, which is famous internationally. The Maranggo Airport in Tomia has a direct connection from Denpasar Bali to Tomia and Wakatobi Dive Resort (Karim, 2022). Denpasar Bali –

Tomia flights occur twice a week, namely on Tuesday and Friday. This flight causes Tomia's accessibility score to be almost equal to Wangi-Wangi Island. Table 3 inventories approximately 160 attractions in the form of geographic destinations, including activities.

Table 4 is a list of accessibility strengths. Wangi-Wangi also has the highest access score because there is one government-owned public ferry port terminal, one naval terminal that is open to the public and can be used by private vessels, and one airport terminal called Matahora Airport. Table 5 is the amenity assessment score. Here, you can see that Wangi-Wangi still has the highest score because Wangi-Wangi is the center of the district capital, and the South Kaledupa sub-district has the lowest score. The shopping center score is worth hundreds due to the combination of all shopping centers, small shops, and large shops spread across the sub-district.

TABLE 4. Accessibility scores

No	Tourism destination	$A2_1$	$A2_2$	$A2_3$	$A2_4$	Score
1	Wangi-Wangi	2	3	2	2	9
2	South Wangi-Wangi	2	2	2	2	8
3	Kaledupa	1	1	1	1	4
4	South Kaledupa	1	1	1	1	4
5	Tomia	2	1	2	2	7
6	East Tomia	2	2	2	2	8
7	Binongko	1	1	1	1	4
8	Togo Binongko	1	1	1	1	4

Source: own work.

TABLE 5. Amenities scores

No	Tourism destination	$A3_1$	$A3_2$	$A3_3$	$A3_4$	Score
1	Wangi-Wangi	20	31	3	265	319
2	South Wangi-Wangi	15	29	3	352	399
3	Kaledupa	10	3	3	69	85
4	South Kaledupa	1	1	3	61	66
5	Tomia	10	4	3	95	112
6	East Tomia	3	4	3	98	108
7	Binongko	2	6	3	62	73
8	Togo Binongko	2	2	3	63	70

Source: own work.

Agustan, Rianse, U., Sukotjo, E., Faslih, A. (2024). Exploration and implementation of a smart tourism destination with the 6As framework & TOPSIS (case study: Wakatobi, Indonesia). *Sci. Rev. Eng. Env. Sci.*, *33* (4), 419–442. DOI 10.22630/srees.9760

Table 6 is a combined score of the number of available packages and the number of activities that can be carried out. Almost all tour packages are prepared by professionally managed resort companies, so only islands that have resorts have scores. Some activities that can be done include cycling, swimming, diving, snorkeling, fishing, beach views/sunbathing, mountain views/caves, culinary, craft shopping, cultural heritage exploration, and others. But especially to enjoy the silence at one with nature, Wakatobi is the right choice (Syahadat, 2022).

Likewise, the ancillary score in Table 7 shows Wangi-Wangi has the highest score, and Binongko has the lowest score. Ancillary services include communication channels, Internet services, ATM or bank branches, medical services, and postal services. These basic services are each present in the district area of each island. ATMs are found at local banks, not international ones. For Kaledupa and Tomia, only mini ATMs are used and are available in chosen small shops.

TABLE 6. Available packages and activities scores

No	Tourism destination	A4	A5
1	Wangi-Wangi	2	9
2	South Wangi-Wangi	1	8
3	Kaledupa	1	8
4	South Kaledupa	0	7
5	Tomia	1	8
6	East Tomia	1	8
7	Binongko	0	6
8	Togo Binongko	0	6

Source: own work.

TABLE 7. Ancillary services scores

No	Tourism destination	$A6_1$	$A6_2$	$A6_3$	$A6_4$	$A6_5$	Score
1	Wangi-Wangi	1	1	9	1	1	13
2	South Wangi-Wangi	1	1	4	1	1	8
3	Kaledupa	1	1	2	1	1	6
4	South Kaledupa	1	1	2	1	1	6
5	Tomia	1	1	1	1	1	5
6	East Tomia	1	1	1	1	1	5
7	Binongko	1	1	0	1	1	4
8	Togo Binongko	1	1	0	1	1	4

Source: own work.

Result of TOPSIS implementations

Table 8 is an accumulation of the 6As scores for the four islands: attractions, accessibility, amenities, available packages, activities, and ancillary services. With Table 8 as the initial matrix, the requirements have been met to execute the TOPSIS procedure. As a first step, Equation 1 leads to the normalization of the values in Table 8, and the results can be seen in Table 9.

TABLE 8. TOPSIS requirement scores

No	Tourism destination	A1	A2	A3	A4	A5	A6
1	Wangi-Wangi	30	9	319	2	9	13
2	South Wangi-Wangi	20	8	399	1	8	8
3	Kaledupa	18	4	85	1	8	6
4	South Kaledupa	18	4	66	0	7	6
5	Tomia	9	7	112	1	8	5
6	East Tomia	12	8	108	1	8	5
7	Binongko	28	4	73	0	6	4
8	Togo Binongko	25	4	70	0	6	4

Source: own work.

TABLE 9. Normalized performance for TOPSIS requirement scores

No	Tourism destination	A1	A2	A3	A4	A5	A6
1	Wangi-Wangi	0.501	0.502	0.576	0.707	0.421	0.661
2	South Wangi-Wangi	0.334	0.446	0.720	0.354	0.374	0.407
3	Kaledupa	0.301	0.223	0.153	0.354	0.374	0.305
4	South Kaledupa	0.301	0.223	0.119	0.000	0.327	0.305
5	Tomia	0.150	0.390	0.202	0.354	0.374	0.254
6	East Tomia	0.201	0.446	0.195	0.354	0.374	0.254
7	Binongko	0.468	0.223	0.132	0.000	0.280	0.203
8	Togo Binongko	0.418	0.223	0.126	0.000	0.280	0.203

Source: own work.

The weights shown in Table 10 are taken from the percentage weights determined by Huertas et al. (2019) through the results of AHP analysis. The weights are integrated so that the highest and lowest values can be known and taken. Thus, the Excel table data can automatically work on Equations 3, 4, and 5, which then produces the TOPSIS ranking score indicator in Figure 5.

Agustan, Rianse, U., Sukotjo, E., Faslih, A. (2024). Exploration and implementation of a smart tourism destination with the 6As framework & TOPSIS (case study: Wakatobi, Indonesia). *Sci. Rev. Eng. Env. Sci.*, *33* (4), 419–442. DOI 10.22630/srees.9760

TABLE 10. Indicators weight

No	Tourism destination	Weight [%]
1	Attractions	27.27
2	Accessibility	27.27
3	Amenities	13.64
4	Available packages	9.09
5	Activities	9.09
6	Ancillary services	13.64

Sources: Huertas et al. (2019).

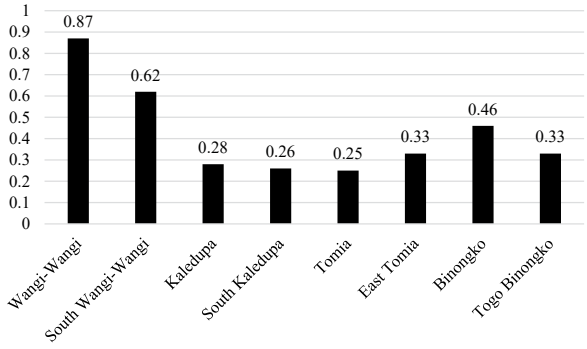

FIGURE 5. TOPSIS analysis priority scores

Source: own work.

The TOPSIS analysis ranked the islands according to their tourism potential considering the six components of the 6As framework (Fig. 5):

1. Wangi-Wangi: This island topped the list with a TOPSIS score of 0.87, showing its strong performance in all components, especially attractions, amenities, and accessibility.
2. South Wangi-Wangi: This island came in second with a score of 0.62. Its closeness to Wangi-Wangi and shared infrastructure boosted its ranking.
3. Binongko: Scoring 0.46, this island stood out for its one-of-a-kind attractions and rich culture. However, it needs better amenities and accessibility.
4. East Tomia and Togo Binongko: These islands scored (0.331 and 0.334) suggesting they have balanced potential that could grow with focused development.
5. Tomia, South Kaledupa, and Kaledupa: These islands scored lower, showing they need big investments in infrastructure and services to reach their full tourism potential.

Conclusions

The application of the 6As and TOPSIS methods to explore and implement the smart tourism destination framework has provided a comprehensive assessment concerning the Wakatobi tourism potential. Key findings and implications for the development of the region's tourism industry have been drawn from this research.

First and foremost, Wangi-Wangi Island becomes the leading destination since it has the highest score for all variables: attractions, accessibility, amenities, available packages, activities, and ancillary services. Of course, it is well-explained that the highly developed infrastructure, several types of natural and cultural attractions, and strong tourism facilities enable the island to become one of the potential candidates for further investment and promotion as one of the smart tourism destinations; its success can set an example for other islands in the region.

Secondly, these huge disparities in the potential for tourism among the islands demand focused development strategies. For example, Kaledupa and South Kaledupa scored the lowest due to poor access and insufficient visitor facilities. To increase the islands' attractiveness to tourism, better transport links, improved accommodation and dining, as well as more tourist activities must be developed. Indeed, investments in infrastructure and services are needed to foster an evenly distributed and inclusive tourism industry inside Wakatobi.

Thirdly, the application of the 6As framework and the TOPSIS method has been effective in providing structure and objectivity as a measure of tourism potential. These tools provide opportunities for comparative analyses of different destinations, outlining strengths and weaknesses. As such, these tools have assisted in the prioritization of issues that need to be improved. This approach can be replicated in other regions for the systematic assessment and enhancement of tourism potential.

The findings of this study also underline the importance of sustainable tourism. Maintenance of the untouched natural and cultural features of Wakatobi forms the basis for the islands' continued attractiveness to tourists. It is therefore important to engage local communities in tourism development, promote eco-friendly practices, and ensure that tourism growth does not come at the expense of the islands' ecological integrity.

The findings of this research may also be useful in policy decision-making. Based on a detailed assessment, this research study can convince stakeholders to invest strategically in enhancing the tourism infrastructure and services in Wakatobi. This will again increase the satisfaction level of tourists and their visitation rates, which will lead to economic development within the region.

Wakatobi has great potential as a smart tourism destination. A capitalization strategy in their natural and cultural assets, improvement of infrastructure and facilities, combined with best practices on the ground, would ensure balanced and inclusive growth in tourism for the islands. Further research is needed, specifically on accessibility, which focuses on transportation route modeling, monitoring the impacts of tourism development, and refining strategies toward sustainable and equitable growth of the tourism sector in Wakatobi.

References

Aida, N., Atiqasani, G., & Palupi, W. A. (2024). The effect of the tourism sector on economic growth in Indonesia. *WSEAS Transactions on Business and Economics*, *21*, 1158–1166. https://doi.org/10.37394/23207.2024.21.95

Andrianto, T., & Sugiama, A. G. (2016). The analysis of potential 4A's tourism component in the Selasari rural tourism, Pangandaran, West Java. In *Proceedings of the Asia Tourism Forum 2016 – the 12th Biennial Conference of Hospitality and Tourism Industry in Asia, 2016* (pp. 138–144). Atlantis Press. https://doi.org/10.2991/atf-16.2016.21

Arif, Y. M., Nugroho, S. M. S., & Hariadi, M. (2019). Selection of tourism destinations priority using 6AsTD framework and TOPSIS. In *2019 International Seminar on Research of Information Technology and Intelligent Systems (ISRITI)* (pp. 346–351). IEEE. https://doi.org/10.1109/ISRITI48646.2019.9034671

Bauer, T. G. (2022). *Final report version 3–14 December 2022: integrated tourism master plan, Wakatobi*. https://drive.google.com/file/d/1_Ljur5wpW_nwr6HcDJbuYuLA7ZRps4oR/view?usp=sharing

Buhalis, D. (2000). Marketing the competitive destination of the future. *Tourism Management*, *21* (1), 97–116. https://www.academia.edu/164837/Marketing_the_competitive_destination_of_the_future

Buhalis, D., & Amaranggana, A. (2015). Smart tourism destinations enhancing tourism experience through personalisation of services. *Information and Communication Technologies in Tourism 2015: Proceedings of the International Conference*. Springer International Publishing. https://doi.org/10.1007/978-3-319-14343-9_28

Buonincontri, P., & Micera, R. (2016). The experience co-creation in smart tourism destinations: a multiple case analysis of European destinations. *Information Technology & Tourism*, *16*, 285–315. https://doi.org/10.1007/s40558-016-0060-5

Chakraborty, S. (2022). TOPSIS and modified TOPSIS: A comparative analysis. *Decision Analytics Journal*, *2*, 100021. https://doi.org/10.1016/j.dajour.2021.100021

Damanik, F. K., Ulinnuha, H., Tarigan, W. P., Lutfianti, E., Wijaya, T. E., & Oh, O. (2022). Smart tourism destination: a comparative study for five super priority destinations in Indonesia. In *Proceedings of the 3rd South American International Industrial Engineering and Operations Management Conference*, *2022* (pp. 538–552). IEOM Society International. https://doi.org/10.46254/SA03.20220151

Framke, W. (2002). The destination as a concept: A discussion of the business-related perspective versus the socio-cultural approach in tourism theory. *Scandinavian Journal of Hospitality and Tourism*, *2* (2), 92–108. https://doi.org/10.1080/15022250216287

Fyall, A., & Garrod, B. (2020). Destination management: a perspective article. *Tourism Review*, *75* (1), 165–169. https://doi.org/10.1108/TR-07-2019-0311

Gidebo, H. B. (2021). Factors determining international tourist flow to tourism destinations: a systematic review. *Journal of Hospitality Management and Tourism*, *12* (1), 9–17. https://doi.org/10.5897/JHMT2019.0276

Giglio, V. J., Aued, A. W., Cordeiro, C. A., Eggertsen, L., S. Ferrari, D., Gonçalves, L. R., Hanazaki, N., Luiz, O. J., Luza, A. L., Mendes, T. C., Pinheiro, Segal. B., Waechter, L. S. & Bender, M. G. (2024). A global systematic literature review of ecosystem services in reef environments. *Environmental Management*, *73* (3), 634–645. https://doi.org/10.1007/s00267-023-01912-y

Goeldner, C. R., & Ritchie, J. B. (2011). *Tourism: principles, practices, philosophies* (12th ed.). Hoboken, NJ: John Wiley & Sons.

Grzunov, J. (2022). Can "smartness" of a destination be measured? Building and testing a generalized framework for measuring smart tourism destination development on the example of Croatia. *Zbornik radova Međunarodne naučne konferencije o digitalnoj ekonomiji DIEC*, *5*, 33–47.

Hamzah, S., Pangemanan, D., & Aprianti, E. (2023). The environmental and sustainable factors on the special economic zones development. *Civil Engineering Journal*, *9* (2), 334–342. http://dx.doi.org/10.28991/CEJ-2023-09-02-06

Hawati, H., Mustafa, M., Yusuf, Y., Putra, A., & Suriadin, H. (2024). Study of coral reefs in the tourism zone of Hoga Island, Wakatobi National Park, Southeast Sulawesi, Indonesia. *Journal La Lifesci*, *5* (1), 27–36. https://doi.org/10.37899/journallalifesci.v5i1.905

Hardi, Saptaputra, S. K., & Asriati (2024). Analysis of factors influencing work accidents among Bajo Tribe Fishermen in the coastal area of Nelayan Bhakti Village, South Wangi-Wangi District, Wakatobi Regency 2023. *World Journal of Advanced Research and Reviews*, *21* (1), 1147–1156. https://doi.org/10.30574/wjarr.2024.21.1.02656

Huertas, A., Moreno, A., & My, T. H. (2019). Which destination is smarter? Application of the (SA) 6 framework to establish a ranking of smart tourist destinations. *International Journal of Information Systems and Tourism (IJIST)*, *4* (1), 19–28. http://www.uajournals.com/ojs/index.php/ijist/article/view/437

Jan, A. & Chaudhry, A. G. (2024). Importance of tourism in livelihoods. *Journal of Policy Research*, *10* (2), 533–536. https://doi.org/10.61506/02.00265

Kalaivani, R. M., Andrews Scoot, D., Latha, S. (2023). The role of value added services between customers and service providers in tourism industry. *International Journal for Multidisciplinary Research*, *5* (6), 1–5. https://doi.org/10.36948/ijfmr.2023.v05i06.8972

Karim, L. O. M. (2022). Criminal sanctions for coral reef destroyers Tomia Island Study, Wakatobi Regency. *Journal of Research Trends in Social Sciences and Humanities*, *1* (1), 60–64. https://doi.org/10.59110/aplikatif.v1i1.49

Khairi, M., & Darmawan, D. (2021). The relationship between destination attractiveness, location, tourism facilities, and revisit intentions. *Journal of Marketing and Business Research (MARK)*, *1* (1), 39–50.

Klepers, A., & Ābols, I. (2022). Operationalizing business intelligence for local level tourism destination performance. In J. L. Reis et al. (Eds), *Marketing and Smart Technologies. ICMarkTech 2022* (Vol. 344, pp. 595–601). Singapore: Springer. https://doi.org/10.1007/978-981-99-0333-7_42

Komilova, N. K., Usmanov, M. R., Safarova, N. I., Matchanova, A. E., & Murtazaeva, G. I. (2021). Tourist destination as an object of research of social and economic geography. *Psychology and Education Journal*, *58* (1), 2058–2067.

Lai, Y-J., Liu, T-Y., & Hwang, C-L. (1994). Topsis for MODM. *European Journal of Operational Research*, *76* (3), 486–500.

Lin, K. J., Ye, H., & Law, R. (2022). Conceptualizing accessible tourism with smart technologies. *Journal of Smart Tourism*, *2* (2), 5–14. https://doi.org/10.52255/smarttourism.2022.2.2.2

Leask, A. (2016). Visitor attraction management: a critical review of research 2009–2014. *Tourism Management*, *57*, 334–361. https://doi.org/10.1016/j.tourman.2016.06.015

McMellor, S., & Smith, D. J. (2010). Coral reefs of the Wakatobi: abundance and biodiversity. In J. Clifton, R. K. F. Unsworth & D. J. Smith (Eds.), *Environmental Sciences, Engineering, & Technology Series*. *Marine Research and Conservation in the Coral Triangle. The Wakatobi National Park* (pp. 18–32). Kabupaten Wakatobi: Operation Wallacea.

Madanchian, M., & Taherdoost, H. (2023). A comprehensive guide to the TOPSIS method for multi-criteria decision making. A comprehensive guide to the TOPSIS method for multi-criteria decision making. *Sustainable Social Development*, *1* (1), 2220. https://doi.org/10.54517/ssd.v1i1.2220

Mandić, A., & Kennell, J. (2021). Smart governance for heritage tourism destinations: Contextual factors and destination management organization perspectives. *Tourism Management Perspectives*, *39*, 100862. https://doi.org/10.1016/j.tmp.2021.100862

Nichols, A. (n.d.). *What are ancillary services in tourism?* Luxurytraveldiva. https://luxurytraveldiva.com/what-are-ancillary-services-in-tourism [accessed: 26.03.2024].

Peraturan Pemerintah Nomor 50 Tahun 2011 tentang Rencana Induk Pembangunan Kepariwisataan Nasional Tahun 2010–2025 [Government Regulation No 50 of 2011. Master plan for national tourism development 2010–2025]. JDIH – Sekretariat Kabinet RI. https://jdih.setkab.go.id/PUUdoc/17379/PP0502011.pdf [accessed: 26.03.2024].

Put-van den Beemt, W., & Smith, R. (2016). *Smart tourism tools: linking technology to the touristic resources of a city*. Smart tourism congress, Barcelona, Spain. https://www.cett.es/fitxers/MiniWebs/145/papers/PUT_SMITH.pdf [accessed: 24.04.2024].

Rahmawati, R., Ramdani, T., & Juniarsih, N. (2022). Potential development of bau nyale tradition as cultural tourism in Lombok. *Sangkép: Jurnal Kajian Sosial Keagamaan*, *5* (2), 149–156. https://doi.org/10.20414/sangkep.v5i2.6790

Risty, F. I. N. (2024). Keterlibatan *Multistakeholders* dalam Mengembangkan Produktivitas dan Daya Saing Industri Kreatif Berbasis Pariwisata. *Journal of Tourism and Creativity*, *8* (2), 103–108. https://doi.org/10.19184/jtc.v8i2.47818

Shen, S., Sotiriadis, M., & Zhang, Y. (2020). The influence of smart technologies on customer journey in tourist attractions within the smart tourism management framework. *Sustainability*, *12* (10), 4157. https://doi.org/10.3390/su12104157

Sinambela, E. A. (2021). Examining the relationship between tourist motivation, touristic attractiveness, and revisit intention. *Journal of Social Science Studies (JOS3)*, *1* (1), 25–30. https://doi.org/10.56348/jos3.v1i1.4

Syahadat, R. M. (2022). Inventarisasi dan identifikasi objek daya tarik wisata dalam perencanaan pariwisata Wakatobi [Inventory and identification of tourism attractions in Wakatobi tourism planning]. *Journal of Regional and Rural Development Planning* [*Jurnal Perencanaan Pembangunan Wilayah Dan Perdesaan*], *6* (1), 30–46. https://doi.org/10.29244/jp2wd.2022.6.1.30-46

Taali, M., Amri, L. H. A., Puspitasari, D. A. K., & Anwar, R. (2024). Analysis of the harmonious development of the National Tourism Strategic Area and Tourism Master Plan. *KnE Engineering*, *6* (1), 44–50. https://doi.org/10.18502/keg.v6i1.15348

Tamin, O. Z. (1997). *Perencanaan & Pemodelan Transportasi* (2nd ed.). Institut Teknologi Bandung.

Thu, H. T. Q., & Lee, J. (2022). The perceived attractiveness of Vietnam tourism destinations for Korean tourists: a comparison between visitors and non-visitors. *호텔경영학연구* [*Korean Journal of Hospitality & Tourism*], *31* (7), 237–252. https://doi.org/10.24992/KJHT.2022.10.31.07.237

Tran, H. M., Huertas, A., & Moreno, A. (2017). *(SA)^6: A new framework for the analysis of smart tourism destinations. A comparative case study of two Spanish destinations. Topic 2. The development of STD: limiting & success factors. Case studies & best practices.* Actas Del Seminario Internacional Destinos Turísticos Inteligentes: nuevos horizontes en la investigación y gestión del turismo. San Vicente del Raspeig: Universidad de Alicante. https://doi.org/10.14198/Destinos-Turisticos-Inteligentes.2017.09

Um, T., & Chung, N. (2021). Does smart tourism technology matter? Lessons from three smart tourism cities in South Korea. *Asia Pacific Journal of Tourism Research*, *26* (4), 396–414. https://doi.org/10.1080/10941665.2019.1595691

United Nations Educational, Scientific and Cultural Organization [UNESCO] (2019). *Wakatobi Biosphere Reserve, Indonesia*. UNESCO. https://en.unesco.org/silkroad/silk-road-themes/biosphere-reserve/wakatobi [accessed: 24.04.2024].

United Nations World Tourism Organization [UNWTO] (2019). *UNWTO Tourism Definitions*. UNWTO. https://drive.google.com/file/d/1ZRwPry2iw3WqFMCY3c5iWk9jZiRp-y5f/view?usp=sharing [accessed: 24.04.2024].

Vries, V. de (2019, 6 May). Wakatobi Islands: Underwater nirvana like no other. The Jakarta Post. https://www.thejakartapost.com/travel/2019/05/06/wakatobi-islands-underwater-nirvana-like-no-other.html [accessed: 26.03.2016].

Wakatobi Tourism Authority (2024). *Wakatobi Tourism Events*. Wakatobi Tourism Authority. https://www.wakatobitourism.com/events/#projects_widget-0-0-0-tourism-events [accessed: 26.03.2024].

Winfield, R. (2024, 4 April). *Kabupaten Wakatobi*. Wikipedia. https://id.wikipedia.org/wiki/Kabupaten_Wakatobi#Pranala_luar [accessed: 23.03.2024].

Withanage, N. C., Wijesinghe, D. C., Mishra, P. K., Abdelrahman, K., Mishra, V., & Fnais, M. S. (2024). An ecotourism suitability index for a world heritage city using GIS-multi criteria decision analysis techniques. *Heliyon*, *10* (11), e31585. https://doi.org/10.1016/j.heliyon.2024.e31585

Xu, J., Su, T., Cheng, X., & Chen, H. (2024). Exploring the destination network in the context of tourism mobility: a multi-scale analytical framework. *Current Issues in Tourism*, *2024*, 1–23. https://doi.org/10.1080/13683500.2024.2334830

Zhang, H., & Long, S. (2023). Evaluation of attraction and spatial pattern analysis of world cultural and natural heritage tourism resources in China. *PLOS ONE*, *18* (8), e0289093. https://doi.org/10.1371/journal.pone.0289093

Summary

Exploration and implementation of a smart tourism destination with the 6As framework & TOPSIS (case study: Wakatobi, Indonesia). Wakatobi represents huge potential for smart tourism due to the rich natural, cultural, and man-made resources available. The objective of the research is to identify and analyze the tourism potential of Wakatobi by using the 6As framework (attractions, accessibility, amenities, available packages, activities, and ancillary services) and applying the Technique for Order Preference by Similarity to Ideal Solution (TOPSIS) method to rank the potential tourist destinations. Field observations, collection of secondary data, and stakeholder interviews were conducted to arrive at comprehensive data on the tourism assets of the islands. The result of the exploration successfully recorded 160 attractions in the form of geographical destinations and activities with a variety of visitor facilities around them, which were measured using the 6As framework. The TOPSIS results indicated that Wangi-Wangi Island had the highest rank (0.87) in overall tourism potential compared to the others due to better infrastructural conditions, diverse attractions, and better facilities. Furthermore, it revealed major discrepancies among the islands, thus requiring focused improvements related to accessibility and services for less developed areas like Kaledupa (0.28), South Kaledupa (0.26), and Tomia (0.25). This study provides the basic insights for policymakers and stakeholders to invest in the right areas to ensure balanced and inclusive growth, increasing the tourism attractiveness of Wakatobi with a focus on sustainability and community involvement.

Instruction for Authors

The journal publishes in English languages, peer-reviewed original research, critical reviews and short communications, which have not been and will not be published elsewhere in substantially the same form. Author of an article is required to transfer the copyright to the journal publisher, however authors retain significant rights to use and share their own published papers. The published papers are available under the terms of the principles of Open Access Creative Commons CC BY-NC license. The submitting author must agree to pay the publication charge (see Charges).

The author of submitted materials (e.g. text, figures, tables etc.) is obligated to restricts the publishing rights. All contributors who do not meet the criteria for authorship should be listed in an Acknowledgements section of the manuscript. Authors should, therefore, add a statement on the type of assistance, if any, received from the sponsor or the sponsor's representative and include the names of any person who provided technical help, writing assistance, editorial support or any type of participation in writing the manuscript.

Uniform requirements for manuscripts

The manuscript should be submitted by the Open Journal System (OJS) at https://srees.sggw.edu.pl/about/submissions. All figures and tables should be placed near their reference in the main text and additionally sent in a form of data files (e.g. Excel, Visio, Adobe Illustrator, Adobe Photoshop, CorelDRAW). Figures are printed in black and white on paper version of the journal (color printing is combined with an additional fee calculated on a case-by-case basis), while on the website are published in color.

The size of the manuscript should be limited up to 10 pages including overview, summary, references and figures (the manuscript more than 13 pages is unacceptable); Please set the text format in single column with paragraphs (A4 paper format), all margins to 25 mm, use the font Times New Roman, typeface 12 points and line spacing one and half.

The submitted manuscript should include the following parts:

- name and SURNAME of the author(s) – up to 5 authors
- affiliation of the author(s), ORCID Id (optional)
- title of the work
- key words
- abstract (about 500 characters)
- text of the paper divided into: Introduction, Material and Methods, Results and Discussion, Conclusions, References and Summary
- references in APA style are listed fully in alphabetical order according to the last name of the first author and not numbered; please find the details below
- post and mailing address of the corresponding author:

  Author's address:
  Name, SURNAME
  Affiliation
  Street, number, postal code, City
  Country
  e-mail: adress@domain

- Plagiarism statement (https://srees.sggw.edu.pl/copyright)

Reference formatting

In the Scientific Review Engineering and Environmental Sciences the APA 7th edition style is used.

Detailed information

More information can be found: https://srees.sggw.edu.pl